5-2003

Viscoelastic Roll Coating Flows

Mitchell A. Johnson

VISCOELASTIC ROLL COATING FLOWS

By

Mitchell A. Johnson

B.Ch.E. University of Minnesota, 1995

M.S. Institute of Paper Science and Technology, 1997

A THESIS

Submitted in Partial Fulfillment of the

Requirements for the Degree of

Doctor of Philosophy

(in Chemical Engineering)

The Graduate School

The University of Maine

May, 2003

Advisory Committee:

Douglas W. Bousfield, Professor of Chemical Engineering, Advisor

Adriaan R. P. van Heiningen, J. Larcom Ober Professor of Chemical Engineering

Albert Co, Associate Professor of Chemical Engineering

Vincent Caccese, Associate Professor of Mechanical Engineering

Stephen A. Austin, Ph. D., Gerber Technologies

COPYRIGHT NOTICE

VISCOELASTIC ROLL COATING FLOWS

By Mitchell A. Johnson

Thesis Advisor: Dr. Douglas W. Bousfield

An Abstract of the Thesis
Presented in Partial Fulfillment of the Requirements for the
Degree of Doctor of Philosophy
(in Chemical Engineering)
May, 2003

The physics of a fluid flow between two rotating cylinders is important in processes such as bearing lubrication, roll coating, and printing. A small amount of dissolved polymer in the fluid can have a large impact on the behavior of the process. Viscoelasticity affects the stability of application and metering processes, and reduces the maximum speed at which a uniform film can be coated onto a substrate.

The goal of this work is to characterize the effect of viscoelasticity on the forward roll coating operation. A bench-top apparatus simulated the process. Measurements of the gap between the roll surfaces, pressure profile, and film thickness were made for a known roll speed and external load. Newtonian, Boger, and shear-thinning viscoelastic fluids were characterized and tested. Two-dimensional finite element analysis of forward roll coating between two rigid rolls was completed for Newtonian, Oldroyd-B, and Giesekus fluids.

The results for the Newtonian liquid were consistent with published experimental and theoretical data after the elasticity of the deformable cover was included in the analysis. A dimensionless empirical expression described the results. A lubrication analysis with non-

Hertzian cover deformation and visco-capillary boundary conditions at the film-merge and film-split corresponded with experimental measurements over a limited load range.

The viscoelastic fluids showed a trade-off between shear thinning and elasticity. Three fluids were Boger-like in that they exhibited nearly constant viscosity in simple shear but had significant elasticity. Two liquids obeyed the Carreau model but showed significant elasticity. All five liquids exhibited varying degrees of the Weissenberg effect. The Boger fluids produced larger gaps and showed increased sensitivity to roll speed compared to the Newtonian liquid. The two shear-thinning elastic fluids produced larger gaps and increased sensitivity to the external load. Dimensionless, empirical expressions described the results.

The finite element analysis revealed the presence of a stress boundary layer at the free surface downstream of the film-split for the Oldroyd-B fluid; the Giesekus fluid, under the same conditions, did not produce the stress boundary layer. Competing effects of shear thinning and elasticity were revealed as a reduction of roll separating force produced by the Giesekus fluid.

ACKNOWLEDGEMENTS

I would like to express my gratitude to my advisor Dr. Douglas W. Bousfield for providing me with the opportunity and means to undertake a fundamental study of the behavior of viscoelastic liquids in a coating environment. Dr. Albert Co, Dr. Adriaan van Heiningen, Dr. Steve Austin, and Dr. Vince Caccese have provided perspective and valuable expertise, which helped me to develop and undertake this project. I would like to thank Dan Jolicoeur and Amos Cline for their efforts in the design and construction of the experimental apparatus. The continuous support and enthusiasm from my parents, Sharon and David, is very much appreciated. David's vast expertise in all things mechanical, and genuine interest in my endeavors, were invaluable resources.

I would especially like to thank Kerry. Her support and encouragement was instrumental to our success in the trials of the past years of which this project was just small part. Thank you Kerry.

TABLE OF CONTENTS

LIST OF TABLES

LIST OF FIGURES

1 INTRODUCTION

1.1 Coating Processes

Coatings are applied to paper and paperboard, metal, plastic films, woven, and non-woven materials as liquids and then solidified in order to increase the functionality or improve the appearance of the substrate. Plastic films or disks are improved by coating with magnetic media, photographic, x-ray, or photo-resist materials. Pressure sensitive adhesives are coated to create fasteners. Anticorrosion coatings improve the life of steel, mineral pigments applied to a paper substrates increase brightness and printability. Ultra-thin layers of silicone are applied to paper and polymer film as release agents. Hydrophobic materials applied to papers protect foods and increase the water repellency of fabrics. Embossed polymer coatings applied to road signs and LCD computer displays increase their brightness and visibility.

The goal of most coating operations is to apply a uniform liquid film to a substrate which is usually a continuous web. Uniform film thickness is not the only important factor; the internal microstructure of the film often affects the mechanical, chemical, optical, and electrical properties of the finished product. There are many devices used by the industry to apply liquid films to substrates (Booth 1970). Industrial coaters can be classified by the methods they employ to feed, distribute, meter, and apply the liquid to the substrate.

1.1.1 Roll Coating

There are many unit operations contained in the coating process, however, the main function of the coater is the deposition of the liquid onto the substrate. Of the many ways to apply a coating to a substrate, one of the more versatile, inexpensive, and mechanically simple processes is roll coating. The roll coating process forms a thin liquid film on a

continuous web by the use of two or more rotating rolls (Higgins 1965, Zink 1979, Satas 1984). A roll coater can apply a wide range of film thickness for a variety of liquid properties. However, in general, the films applied by roll coaters are not as uniform as those applied by a pre-metered coating device except when an expensive precision roll coater is used.

1.1.2 Equipment

The two major types of roll coaters are designated by the direction that the roll surfaces move in the nip. In forward mode roll coaters, the roll surfaces move in the same direction. The surfaces of the rolls move in opposite directions in reverse mode coaters. Schematics of these systems are shown in Figure 1.1 where it should be noted that the gaps between the roll surfaces have been greatly exaggerated.

Forward roll coaters, or meniscus roll coaters, are used to apply optical quality films 10-200 μm thick of low viscosity, 20-1000 mPas, liquids at relatively low speeds 0.05-2 m/s (Zink 1979, Satas 1984). The forward roll coating process is sensitive to speed, viscosity, and the gap between the rollers. Reverse roll coaters are more versatile than forward machines, however, they are very complex and expensive. A wider range of film thicknesses from 5 – 400 μm can be applied at speeds up to 400 m/min for liquids with viscosities ranging from 100 – 50,000 mPas.

Roll coating systems can be further characterized by whether or not the application and metering elements deform, in terms of their shape or position, as a result of the balance of forces in the application or metering zones. In the rigid systems shown in Figure 1.1, a narrow gap is set between two rigid rollers. The film thickness and uniformity is determined by the gap width and roll speeds. A detailed review of the rigid roll coating literature can be found in (Coyle 1997).

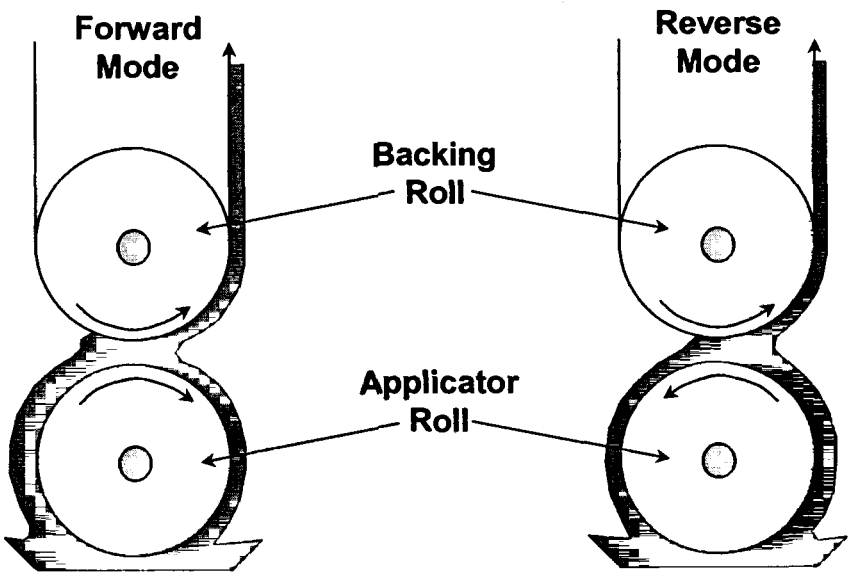

Figure 1.1 Rigid roll coating systems

In the schematics shown in Figure 1.2, application and metering of the liquid are controlled by the interaction between the elastic forces of the deformable applicator or metering element and the hydrodynamic viscous forces. In these elasto-hydrodynamic roll coating systems, one of the boundaries deforms to an equilibrium shape or position determined by the balance between the elastic restoring forces of the deformable element, external loading, and the hydrodynamic forces generated by dragging the liquid into the nip. Elasto-hydrodynamic coating systems are more versatile than rigid systems because they can apply greatly reduced film thicknesses with less sensitivity to mechanical tolerances, process disturbances, and operating parameters. The direct gravure coater, Figure 1.2a, operates differently from the other operations. In this configuration, the elasto-hydrodynamic interaction is used to ensure transfer of the liquid from the gravure cells to the substrate by allowing the substrate, which is wrapped around the deformable backing roll, to conform to the engraved surface of the gravure roll. Figure 1.2b is a two-sided squeeze roll coater, a

high speed metered-size-pressure coater is shown in Figure 1.2c, a five roll film transfer coater is shown in Figure 1.2d and a printing press ink train is shown in Figure 1.2e.

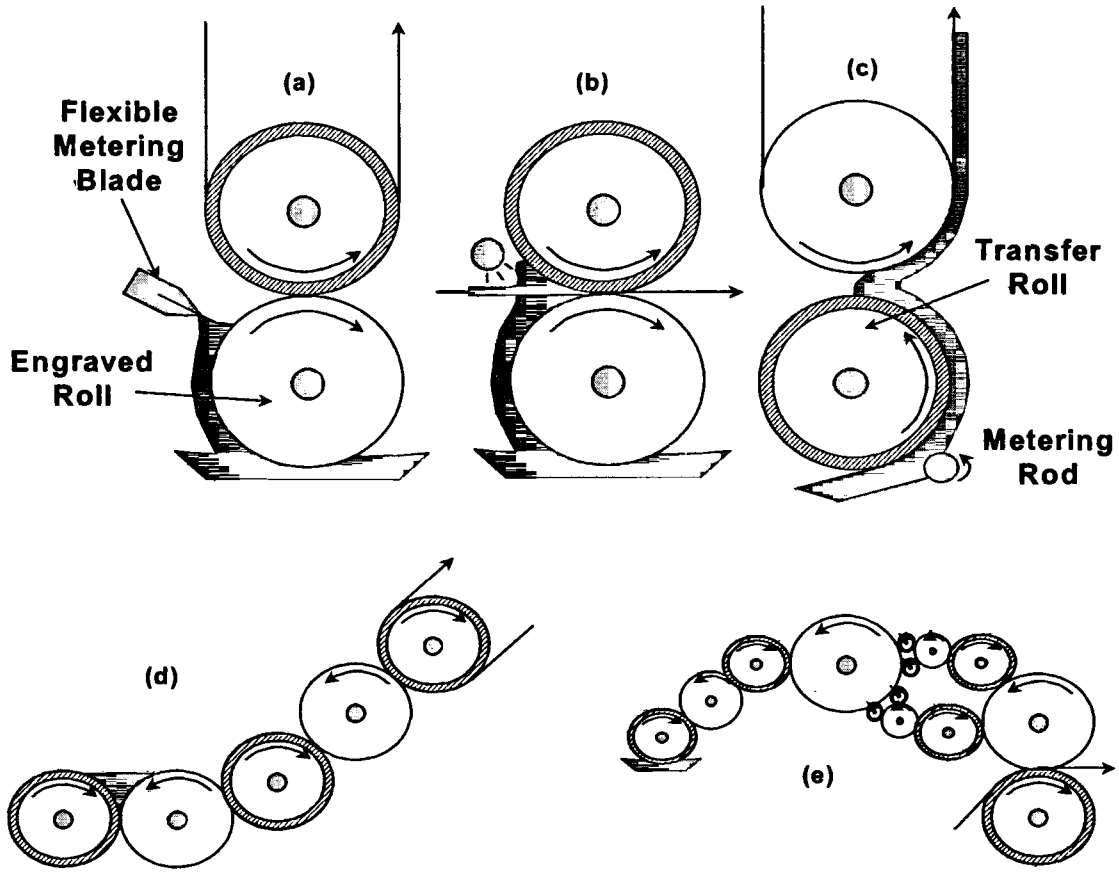

Figure 1.2 Elasto-hydrodynamic roll coating systems

Schematics of other elasto-hydrodynamic coating arrangements, which may or may not contain a roll, are shown in Figure 1.3. In Figure 1.3a, the tensioned web kiss coater uses the flexible substrate to control the film thickness but the pump that supplies liquid to the die in the tensioned web slot coater, Figure 1.3b, determines the film thickness rather than the balance of forces. In Figure 1.3c, a flexible doctor blade is used to control the coated film thickness. Prankh and Coyle (1997) provide a recent review and analysis of elasto-hydrodynamic coating systems.

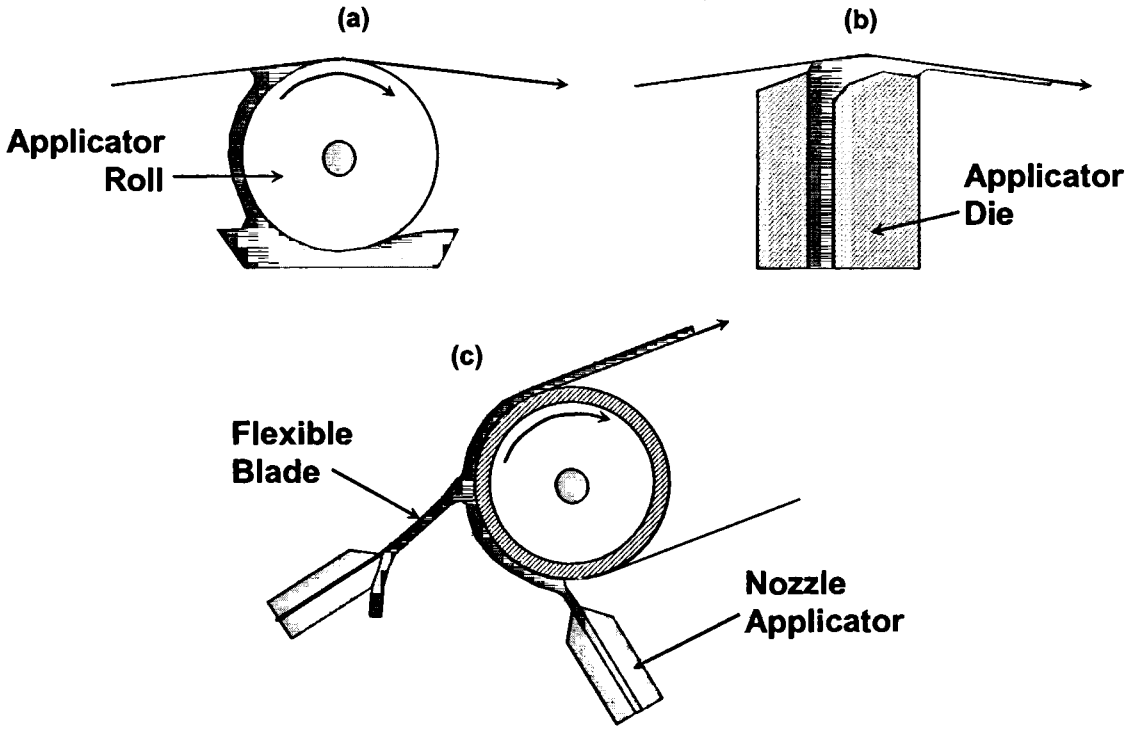

Figure 1.3 Elasto-hydrodynamic coating systems

Elasto-hydrodynamic coating systems are much more versatile than their rigid counterparts because they can apply greatly reduced film thickness and are less sensitive to mechanical tolerances. Roll speed, viscosity, and external loads have a smaller effect on these systems with the added bonus of being less sensitive to process perturbations; however, this is not always achieved because the stability of the process is determined by the interactions of many parameters.

1.1.3 Process Stability

Roll coating flows have been studied for many decades both experimentally and mathematically, with the goal of predicting the film thickness, interface locations, roll velocities, pressure profiles, separation forces, recirculation locations, and flow stability. Even though the flow in the narrow gap region of a roll coater can be considered as a one-

dimensional lubrication flow, it is complicated by the influences of air-liquid interfaces, deformable boundaries, static and dynamic contact lines, adjacent high and low shear areas, and extensional flows at the inlet and film split regions. Figure 1.4 is a schematic of the gap flow.

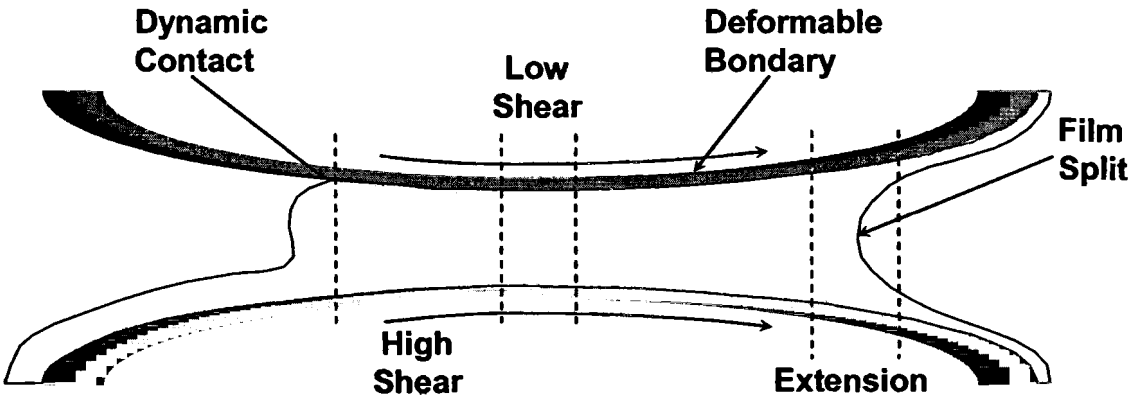

Figure 1.4 Gap flow in a forward roll coater

The roll coating process can become unstable to process disturbances at both the inlet and film split regions and defects in the coated film are the result. The occurrence of defects usually requires production speeds to be decreased, refinements in the mechanical tolerances of the equipment, or the relaxing of quality control restrictions. Typical sources of disturbances are variations in the gap between the rolls either through mechanical tolerances or substrate thickness. Roll eccentricity can also cause disturbances. Fluctuating roll speeds and mechanical vibrations are other triggers of instabilities.

The inlet region of the roll coater contains a rolling bank of liquid that has multiple vortices rotating on an axis perpendicular to the machine direction depending on process conditions. Rotating flows are susceptible to inertial instabilities through an imbalance of rotational momentum. Coating flows that exhibit inertial instabilities are found in short-dwell and puddle coater ponds Figure 1.5.

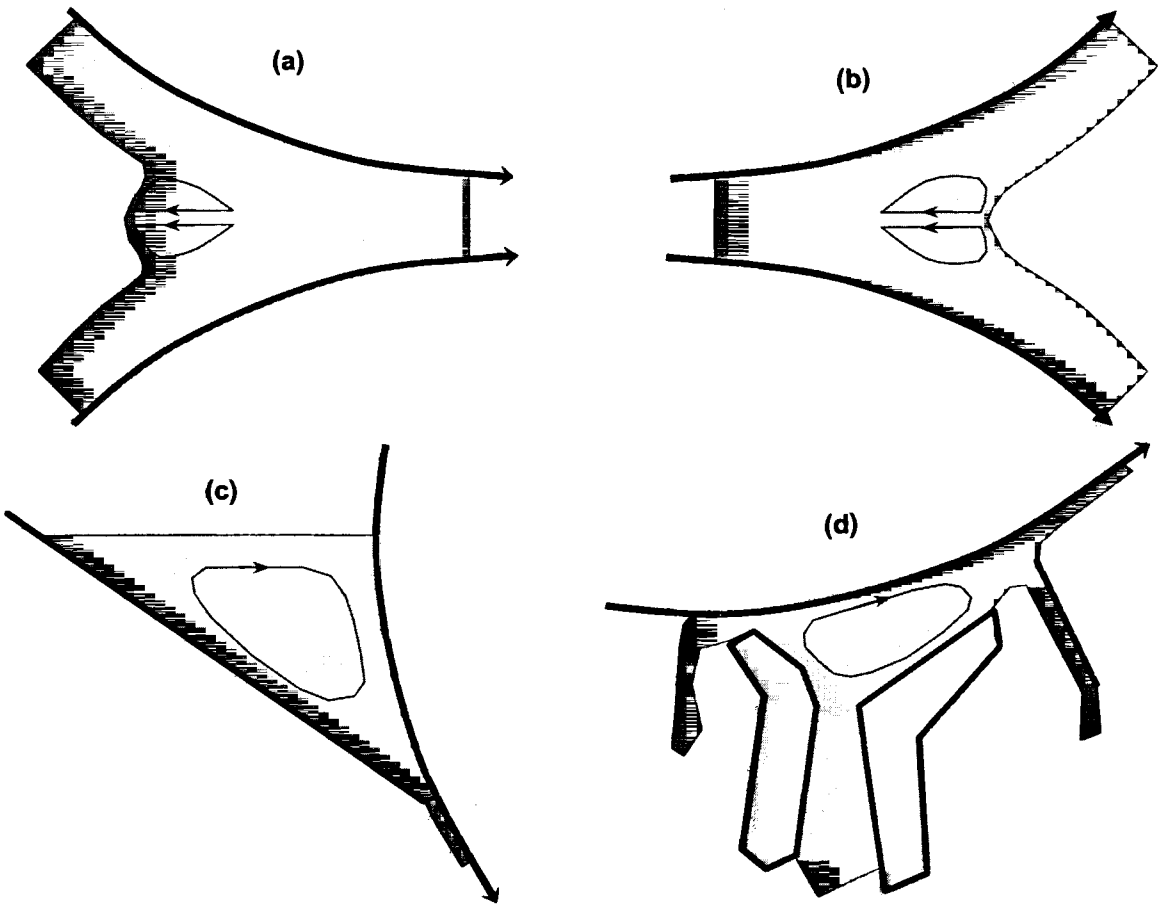

Figure 1.5 Rotational coating flows

It is possible that the vortices in the rolling bank at the inlet region of a forward roll coater could be even more susceptible to the inertial instability mechanism because of the free surface boundary. The inertial instability mechanism has also been shown to cause ribbing in film flows of liquids on rotating rolls (Yih, 1960). However, it would require an extreme set of operating conditions, such as very low viscosities and wide gaps, for ribs to form near the inlet region during a forward roll coating operation.

Roll coating operations are prone to air entrainment at the dynamic wetting line. Entrained air bubbles tend to agglomerate and cause coating thickness variations across the web. Air entrainment may also occur where the rolling bank meets the free surface of a second incoming film.

Excessive feed to nip may disturb the flow. The liquid not drawn into the nip or the rolling bank may run back down the film and cause instabilities, which could perturb the flow; this flow situation may lead to air entrainment as well.

Starving the nip of coating liquid can also lead to film thickness variations. When the nip is starved, the coating thickness remains nearly constant in the center of the web but decreases toward the edges. This failure mode is common in meniscus coating where both viscosity and roll speeds are low. However, in printing applications, all of the unit nips are starved from the metering roll to the blanket.

The film split region of the roll coater is also susceptible to instability. The balance between surface tension and viscous forces at the film split meniscus shows that the diverging flow field is always unstable to three-dimensional disturbances. If the coating speed and viscosity are high, then the stabilizing effect of surface tension can be overcome and a three-dimensional flow will result. This flow forms a pattern known as ribbing. The uniformity of the coated layer is then determined by the ability of the film to level the defects. Figure 1.6 shows examples of the defects in the film split region.

Other defects occur at the film split region as the roll speeds increase. Booth (1970) called the thin membranes of coating liquid that form in the diverging nip "webs". Dontula *et al.* (1996) labeled them septae. When the process is disturbed, the webs rupture and filamentation occurs.

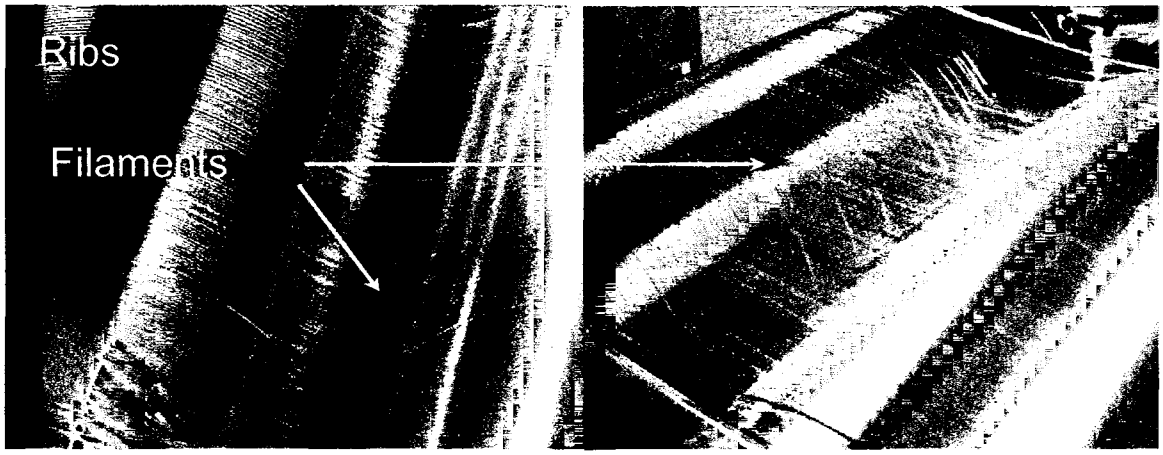

Figure 1.6 Film split defects

Cavitation of the liquid phase has also been proposed as a mechanism leading to filamentation. The filament ruptures as it is stretched and, depending on the number of places it breaks, it can leave behind a stalagmite of liquid on the web or it can eject a droplet of liquid into the air. Adachi *et al.* (1988) reported that liquid droplets were ejected from the nip from the edges of the roll due to the presence of the thicker edge beads.

Ejected droplets, called mist, leaves behind defects after the coating is solidified and can become an environmental hazard. The metered-size-press process and printing operations can suffer from misting (Roper *et al.* (1997), Grön *et al.* (1998), and Roper *et al.* (1999), Voet (1956), Miller and Myers (1958), Myers and Hoffmann (1961), Christiansen (1995), MacPhee (1997), and Blayo *et al.* (1998)). Alonso and Tanguy (2001) reported that the rheological behavior of the coating liquid affects the misting behavior in a metered size press coater.

Physical destruction of the substrate, especially in printing operations, can occur depending on the fluid properties and operating parameters. The tensile stress generated at the nip exit can be so great that the liquid, rather than rupturing the filament, will pick fibers

from the web to relieve the stress. Picking occurs readily at high production speeds (Fetsko *et al.* (1963) and Jorgenson and Lavi (1973)).

1.1.4 Non-Newtonian Effects

Nearly all industrially significant coating liquids have some form of non-Newtonian behavior: shear thinning, dilatancy, or viscoelasticity. Coating liquids are commonly suspensions of mineral pigments, solutions of dissolved polymers, or combinations of both, as shown in Figure 1.7. A wide range of non-Newtonian behavior in roll coating flows is caused by the behavior of the complex liquid in the flow domain. In fixed gap, rigid roll coaters, shear-thinning fluids increase the flow rate through the nip. Shear-thinning liquids tend to be split nearly evenly between the rolls even when the roll speeds are unequal (Coyle *et al.* 1987, Benkreira *et al.* 1981). The faster roll will carry away more of a Newtonian liquid. The onset of the ribbing instability is usually delayed to higher roll speeds for shear-thinning liquids.

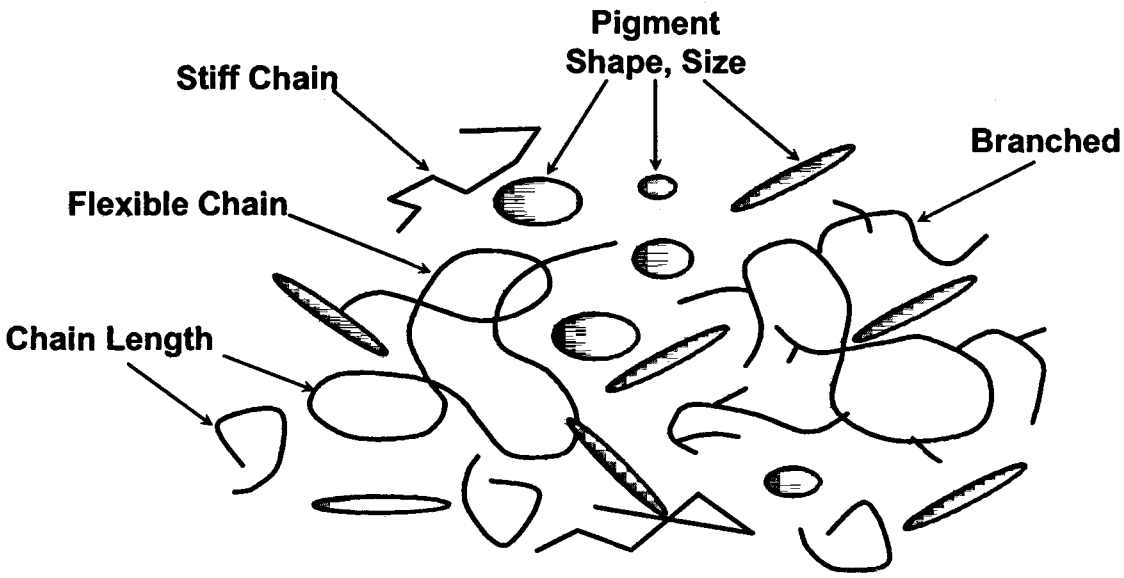

Figure 1.7 Coating liquid

Adding small amounts of long chain polymers to the coating liquid, however, can trigger the onset of ribbing at much lower machine speeds through the effects of elasticity and elongational viscosity. Studies with polymer solutions have shown that instabilities caused by elasticity may lead to air entrainment Cohu and Benkreira (1998). Ink formulations that have high extensional viscosities have shown increased tack and propensity for filamentation and picking. Viscoelastic coating liquids have also been shown to decrease the flow through a blade coater nip and increase the separating force against the blade.

1.2 Motivation

It is important to understand how viscoelastic liquids affect the roll coating process to meet the demand for high quality coated products. The goal of this work was to establish a technique to measure the effects of viscoelasticity on forward roll coating flow. Both experimental and computer-aided techniques were used. The unique aspect of the experimental work is the simultaneous measurement of applied load, film thickness, pressure

profile, and the gap between the roll surfaces. In general, little information is available on how viscoelasticity affects the flow of the liquid through the nip of a roll coater. For instance, are the pressure profile, or the positions of the inlet and film split menisci, altered by the presence of elasticity? Does the shear in the nip region generate normal stresses that could change the flow rate by deforming further the elastic boundary in an elasto-hydrodynamic system? What happens when shear-thinning and elasticity compete? Does elasticity trigger its own instability mechanism unique to roll coating flows? These questions should be answered if a more complete understanding of the viscoelastic roll coating flow is desired.

1.3 Thesis Layout

The bulk of the work performed in this research was to establish techniques to measure the effects of viscoelasticity on roll coating flows. An experimental roll coating apparatus was constructed and measurements of the film thickness and pressure profile were made for both Newtonian and non-Newtonian test fluids. The effects of viscoelasticity could then be determined based on the differences in film thickness and pressure between the Newtonian fluids and non-Newtonian fluids. Computer aided techniques were used to study the parameters of various viscoelastic fluid models to determine their effect of the fixed rigid roll coating flow. A discussion of the results obtained for Newtonian fluids is presented in Chapter 2 and the results for the viscoelastic fluids are presented in Chapter 3. A summary of the thesis and recommendations for future work are presented in Chapter 4.

2 NEWTONIAN COATING FLOWS

2.1 Introduction

Many studies have been presented for two rigid rolls with a fixed gap; detailed reviews of the literature on rigid roll coating flow studies are presented in Coyle (1992), Benjamin (1994), and Coyle (1997). However, many roll coating systems employ a roll with a deformable elastomer cover on backing roll to produce the coated film. The elastic layer on the backing roll creates an elasto-hydrodynamic system, one where the flow geometry, thickness and uniformity of the coated film, depend on the balance between the hydrodynamic forces generated by the liquid, external loads, and the elastic restoring force of the cover. Elasto-hydrodynamic coating systems are quite prevalent throughout the industry. There is also a vast amount of information in the literature concerning a similar flow system, the lubrication flow in bearings and gear teeth. A recent review of elasto-hydrodynamic coating systems can be found in Prankh and Coyle (1997). Information on bearing lubrication is contained in Dowson and Higginson (1966).

2.1.1 Theoretical Analyses

The forward mode squeeze-roll coater has an elastomeric cover on one or both rolls. In this system, the fluid is dragged into the nip by the moving roll surfaces through the action of viscosity. High pressure is generated at the inlet of the nip. The fluid pressure causes the deformable roll surface, and possibly the substrate, to deflect. The coated film thickness becomes a function of two dimensionless groups. The elasticity number Ne, is the ratio of the viscous stresses to the elastic restoring forces,

$$Ne = \mu \bar{V} / ER \tag{2.1}$$

where μ is the liquid viscosity, $\bar{V}$ is the average velocity of the rolls, E is an effective plain strain modulus for the two rolls which are assumed to be Hookean solids:

$$\frac{1}{E} = \frac{1-\nu_1^2}{E_1} + \frac{1-\nu_2^2}{E_2} \tag{2.2}$$

where ν is the Poisson ratio and E is the Young's modulus for a roll material and R is an effective radius for the two rolls:

$$\frac{1}{R} = \frac{1}{R_1} + \frac{1}{R_2} \tag{2.3}.$$

The second dimensionless group is the load number N_w, the ratio of any external, linear load applied to the system, W, and the elastic restoring forces:

$$N_w = W / ER \tag{2.4}$$

Because the steel roll is much harder than the covered roll, its effect is negligible. Surface tension forces can also be neglected except in the rigid roll limit at low capillary number Ca defined in Equation 2.12. The elasto-hydrodynamic roll coating systems have three distinct operating regimes and these can be examined if N_e and N_w are combined into a single parameter g_3 after Johnson (1970) and Herrebrugh (1968). The parameter g_3 is defined as:

$$g_3 = \frac{N_w}{N_e^{1/2}} \tag{2.5}.$$

Two limiting cases of the flow are the rigid roll limit at $g_3 = 0$ and the dry contact limit at $g_3 >> 1$. In the rigid roll limit, hydrodynamic forces control the flow in the nip and elastic deformation is negligible. High speeds and low external loads can produce flows in the rigid limit. In the dry contact limit, elastic forces dominate the flow and the hydrodynamic forces are negligible. The primary variable of interest in coating flows is the flow rate through the

roll nip, which can be expressed, in dimensionless form as $\frac{H}{R}$ where H is the local gap between the roll surfaces at the point in the nip where the maximum fluid pressure occurs. Hooke (1986) has shown that the thickness of the roll cover material can influence the flow if the ratio of the cover thickness b to the Hertzian contact half width a is less than 1 where a is:

$$a = \left(\frac{4WR}{\pi E} \right)^{1/2} \tag{2.6}.$$

Herrebrugh (1968) solved the elasto-hydrodynamic lubrication flow between a rigid roll and a roll with a semi-infinite thickness deformable cover, for large values of g_3 and a constant viscosity liquid. Hall and Savage (1988) used improved numerical methods and obtained similar results. Coyle (1988b) used a one-dimensional model for a finite thickness cover but his model only produced qualitative predictions of the flow rate. Hooke (1986) produced solutions for a wide range of loads and layer thicknesses. Coyle (1990) incorporated the effects of nonlinear finite deformation of the elastic solid layer and also investigated the influence of a viscoelastic cover layer. The calculations by Bapat and Batra (1984) for dry rolling contact of viscoelastic solids have shown that viscoelasticity is important. Carvalho and Scriven (1994) used several one-dimensional spring models and a two-dimensional model coupled with the lubrication approximation to study the deformable roll coating flow. Carvalho and Scriven (1997a) employed finite element methods to study the two-dimensional flow and roll cover deformation. Carvalho and Scriven (1997b) also performed a perturbation analysis of the two-dimensional deformable roll coating flow.

2.1.2 Experimental Analyses

There is a vast body of experimental data concerning the flow in a narrow, fixed gap between two rigid rollers Pitts and Greiller (1961), Savage (1982), Benjamin *et al.* (1995). However, many coating systems employ a deformable layer on one of the rollers. Crook (1958) first measured the deformed gap profiles for a lubricated elasto-hydrodynamic contact with a fixed external load. At high loads, a nearly parallel gap region forms between the two roll surfaces over which the pressure profile is nearly Hertzian. Examples of the surface profile are shown in Figure 2.1. In this figure, there was an initial 10 μm gap between the roll surfaces and the flow rate was specified. As the load increases, the hydrodynamic forces generated by dragging the liquid into the nip increase and overcome the elastic restoring force of the deformable cover. The cover deflection increases and a nearly parallel channel forms between the rolls.

Many investigators have performed experiments with constant external load operation of the nip for Newtonian liquids. Smith and Maloney (1966) provide the most extensive set of data that correlates the flow rate with the operating parameters. Swales *et al.* (1972), Varnam and Hooke (1977), and Coyle (1988a) have also presented empirical correlations for the flow rate through the nip.

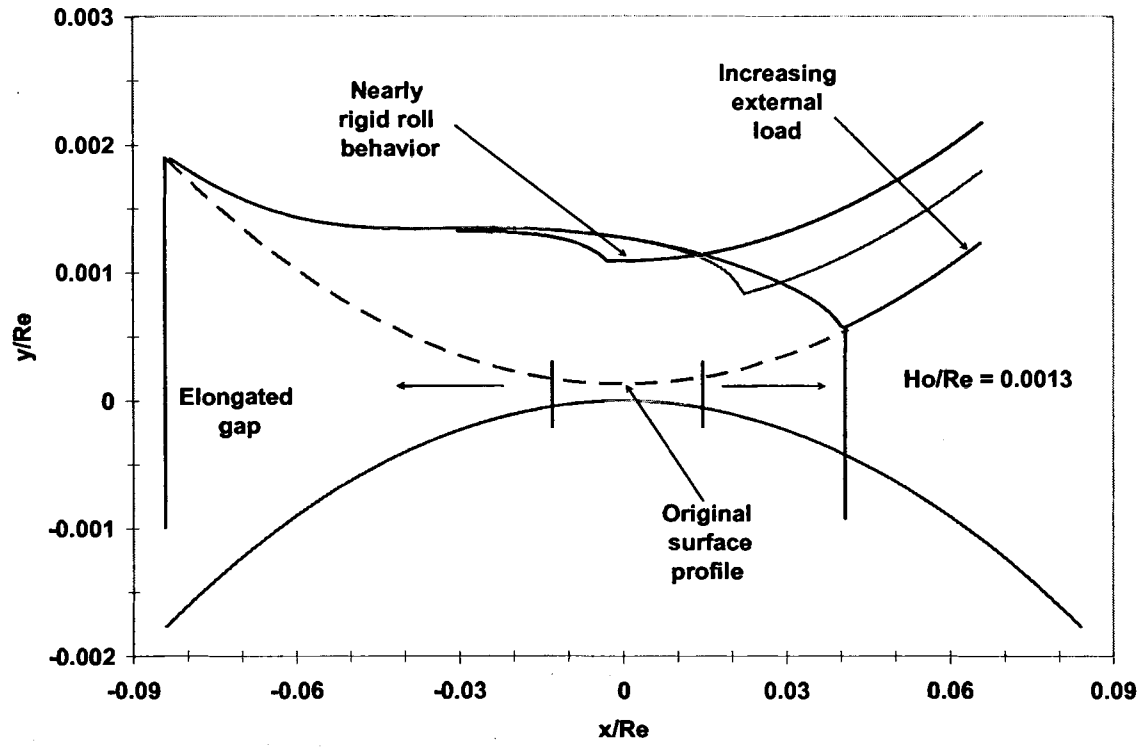

Figure 2.1 Elasto-hydrodynamic gap profiles

Adachi *et al.* (1988) and Kang, Lee, and Liu (1991) presented coating thickness data for squeeze roll nips. In this configuration, the rolls are engaged to create a particular amount of deflection of the deformable cover and then held in place. These systems can either have an initial gap between the roll surfaces, or be operated with a negative gap, or nip. Benjamin (1994) examined both positive and negative fixed gaps for a deformable roll operation where the inlet was flooded with a Newtonian liquid. He varied the roll speed ratio and found that the film split ratio of the outgoing films had a much more significant dependence on the roll speed ratio compared to similar conditions with two rigid rollers.

Cohu and Mangin (1997) measured the flow rate of Newtonian liquids for fixed external loads. Their results agreed quantitatively with the finite element analysis by Coyle (1988a) for a thick deformable cover. In their analysis, Cohu and Mangin (1997) also accounted for the viscoelastic behavior of the cover material by using an elastic modulus that

depended on roll speed. Their results showed that when thin covers were used, the flow rate was significantly reduced. This may have been caused by reduced deflection of the cover.

2.2 Experimental Investigation

The purpose of the Newtonian liquid study was to establish an investigative technique by comparing the results of flow rate and film thickness measurements to published data. The ultimate goal was to examine the effectiveness of a new technique that made it possible to measure the actual gap between the roll surfaces at the point within the nip where the maximum fluid pressure occurred. No one has reported any attempts to repeat or improve upon the measurements of the gap profile first made by Crook (1958). Since that time, investigators have relied mainly on scraping the coated film from the roll surfaces and measuring its mass after a length of time, inferring flow rate from this measurement. These investigators have reported that incomplete scraping was a significant cause of error in their measurements. The gap measurement technique applied in this investigation eliminated this error and was verified by measurements of the coated wet film thickness. The gap measurement was supplemented with pressure profile and applied load measurements.

2.2.1 Apparatus

Forward roll elasto-hydrodynamic coating flows were studied with a bench-top apparatus. A schematic of the coating rig is shown in Figure 2.2. The device consists of two rolls, both 12.7 cm in diameter and 20.3 cm wide, with 3.6 cm diameter shafts. One roll is a steel tube that has a 2.5 cm thick shell and removable endplates. The other roll is solid steel and has an elastomeric cover that is 6 mm thick.

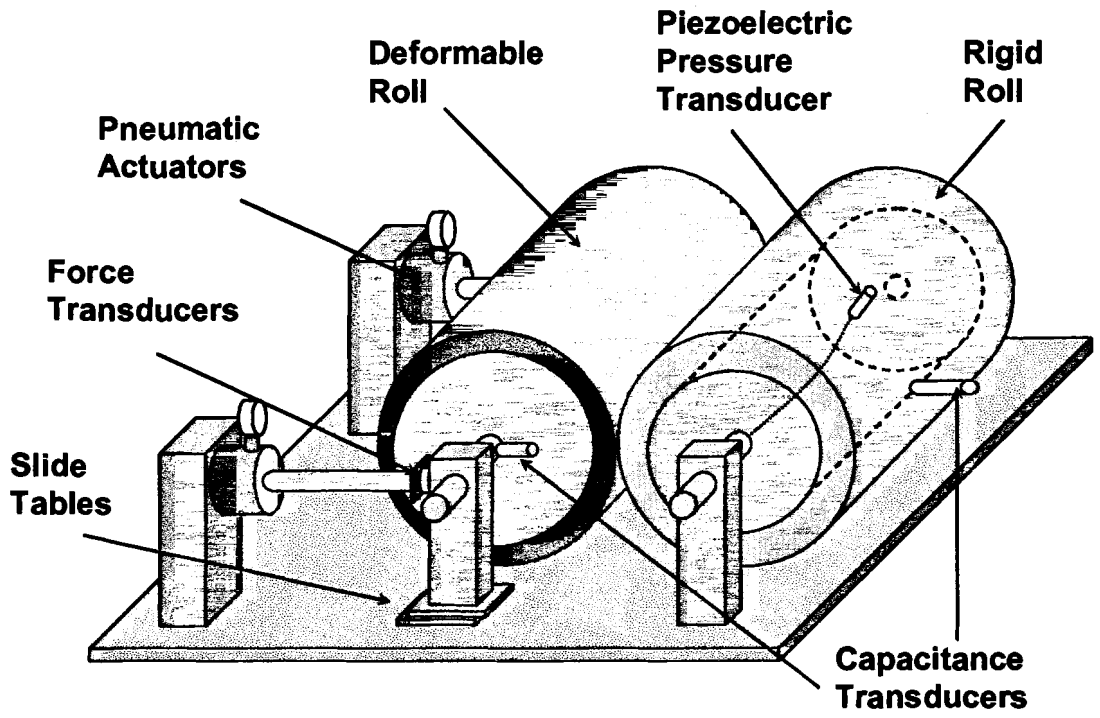

Figure 2.2 Experimental roll coating apparatus

The rolls are supported by pillow block bearing housings model PU-324 (Rexnord Corp., Milwaukee, WI). Both of the rolls are fixed to a steel base plate, however, the deformable roll is mounted on crossed roller slide tables, model NBT-6160 (Del-Tron Precision Inc., Bethel, CT), allowing the roll to change its position with little friction. Two pneumatic, rolling-diaphragm actuators, model S-4 (Marsh Bellofram Corp., Newell, WV), one on each end, are used to load the deformable roll against the rigid roll. A high performance regulator, model 960 (Marsh Bellofram Corp., Newell, WV), controls the pressure in each cylinder. A force transducer, model ELA-B2E-250L (Entran, Fairfield, NJ) sandwiched between the tie-rod and the bearing housing post, monitors the load applied by each actuator. A pair of 5.3 hp servomotors, model MGM-4120, with EN-214 drives (Emerson, St. Louis, MO), rotate the rolls.

A personal computer-based data acquisition system was used to send roll speed information to the drives and acquire data from the sensors. The signal from the pressure transducer was removed from the roll via a slip ring assembly. The system uses a 16 channel, 12 bit, data acquisition board, model PCI-DAS-1002 (Measurement Computing, Middleboro, MA), that can sample up to a total rate of 200 kHz with a 3 microsecond delay between channels and has an analog to digital conversion resolution of 2.44 mV DC. The Visual BASIC based graphical interface of SoftWIRE version 3.0 (SoftWIRE Technology, Middleboro, MA), controls the data acquisition. Sampling is performed based on the position of the roll from the feedback of the encoder in each motor with a resolution of up to 2048 points per revolution.

2.2.2 Measurement Techniques

A non-contact, capacitance technique was used throughout the experiments to determine the coated film thickness applied to the roll surface and the gap between the rolls. The capacitance probe system used in the experiments was the Accumeasure™ 5000 amplifier and the ASP-10-CTA and ASP-10-ILA capacitance transducers (MTI Instruments, Latham, NY). The amplifier has a frequency response of 20 kHz and output noise level of 1.7 mV rms DC and has a linear response of ±0.1% over 10 to 100% of the full scale range of 0 to 10 V DC for either gap or dielectric medium thickness changes. The 3mm diameter capacitance transducers have a range of 500 microns with a sensitivity of 50 microns/V and an accuracy of 0.1% of the range.

Capacitance gauging is a reliable and convenient technique that has been used to measure film thickness in other roll coating applications (Spiers *et al.* 1974, and Tharmalingam and Wilkinson 1978 a and b). Crook (1958) used a capacitance technique to

measure the gap profile in an elasto-hydrodynamic system. Bohan *et al.* (2001) recently applied a capacitance measurement coupled with an inductance sensor to immediately remove the effect of roll eccentricity. Capacitance, and the resulting voltage, changes proportionally to the thickness and dielectric constant, $k = \frac{V_{air}}{V_{liquid}}$, of the measured medium. For this measuring system, the dielectric constant of the test liquid must be predetermined. This was done according to parallel plate capacitor theory, by measuring the change in voltage for a change in gap when the entire gap was filled with the test liquid. The Newtonian test fluid used throughout the investigation was a mixture of two Dow-200 silicone oils. The physical properties, and the components by weight percent, of the test liquid are shown in Table 2.1. Fluid density was measured by pycnometer and the surface tension was measured with a DuNouy Ring. The fluid viscosity was measured with a Bohlin CVO-50 cone and plate rheometer.

Table 2.1 Physical properties of Newtonian test fluid

Test Fluid		ρ (kg/m^3)	σ (N/m)	k	η_o (Pas)
Silicone Oil					
1000 cst	10,000 cst				
0.86	0.14	977	0.021	2.79	1.35

Because of construction limitations, the rolls and shafts have a certain amount of run-out, or eccentricity, that caused the distance from the target to the probe surface to change. The run-out of the deformable roll shaft is on the order of 40 μm and the run-out of the rigid roll is on the order of 20 μm.

A piezoelectric pressure transducer monitored the pressure profile within the nip; the rapid response of the piezoelectric material and integrated circuit make are ideal for this

application. The transducer was mounted in the shell of the rigid roll so that the sensor surface was flush with the roll surface. The sensor, a model 105-C12 (PCB Piezotronics, Depew, NY) is a miniature transducer with a diameter of 2.5 mm. It has a resonant frequency of 250 kHz and a range of ±1000 psi with a sensitivity of 5.385 mV/psi and linearity equal to 0.56% of full scale. The sensor requires a minimum 20 V DC to drive the internal circuitry of the sensor housing. Both the excitation voltage and the signal from the sensor are passed between the roll and the signal conditioner via a slip ring assembly, model IECU 12 (IEC Corp., Austin, TX) that has two silver-graphite brushes per ring.

2.2.3 Roll Cover

The roll cover material is polyurethane; model A-9 (Air Products and Chemicals Inc., Allentown, PA), with a hardness of 70 Shore-A. Dynamic oscillatory measurements of stress and strain in compression mode revealed that this material is quite viscoelastic. A sample of the material was compressed at three different rates and the resulting stress and strain of the material was tracked; the results are shown in Figure 2.3.

The change in the amount of deformation of the roll cover can also be measured on the roll coating apparatus. The results shown in the following figure are plotted with values of deformation predicted by Hertz contact theory using a Young's modulus of the cover as E_1 = 30 MPa. The range of contact times encountered during the experiments was between 0.005 and 0.011 seconds. Therefore, using E_1 = 30 MPa as the modulus in the following calculations is a reasonable approximation. Measurements of the Poisson ratio for materials are difficult to obtain and the value used throughout the experiments and analysis was based on fits to experimental measurements of the pressure profile in dry contact with a non-Hertzian deformation approximation (Johnson, 1985). The estimated value was ν = 0.49.

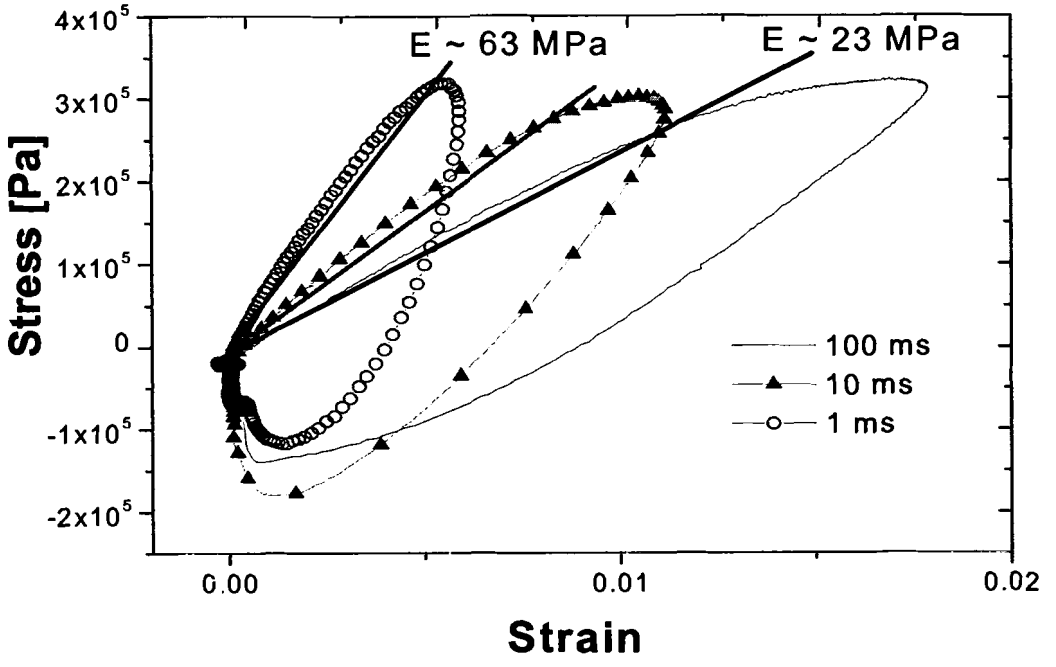

Figure 2.3 Stress vs. strain for the roll cover material

2.2.4 Experimental Procedure

The run-out of the roll surfaces caused each experiment to consist of a preliminary run and test run. Air was the test medium in the preliminary run which was used to establish the distance between the probe face and the target at various points around the circumferences of the rolls. The test liquid was then added to the system in the test run and the output voltage from the probes was obtained at the same points around the circumference of the roll or shaft. The minimum gap and the wet film thickness of the test liquid are proportional to the voltage difference between the baseline run and the run with the test liquid. The procedure is presented schematically in Figure 2.4. After the measurements were obtained, the roll speed was increased and more fluid was added to the system.

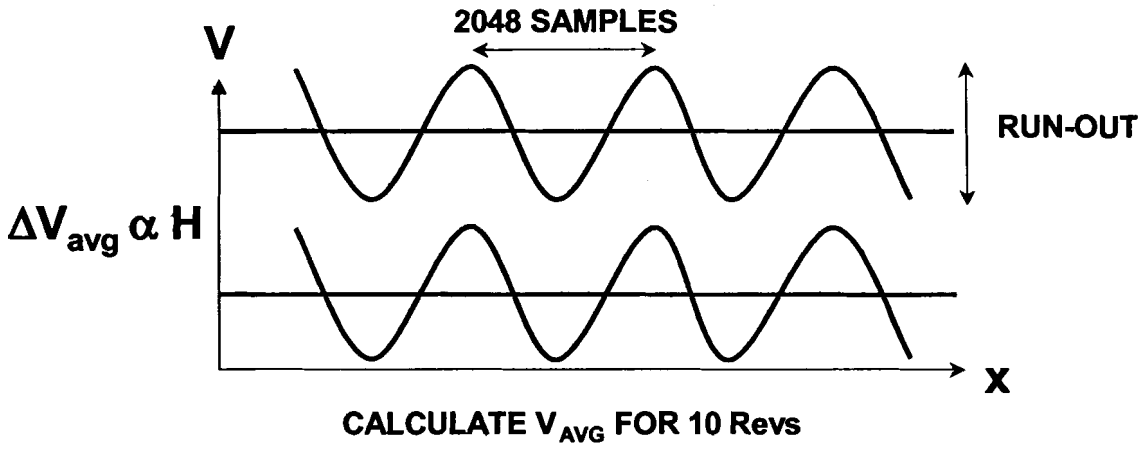

Figure 2.4 Schematic of the experimental procedure

Figure 2.5 is an example of the information obtained from the capacitance gauging technique. After the test liquid is added to the system, it takes about 15-20 revolutions for the system to reach equilibrium. The system remains at steady state for at least 60 revolutions before fluid is lost to the roll edges. All measurements were obtained within the steady-state period. The figure also shows that the measurement of the actual gap at the point of maximum fluid pressure in the nip corresponds with twice the measured film thickness.

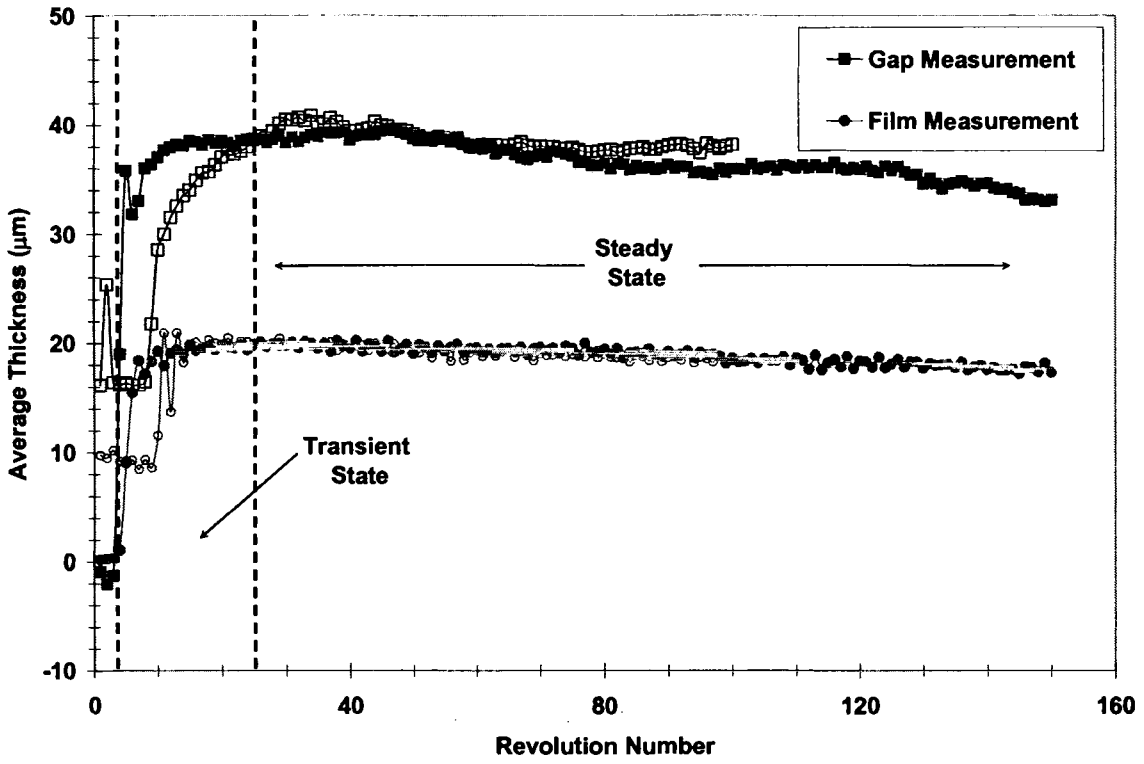

Figure 2.5 Measured gap width and film thickness

2.3 Theoretical Investigation

The forward mode, Newtonian, elasto-hydrodynamic roll coating flow was analyzed with a lubrication approximation based mathematical model. This analysis has been carried out many times before with various methods for treating the deformation of the roll cover including both Hertzian contact and various spring models as well as with a viscoelastic model for the roll cover material. The model in this analysis used non-Hertzian contact theory for a finite thickness cover, a method first suggested by Johnson (1985). This analysis is unique in that the position of the deformable roll is allowed to change with the operating conditions and a visco-capillary boundary condition is employed at the film split. Previous models fixed the positions of the rolls such that a small initial gap or nip was maintained

between the rolls and the resulting elasto-hydrodynamic equilibrium state was allowed to develop. Figure 2.6 is a schematic of the flow domain.

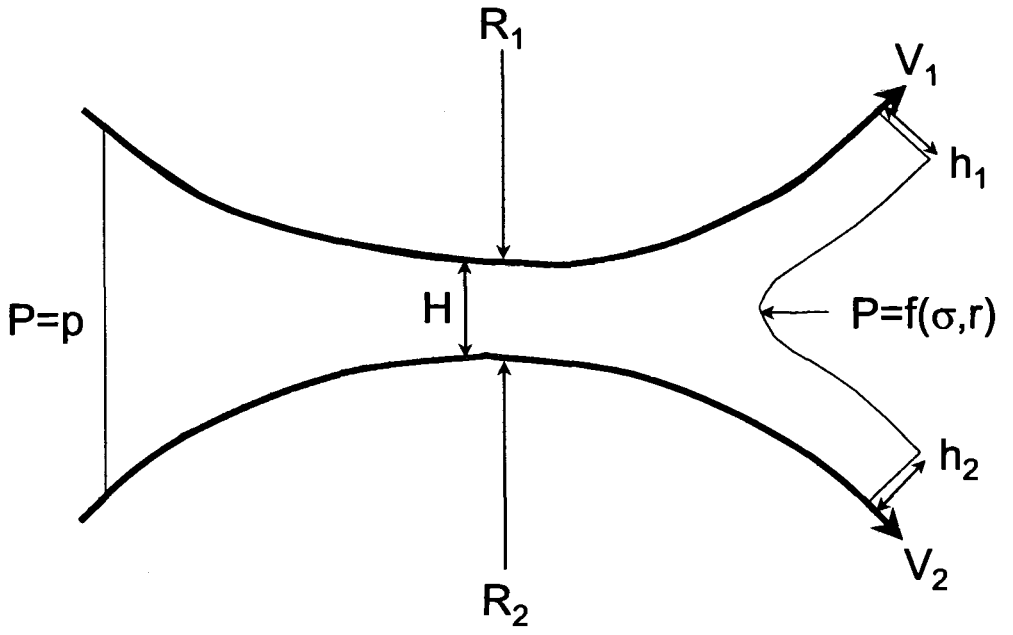

Figure 2.6 Flow domain for the lubrication model

The liquid is taken to be Newtonian and incompressible. The roll radii are much larger than the distance between the roll surfaces, therefore the flow in the gap region is nearly rectilinear and the governing Navier-Stokes system of differential equations can be simplified to the lubrication approximation Cameron (1976). The pressure profile through the gap is given by:

$$\frac{\partial P}{\partial x} = 12\mu\bar{V}\left(\frac{H(x)-H_o}{H(x)^3}\right) \tag{2.7}$$

where $\bar{V}$ is the average roll speed, H_o is an initial gap or engagement, and $H(x)$ is roll surface profile which is well approximated as a parabola in the nip region:

$$H(x) = 2H_o + \frac{x^2}{R} + D(x) \tag{2.8}.$$

In equation 2.8, $D(x)$ is the local deformation of the roll cover, which is dependent on the fluid pressure and the Poisson ratio after Johnson (1985):

$$D(x) = \frac{P(x)}{(1-\nu)^2 E(1-2\nu)b} \tag{2.9}$$

where b is the thickness of the roll cover. This model for deformation does not account for shear stresses in the cover or the effects of neighboring deformations. It is also difficult to use this expression for incompressible materials, such as roll covers, when the Poisson ratio approaches $\nu = 0.5$. Carvalho and Scriven (1997a), suggest that this relation cannot be used when computing elasto-hydrodynamic roll coating flows because of the large deformations encountered. They have proposed a one-dimensional spring model as well as a plane strain model to describe cover deformation and solved the full two-dimensional flow and deformation problem via the finite element method. Equation 2.7 is integrated with an implicit Euler method.

A relatively simple but important aspect of the model is the inclusion of a film-split at the nip exit. The split-point is made to depend on the viscous and capillary forces via a visco-capillary boundary condition for the pressure. At the split-point the capillary pressure in the liquid is given by:

$$P_e = \frac{-\sigma}{r} \tag{2.10}$$

where σ is the surface tension of the liquid and r is the radius of curvature of the film-split meniscus. The radius of curvature is given by:

$$r = \frac{Q}{2.68 Ca^{2/3} \bar{V}} \tag{2.11}$$

where Q is the total flow rate through the nip and Ca is the capillary number defined as:

$$Ca = \frac{\mu \bar{V}}{\sigma} \qquad (2.12).$$

The location of the split-point is found by matching the circular meniscus to the asymptotic solution of the flow on a flat plate being withdrawn from a pool of liquid. For symmetric roll speeds, the height at the exit, h_e, is given by:

$$h_e = \frac{Q}{\bar{V}}\left(1.644 + \frac{2}{2.68Ca^{2/3}\sqrt{1+0.414(3Ca)^{2/3}}}\right) \qquad (2.13).$$

At the film merge the pressure is zero and the position of the film merge is adjusted with an iterative procedure until the radius of the meniscus gives zero pressure.

The model also has the ability to adjust the relative positions of the center points of the rolls until the boundary conditions are met. A final boundary condition is that the integrated pressure profile must be equal to the specified external, linear load W such that:

$$W = \int_{x_{inlet}}^{x_{exit}} P(x)dx \qquad (2.14).$$

An additional approximation was made to account for cavitation of the liquid and the unreasonable, negative exit pressures produced by models. The fluid pressure below -100 kPa was truncated from the calculation of the load. Other boundary conditions, such as Elrod (1981), have been proposed, but experiments showed that the minimum pressures obtained were between -200 kPa and -100 kPa. Truncating below –200 kPa had a negligible effect on the calculated gap width so -100 kPa was used as the cut-off point in the analysis.

2.4 Results and Discussion

The pressure is presented in dimensionless form and scaled with the elastic deformation of the roll cover as:

$$p^* = \frac{P(x)b}{ER} \tag{2.15}.$$

The thickness of the roll cover was used in the scaling to include the effects of a finite thickness cover. Figure 2.7 shows examples of the pressure profiles obtained from the piezoelectric transducer for three external loads given as the load number *Nw* at one roll speed and fluid viscosity *Ne*. Each point is the average of ten measurements and the curves have been shifted so that the pressure peak occurs at $\frac{x}{R} = 0$. As the dry contact limit is approached, at high *Nw*, the gap between the rolls decreases and the magnitude of the pressure peak increases. When conditions near the rigid roll limit, the pressure profile becomes more symmetric; the gap increases and nip length decreases, as the roll surfaces are forced apart.

In Figure 2.8, the applied load is held constant and pressure profiles for four combinations of viscosity and roll speed are plotted. As *Ne* increases, the maximum pressure in the nip increases and the nip length decreases because the system is operating near the rigid limit and viscous forces dominate. If the rolls were fixed in position, there would be a large amount of cover deformation, however, because the external load is fixed, the large viscous force results in an increase in the gap and a small cover deflection.

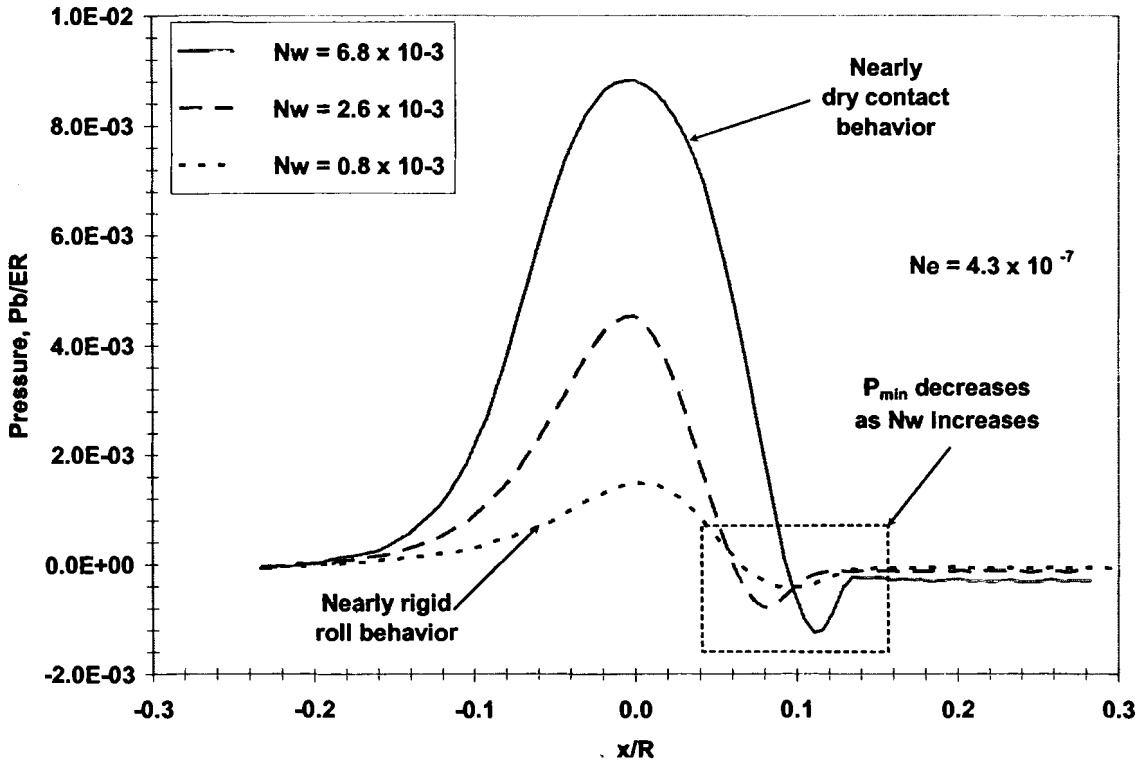

Figure 2.7 Pressure profiles at constant speed

Conversely, as the roll speed decreases, viscous forces diminish, the gap width decreases, and the deformation of the cover increases because the external load dominates the restoring force of the cover material.

Figure 2.9, is a comparison of the integrated pressure profiles measured by the piezoelectric transducer with the force per unit length measured by the force transducers on either end of the deformable roll shaft. The integrated areas, for the entire range of roll speeds, are within 10% of the line loads for the range of conditions in the tests and the effect of the convolution of the pressure signal with nip length is minimal.

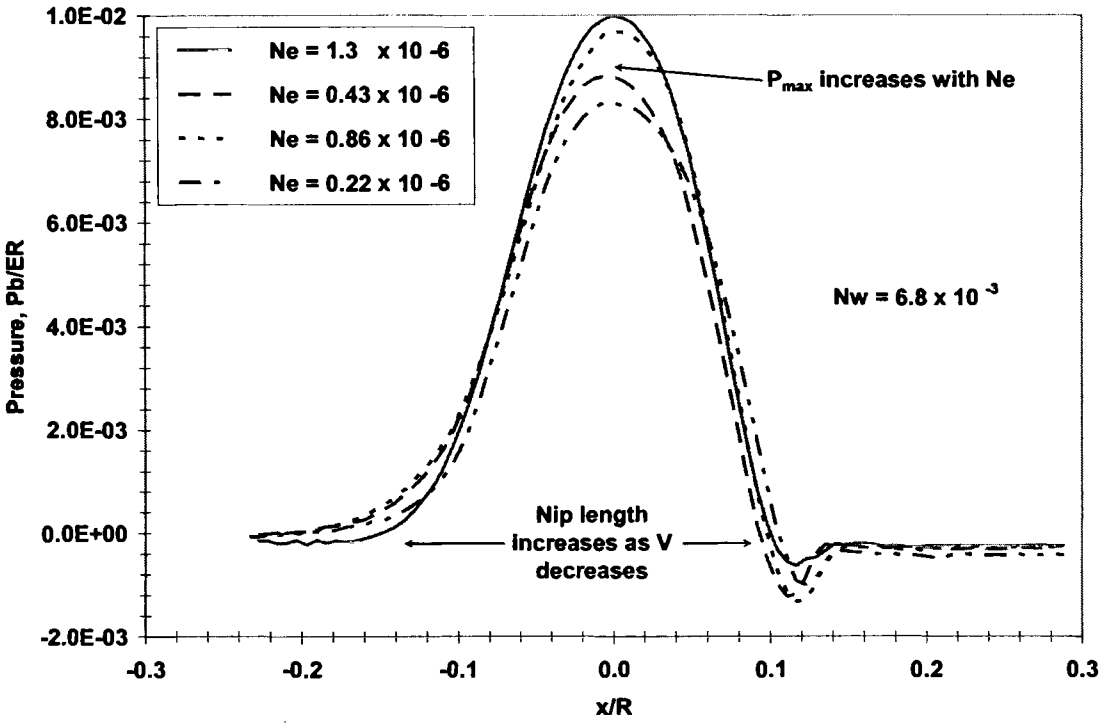

Figure 2.8 Pressure profiles at constant load

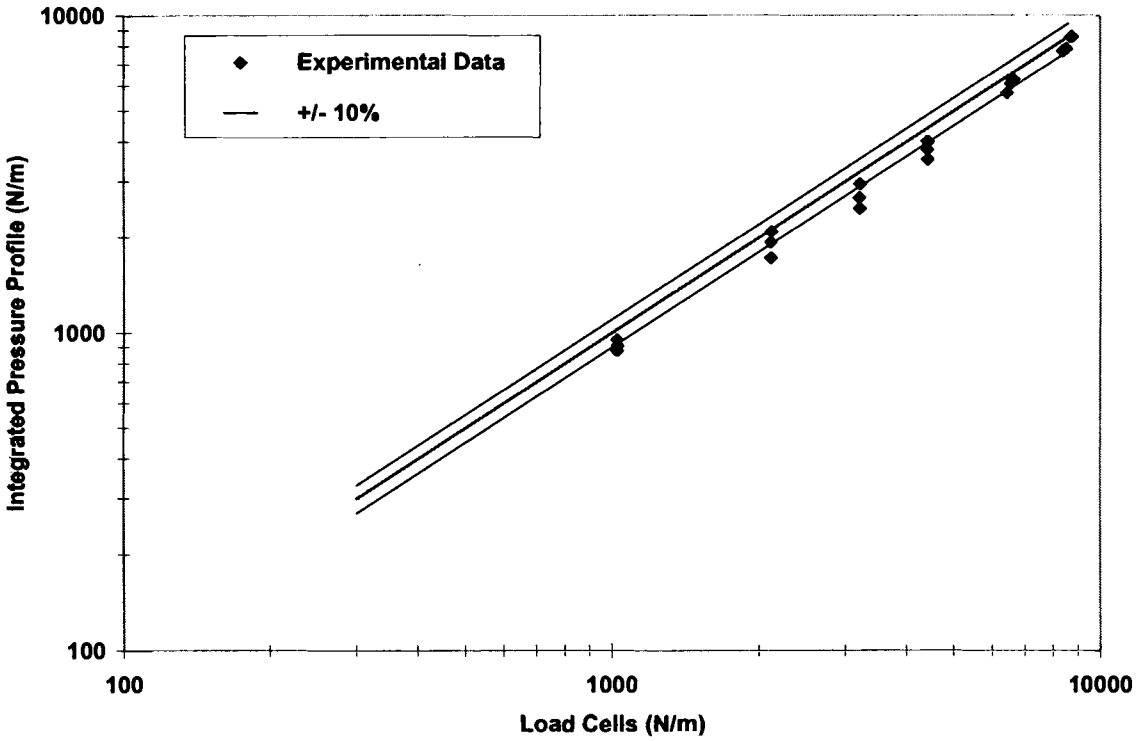

Figure 2.9 Integrated pressure profiles compared to measured load

Figure 2.10 compares the measured pressure profiles with the prediction of the lubrication model for two sets of conditions. The conditions for the comparisons are listed in Table 2.2. For the two conditions compared, the predicted profiles are in excellent agreement with the measured profiles. This is rather remarkable for such a simple model because of the limitations introduced by the non-Hertzian contact deformation model. Even though the model captured the cover deformation well, it limited results to low applied loads.

Table 2.2 Conditions for the model and compared experiments

Parameter	High Load		Low Load	
	Model	Experiment	Model	Experiment
	Dimensional			
σ (N/m)	0.02	0.021	0.02	0.021
μ (Pas)	1.35	1.35	1.35	1.35
ρ (kg/m)	1000	977	1000	977
$\overline{V}$ (m/s)	1	1	1	1
W (N/m)	3000	3210	1000	1027
b (m)	0.006	0.006	0.006	0.006
E (Pa)	39478879	39478879	39478879	39478879
R (m)	0.03175	0.03175	0.03175	0.03175
H (μm)	72	80	117	120
	Dimensionless			
Np	2000		2000	
ν	0.49	0.49	0.49	0.49
Ne	1.1×10^{-6}	1.1×10^{-6}	1.1×10^{-6}	1.1×10^{-6}
Nw	2.4×10^{-3}	2.4×10^{-3}	0.8×10^{-3}	0.8×10^{-3}
g_3	2.3	2.3	0.8	0.8
Ca	67.5	64.3	67.5	64.3
Re	0.05	0.06	0.09	0.09

The results indicate that the non-Hertzian contact model and the requirement that the roll positions be changed to accommodate the visco-capillary boundary condition can accurately represent an elasto-hydrodynamic coating system for low applied loads where the deflection of the cover is small. It is important to note that the results of the calculations have the portion of the negative pressure peak below –100 kPa subtracted from the load

calculation. Without the correction, the maximum pressure was significantly overestimated resulting in gap predictions significantly lower than the measured width.

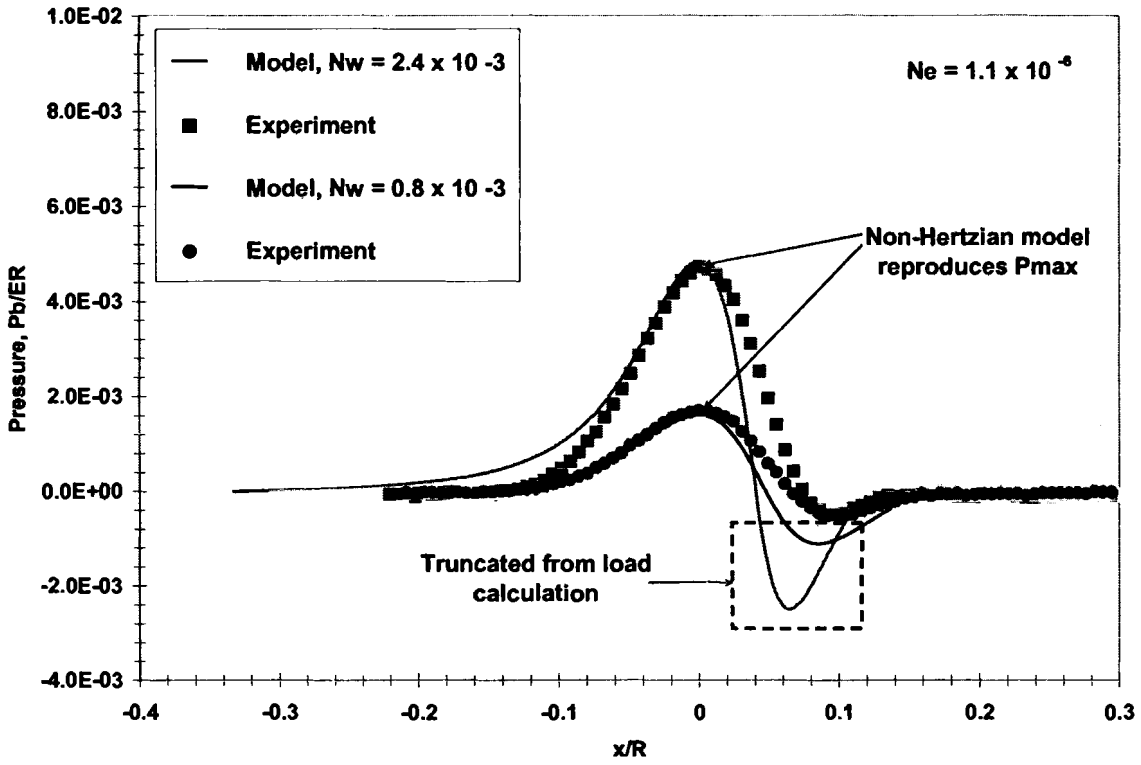

Figure 2.10 Comparison of the calculated and measured pressure profiles

In the experiments, the minimum pressure varied between -100 kPa to -200 kPa, likely due to the amount of dissolved air in the test liquid. These results are quite surprising because they capture the behavior of the system so well. However, the roll cover in this system undergoes much smaller deformation than a typical system because the material is so hard E = 30 MPa. This also explains why we were unable to obtain solutions at higher loads when the cover would have much higher deformation.

Figure 2.11 is a plot of the measured gap width, scaled with the effective roll radius, as a function of the elasticity number *Ne* for several levels of applied load expressed as the load number *Nw*. Each point on the graph is the average of 10 measurements with

deviations from the mean of less than 1 μm. The operating conditions are presented in Table 2.3.

Table 2.3 Experimental operating conditions

Parameter	Dimensional	Dimensionless
σ (N/m)	0.021	
μ (Pas)	1.35	
ρ (kg/m)	977	
$\bar{V}$ (m/s)	0.1-1.4	
W (N/m)	900-8700	
b (m)	0.006	
E (Pa)	39478879	
R (m)	0.03175	
H (μm)	7-140	
ν		0.49
Ne		$0.11 - 1.1 \times 10^{-6}$
Nw		$0.8 - 6.9 \times 10^{-3}$
g_3		0.8 - 6.6
Ca		>> 1
Re		<< 1

Increasing the roll speed strengthened the effect of the viscous forces and caused the rolls to separate and sustain higher flow rates through the nip. Increasing the applied load overcame the viscous forces and reduced the gap width. The sensitivity of the gap width to the elasticity number is represented in terms of the slope of the best-fit line. The slope is less than 1 so a large change in roll speed is required to make a significant change in the gap width.

The effect of the applied load on the gap width is plotted in Figure 2.12 as a function of the load number at several levels of *Ne*. As the load is increased, the viscous forces are overcome and the gap decreases. The conditions that were tested indicate that the gap width is even less sensitive to applied load than to the roll speed. Both of these trends make the roll coater with a deformable cover robust and relatively easy to install and operate because of the insensitivity to process perturbations.

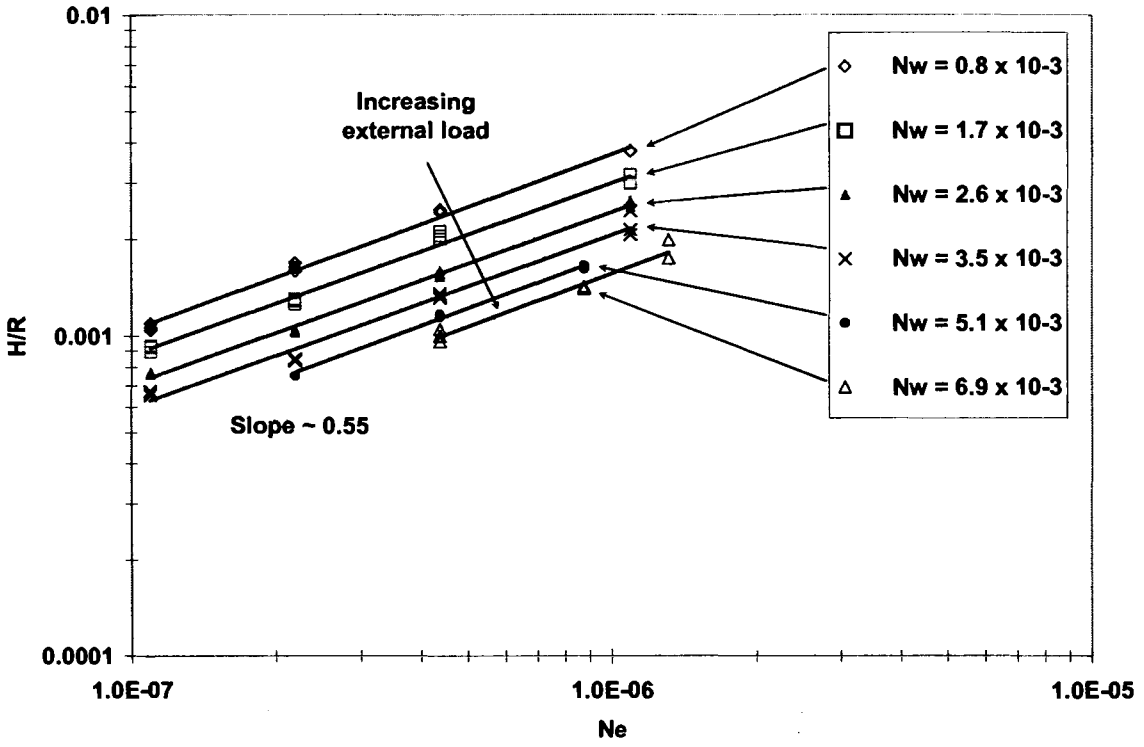

Figure 2.11 Measured gap width as a function of Ne

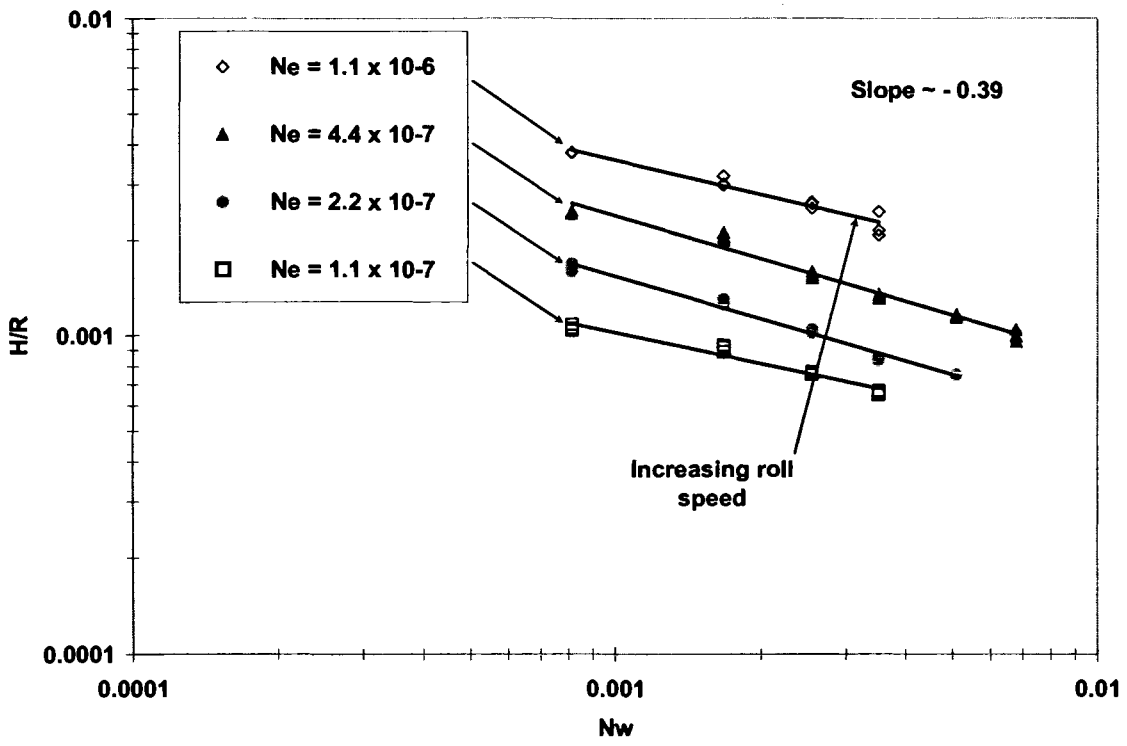

Figure 2.12 Measured gap width as a function of Nw

The best-fit lines in the preceding two figures were obtained by fitting all of the data to an empirical relation. The dimensionless gap width, or flow rate, H/R, can be fit with the equation:

$$\frac{H}{R} = 0.42 Ne^{0.55} Nw^{-0.39} \qquad (2.16).$$

Equation 2.16 can be rearranged to show the dependence of the gap on the operating variables, input in MKS units, as:

$$H = 0.42\left(\mu \bar{V}\right)^{0.55} W^{-0.39} E^{-0.16} R^{0.84} \qquad (2.17).$$

It should be noted that only one value of roll radius and a single value of elastic modulus were used throughout the experiments and in the fitting procedure. Therefore, it can't be confirmed that the indicated dependencies on these two quantities are true. However, 95% of the data agree within ± 5% of the empirical correlation. The empirical correlation is compared with the experimental data in Figure 2.13.

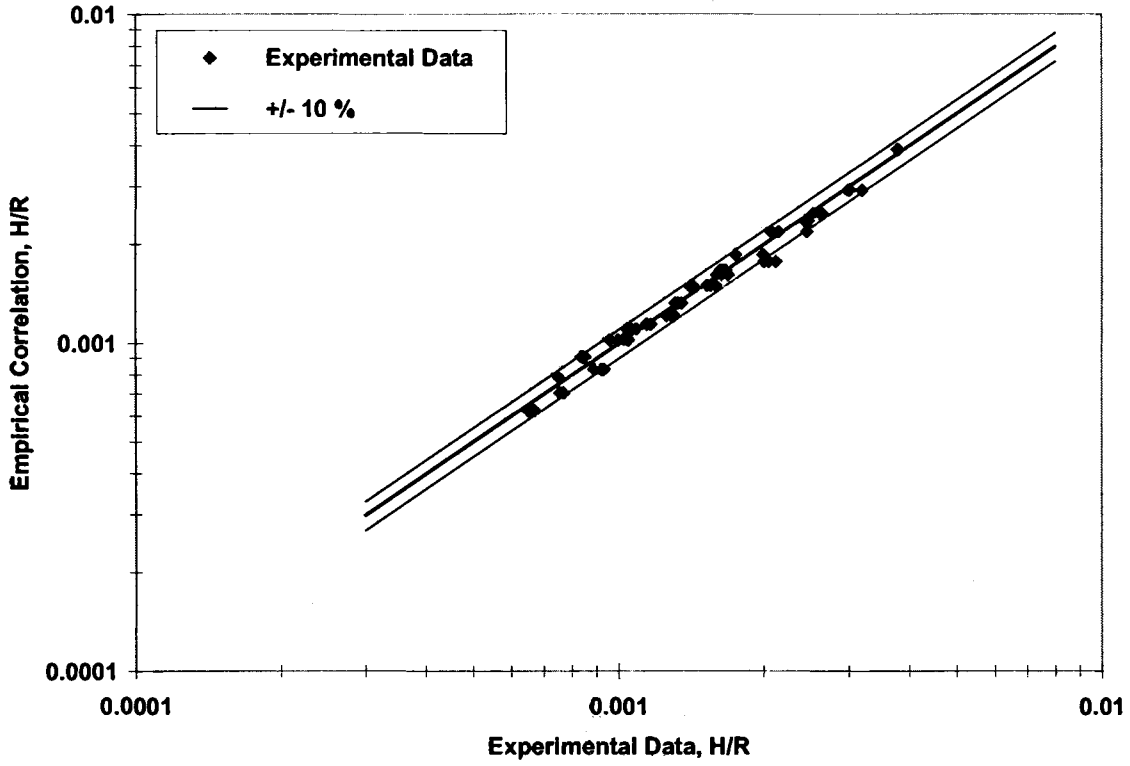

Figure 2.13 Best-fit of experimental data

In the next figure, 2.14, the experimental data are plotted in terms of a modified elasticity number, $\frac{H}{R}Ne^{-0.6}$ so that they can be compared with published data. Throughout the analysis, a single value of the elastic modulus of the roll cover was used. Even though dynamic oscillatory tests on the cover show that it behaves viscoelastically, the measurements indicate that the gap width is relatively insensitive to the viscoelastic behavior of the cover in the speed ranges tested. Cohu and Mangin (1997) made a similar conclusion.

The data are in very good agreement, in terms of the magnitude of the gap, with the analysis of Herrebrugh (1968). The difference between the two sets of data appears in the sensitivity to the load parameter. The experimental data are more sensitive to the applied load. A possible cause of the difference between the two sets is the thin rubber cover that

was used. Cohu and Mangin (1997) have shown increased sensitivity to load when the ratio of the cover thickness to half the nip length approaches 1.

The gap width measurements are in very good agreement with the experimental data of Smith and Maloney (1966). They used a thick, deformable cover in their experiments. At high loads, the experimental data begin to diverge from the correlation of Smith and Maloney (1966) which is more evidence supporting the influence of the cover thickness.

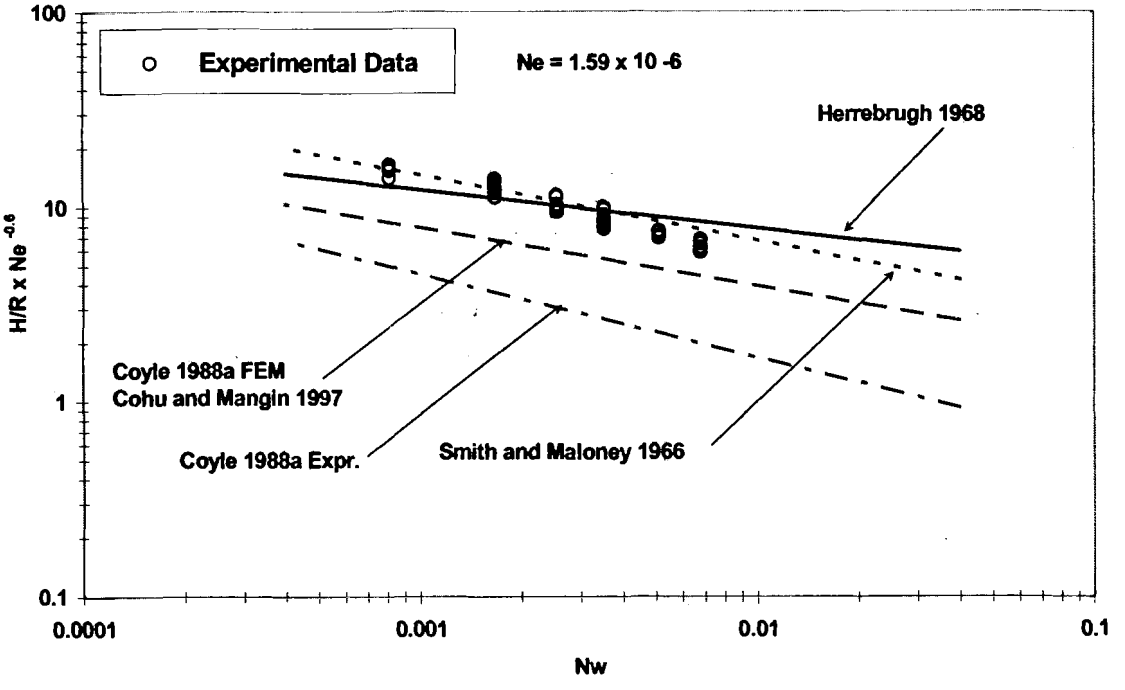

Figure 2.14 Comparison with published data

The data show similar sensitivity to the applied load when compared with the experimental measurements and finite element calculations of Coyle (1988a). However, agreement in terms of magnitude is poor. Coyle (1988a) attributed the discrepancies between his data and other published data, to the influence of the viscoelasticity of the deformable cover. The measurements of flow rate by Cohu and Mangin (1997) agree with the finite element calculations of Coyle (1988a). The data of Adachi *et al.* (1988) are not

plotted because of an unreliable measurement of the elastic modulus of the cover material used in the analysis of their experimental measurements. The data in Figure 2.14 are summarized, in Table 2.4.

Table 2.4 Empirical relations for the gap width

H	$H = k\mu^a \bar{V}^b W^c E^d R^e$					
	k	a	b	c	d	e
Experiment	0.42	0.55	0.55	-0.39	-0.16	0.84
Smith and Maloney, 1966	4	0.64	0.58	-0.34	-0.35	0.58
Herrebrugh, 1968	3.12	0.6	0.6	-0.2	-0.4	0.6
Coyle, 1988a FEM Cohu and Mangin, 1997	0.4	0.6	0.6	-0.3	-0.3	0.7
Coyle, 1988a Exp.	4.1	0.49	0.49	-0.43	-0.41	0.42

Further comparison of the gap width measurements are made with the two-dimensional finite element analysis of Carvalho and Scriven (1997a). The sensitivity of the measured gap width to the load parameter is in very good agreement with the calculations where the exponent is equal to –0.39.

Throughout the experiments, the speed ratio between the rolls was maintained at $\frac{V_2}{V_1} = 1$. In the lubrication equation, the average roll speed is used to predict the gap between the rolls so in effect it will scale it to a set of roll speeds with a ratio of 1. However, the experiments of Benjamin *et al.* (1994), showed that the film split ratio was much more sensitive to the roll speed ratio, for a deformable roll system, compared to two rigid rolls operating with a small gap between the roll surfaces. Contrary to this conclusion, Kang, Lee, and Liu (1991) found the film-split ratio for a fixed engagement, deformable roll system to be relatively insensitive to the roll speed ratio. Future experiments should consider the roll speed ratio as an independent variable.

2.5 Summary

The experiments and calculations from the lubrication model, with symmetric roll speeds for Newtonian liquids in an applied load, deformable, forward roll coating system are summarized as follows:

- A bench-top apparatus was constructed to study elasto-hydrodynamic forward roll coating flows.
- A technique was developed and applied to measure the gap between the roll surfaces. Measurements of the gap corresponded with the expected value at the point of maximum fluid pressure within the nip and the measured wet film thickness.
- The measured gap and its sensitivity to the external load and roll speed were consistent with published experimental data and theoretical analyses.
- There was some evidence of increasing sensitivity to the applied load caused by the influence of the thin, deformable roll cover used in the experiments.
- A model of the deformable roll coating system was developed based on the lubrication approximation with non-Hertzian deformation of the roll cover and a visco-capillary boundary condition at the film-split.
- The lubrication model reproduced the magnitude and shape of the measured pressure, for low external loads, after values of the negative pressure below –100 kPa were removed from the calculations.

3 VISCOELASTIC COATING FLOWS

3.1 Introduction

Previous investigations of roll coating flows have focused on two roll systems with a fixed rigid gap between the roll surfaces. These systems were operated in either forward or reverse mode and used a Newtonian test liquid. These works described the dependence of the coated wet film thickness on the fluid properties and operating variables. Much attention was given to the stability of the system and documenting the appearance of the three-dimensional ribbing instability as a function of the fluid properties and operating conditions.

Many industrially important coating liquids are non-Newtonian, however. In many cases, polymers are added to the coating liquid to modify its viscosity or to act as a binding aid for some other component of the liquid. Often, a molten polymer is applied to a substrate. These liquids exhibit viscoelastic behavior in the roll coating environment. The viscosity of the liquids is often shear-rate dependent. The behavior of the liquid in a particular coating system is often dependent on past deformation events. In some instances, adding only a small amount of polymer to the coating liquid caused a dramatic reduction of the stable operating window. Consequently, much of the current research has focused on the appearance of defects, with the presence of polymer additives, in flows between rigid roll systems. Triantafilopoulos (1996) and Glass and Prud'homme (1997) present recent discussions of the effects of coating liquid rheology in various coating systems.

A system that is used widely throughout the coating and printing industries involves the use one or more deformable rolls to apply and meter a thin film onto a substrate. The deformable roll coating system is simple to operate and relatively insensitive to process perturbations and mechanical tolerances. Surprisingly, little has been published, either

experimental or theoretical, that documents how the viscoelastic behavior of the coating liquid affects the deformable roll coating system.

3.1.1 Theoretical Analyses

Most past theoretical analyses attempted to simulate non-Newtonian behavior by including shear rate dependence of the viscosity in the calculations of flows in rigid roll systems. There have been few attempts to include elastic effects in flow models because of the complexity added to the calculations and the lack of an appropriate fluid model that can adequately describe observed behavior. The available models often describe one behavior well but cannot describe all of the behaviors exhibited by a liquid in a typical roll coating geometry. The wide variety of choices makes it difficult to compare one set of results to another. However, some attempts at viscoelastic calculations in rigid roll coating systems have been made. Tanner (1960) and Greener and Middleman (1975) examined small viscoelastic effects by including first order terms in a Weissenberg number expansion of the lubrication approximation for the flow between two rigid rollers. Tanner used a co-rotational derivative in the Maxwell model and Greener and Middleman used an empirical constitutive relation to describe viscoelastic effects. They observed decreased pressures and reduced separating forces at small Weissenberg numbers.

Davies and Walters (1973) analyzed journal-bearing flow. This system, the flow between two eccentric cylinders with the inner rotating, is similar to the roll coating system and can be described by the lubrication approximation. Davies and Walters used several non-linear models and an Oldroyd model, with a Jaumann derivative to describe viscoelastic effects. They observed that when the normal stresses are much larger than the shear stress, the journal bearing was able to support increased loads, compared to the Newtonian case, at

small eccentricity. Beris *et al.* (1984) used finite element methods, with a variety of fluid models, to simulate the viscoelastic journal-bearing flow. They explored a range of Deborah numbers at low eccentricity to determine the family of stable solutions. The load bearing capacity was not reported. They extended their work to higher levels of eccentricity in Beris *et al.* (1986).

3.1.2 Experimental Analyses

Fukushima (1976) observed markedly different ribbing patterns in flows of butter and printing inks. Glass (1978a-d) performed extensive studies of industrial paint formulations, developing a connection between a rheological property, called "dynamic uniaxial extensional viscosity" and the appearance of ribbing defects. Matsuda and Brendly (1979) found that coatings with high degrees of shear-thinning behavior increased rib amplitude. Doremus and Piau (1981, 1983) measured reduced flow rates and larger separating forces for flows of viscoelastic liquids with high extensional viscosity; however, the gap to diameter ratio used in these experiments is approximately 3 orders of magnitude larger than industrial coating systems and the results may not be applicable. Bauman *et al.* (1982) found that adding a small amount of polymer to the forward roll coating system dramatically reduced the maximum speed at which the ribbing defect occurred. Soules *et al.* (1988) showed that a polymer additive with a rigid backbone and low extensional viscosity, only slightly exaggerated ribbing behavior. Fernando and Glass (1988) studied a variety of polymer additives that had similar steady shear viscosities but a wide range of extensional behavior. The appearance of ribbing at lower roll speeds correlated with increasing extensional viscosity. Kang, Lee, and Liu (1991) observed that viscoelasticity increased both the coating thickness and its sensitivity to roll speed in a fixed engagement, deformable roll

system. Large ribbing defects were also observed. Dontula *et al.* (1996) observed reduced critical capillary numbers for the onset of ribbing with dilute solutions of polymers having different molecular conformations. Both solutions had constant shear viscosities, no measurable elastic properties, and large extensional viscosities. The flow at the film-split was observed to be different from Newtonian flow. Lopez *et al.* (2002) examined the effects of polymer additives on the ribbing instability in an eccentric, rotating cylinder system. For low polymer concentrations, a small reduction in the critical capillary number was observed. At large concentrations, the critical capillary number remained constant for inelastic fluids, while elastic fluids caused it to decrease. A strong effect of elastic properties was observed on ribbing amplitude.

A two roll interface with one roll having a deformable cover commonly occurs in printing press ink trains. Misting has been correlated with the pressure at the nip exit. The pressure at the nip exit is also related to a property of the ink known as "tack" (Reed (1937), Zang *et al.* (1991), Aspler and Taylor (1991), Aspler *et al.* (1994), and Patel and Dealy (1987)). Measurements with inks containing dissolved polymers produced the highest tack values. Adding polymer molecules to ink solutions increased the sensitivity of tack to the film thickness in the nip. Bohan *et al.* (2001) made dynamic measurements of ink film thickness, pressure, and temperature in rolling nip contacts. They observed that the magnitude of the sub-ambient pressure at the nip exit with flows of shear-thinning inks, was larger than the Newtonian fluids tested.

The metered size press coater is commonly used in paper coating and it has the potential to encounter misting defects, (Roper *et al.* (1997), Grön *et al.* (1998), and Roper *et al.* (1999), Voet (1956), Miller and Myers (1958), Myers and Hoffmann (1961), Christiansen (1995) MacPhee (1997), and Blayo *et al.* (1998)). Poranen *et al.* (2000) observed that when

highly elastic starch molecules were added to the coating liquids with suspended pigment particles, higher metering rod loading was needed to produce a particular wet film thickness. Alsonso and Tanguy (2001) reported that the rheological behavior of the coating liquid affected misting in a metered size press coater.

Williamson *et al.* (1997) conducted experiments with polymer-modified oils in a journal bearing geometry. They observed that the load bearing capacity, the extra load required to produce a film thickness, increased with the relaxation time of the polymer modified oils.

The results of past work indicate that non-Newtonian rheology does influence the process in qualitative ways, but experiments where loads, gap, and pressure profile are measured for well-characterized rheology are non-existent. The work summarized in this chapter is intended to add this information to the literature.

3.2 Experimental Investigation

3.2.1 Viscoelastic Fluids

The objective of this study was to study the elasticity of the test liquid independent of shear-thinning behavior. The tool most commonly applied for this purpose is a fluid that has constant, steady shear viscosity but also has elasticity, Boger (1977). The Boger fluid exhibits nearly constant viscosity in steady shear because of the small amount of dissolved polymer it contains. However, because the dissolved polymer is very high molecular weight, it exhibits increasing normal stresses with shear rate in steady shear flow. Adding more polymer to the solution can gradually introduce shear-thinning behavior.

The viscoelastic liquids used in this study were solutions of polyisobutylene (PIB) in a mixed solvent of kerosene (K) and polybutene. The PIB was obtained from Aldrich

Chemical Company. It had a quoted molecular weight of 4,800,000 g/mol and a density of 918 kg/m^3. Small pieces of the PIB were dissolved in kerosene with mild stirring for 3 days. The stock solution had a concentration of 3.4% by weight. The stock solution was diluted with a mixture of low molecular weight polybutenes , MW ~ 750 g/mol (PB 750) and MW ~ 320 g/mol (PB 320), also from Aldrich Chemical Company. The solution was stirred mildly for three additional days to ensure thorough mixing. The preparation and mixing procedure used in this study followed the methods presented by Nguyen and Sridhar (1990). Preparation methods for alternative, water-based, model elastic liquids with polyacrylamide, Prilutski *et al.* (1983) or polyethylene oxide, Dontula *et al.* (1998) are also available. Water based solutions were not used because of the strong dependence of capacitance, the primary indicator of film thickness, on concentration. The physical properties and components by weight percent of the model fluids are given in Table 3.1.

Table 3.1 Physical properties of the test liquids

Test Fluids				ρ (kg/m^3)	σ (N/m)	k
Silicone Oil						
1000 cst		10,000 cst				
0.86		0.14		977	0.021	2.79
Boger Fluids						
PIB	PB 320	PB 750	K			
0.0012	0.3720	0.558	0.0697	857	0.028	2.24
0.0024	0.3710	0.557	0.0696	858	0.028	2.24
0.0036	0.3709	0.556	0.0695	858	0.029	2.23
Elastic, Shear-thinning Fluids						
PIB	PB 320	PB 750	K			
0.0045	0.556	0.370	0.0695	847	0.028	2.22
0.0062	0.5191	0.3461	0.1286	845	0.028	2.20

The steady shear and oscillatory flow behavior of the test liquids were characterized with a cone and plate, Bohlin CVO-50 controlled stress rheometer (Bohlin Instruments Inc., East Brunswick, NJ). The CVO-50 permitted measurements of the apparent viscosity $\eta(\dot{\gamma})$

with shear rate $\dot{\gamma}$ and, for small amplitude oscillations, the dynamic viscosity $\eta'(\omega)$ and the dynamic rigidity $G'(\omega)$ with applied frequency ω. The simple shear flow information was obtained for both the non-Newtonian solutions and their Newtonian solvent components. The apparent viscosity of the test fluids is shown in Figure 3.1 and Figure 3.2.

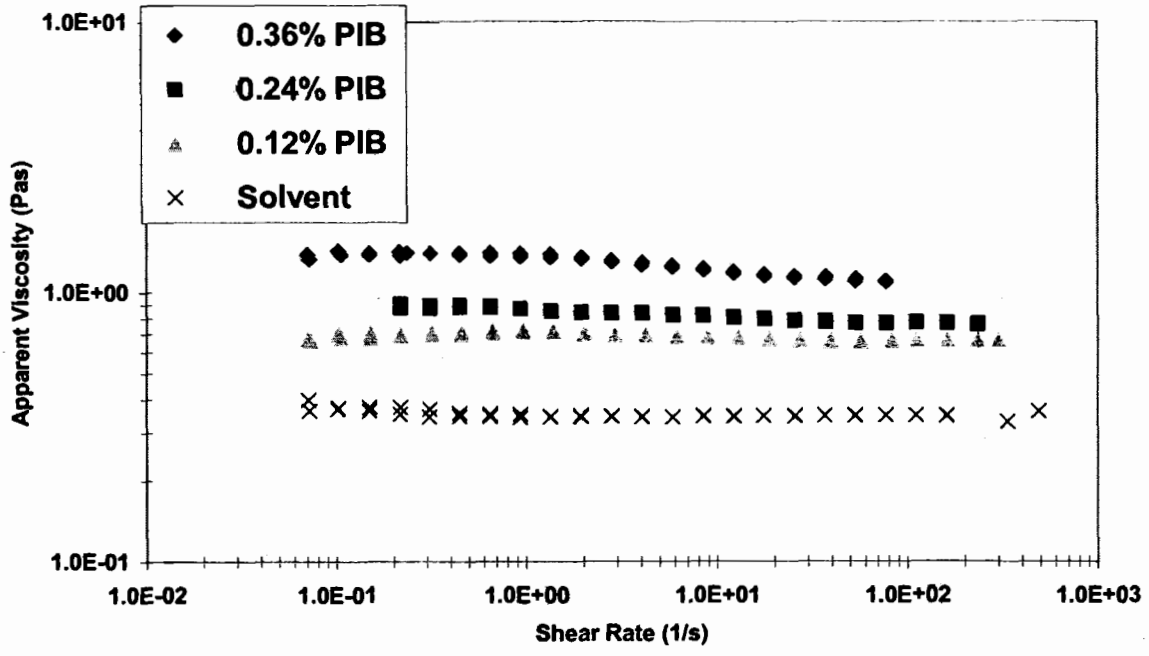

Figure 3.1 Apparent viscosity of the Boger test fluids

Adding more polymer molecules to the Newtonian solvent was intended to create different levels of elasticity and shear thinning. The elastic modulus of the test liquids is presented in Figure 3.3. Adding polymer caused the zero-shear viscosity to increase as well. During the steady shear measurements, instability in the flow in the cone and plate rheometer limited the maximum shear rate at which data could be obtained. The instability manifested itself as a tendency of the test fluid to climb out of the gap from between the cone and plate, then onto the cone. Steiert and Wolff (1990) observed similar behavior. The cause was attributed to the buildup and breakdown of fluid structure through transient

network formation Sridhar (1990). Measurements of apparent viscosity at higher shear rates were not available.

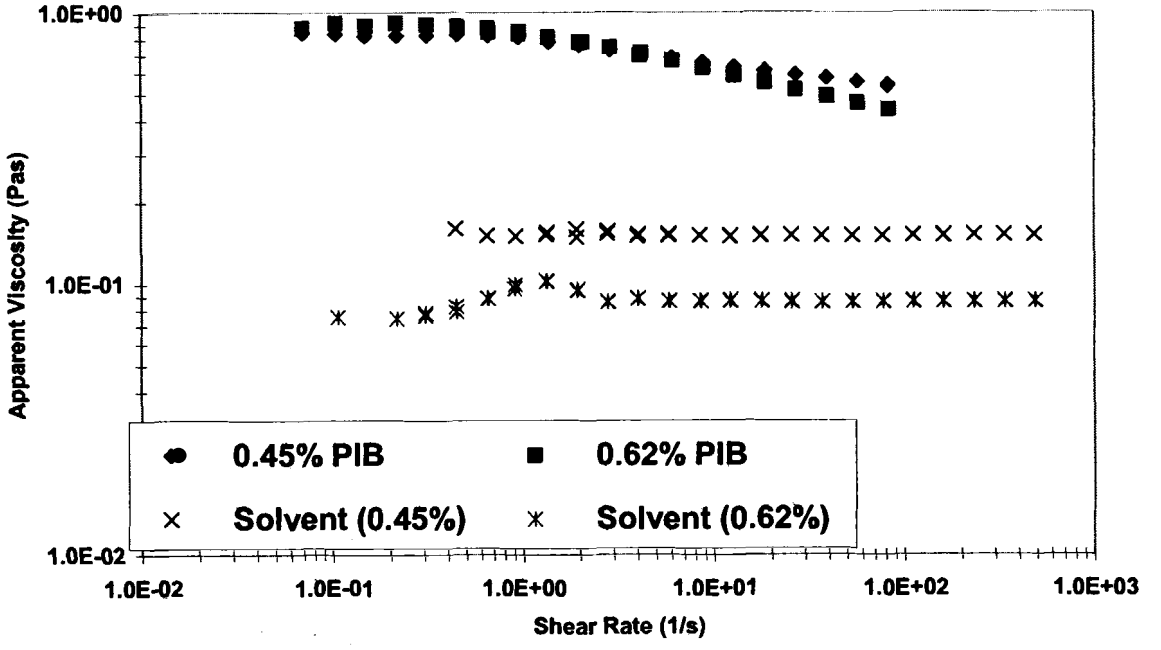

Figure 3.2 Steady shear viscosity for the shear-thinning liquids

Increasing the polymer content above 0.36% PIB required the solutions to be altered. For the 0.45% PIB solution, the amount of PB 750 was decreased and PB 320 was increased, to create a solution with an apparent viscosity in a useable range. It was not possible to mix the solution when the polymer content was increased to 0.62% without increasing the amount of K in the solution. This solution showed the intended increased shear-thinning behavior but at the cost of altered elastic properties; changing the ratio of K to PB caused the elasticity of the solution to be less than intended, as shown in Figure 3.3.

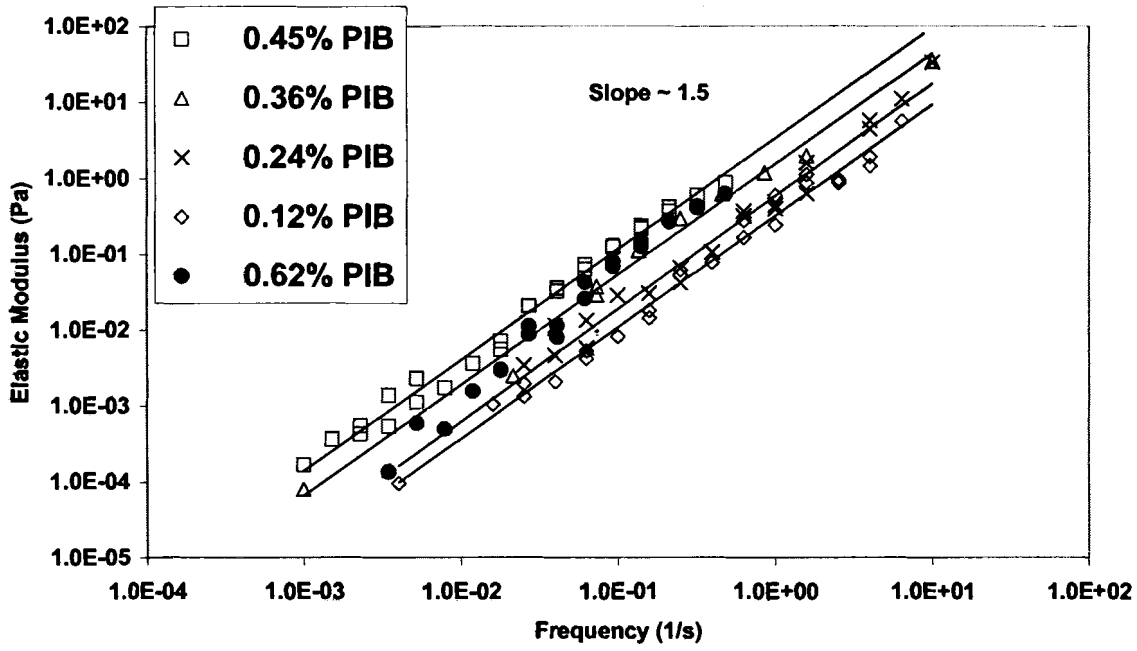

Figure 3.3 Elastic modulus G' vs. frequency of PIB solutions

Measurements of the normal stress and extensional viscosity of the test liquids were not available. However, each of the liquids exhibited the Weissenberg effect, or rod climbing, during mixing; the tendency to climb the stirring rod increased with polymer content indicating increased elasticity. The CVO-50 was not able to reach a frequency small enough to achieve a terminal slope of 2 for the elastic modulus. A wide spectrum of relaxation times may be caused by the polydispersity of the PIB.

The commercial software package POLYMAT, (Fluent Inc. Lebanon, NH), was used to determine the Carreau model parameters in steady shear. The Carreau model is defined as:

$$\eta(\dot{\gamma}) = \eta_\infty + (\eta_o - \eta_\infty)\left(1 + \tau^2 \dot{\gamma}^2\right)^{\frac{n-1}{2}} \qquad (3.1).$$

In the model, n is the power-law index, $\eta(\dot{\gamma})$ is the apparent viscosity, η_o is the zero-shear viscosity, η_∞ is the infinite shear rate viscosity, $\dot{\gamma}$ is the shear rate, and τ is the inverse of

the shear rate at which the power-law behavior begins. The Carreau model parameters and components by weight percent of the test liquids at 23° C are presented in Table 3.2.

Table 3.2 Carreau model parameters

Test Fluids				η_o (Pas)	η_s (Pas)	n	τ (s)
Silicone Oil							
1000 cst		10,000 cst					
0.86		0.14		1.35			
Boger Fluids							
PIB	PB 320	PB 750	K				
0.0012	0.3720	0.558	0.0697	0.69	0.35	0.96	0.23
0.0024	0.3710	0.557	0.0696	0.86	0.35	0.96	0.84
0.0036	0.3709	0.556	0.0695	1.38	0.35	0.92	0.88
Elastic, Shear-thinning Fluids							
PIB	PB 320	PB 750	K				
0.0045	0.556	0.370	0.0695	0.84	0.15	0.88	1.12
0.0062	0.5191	0.3461	0.1286	0.92	0.09	0.81	1.35

Because the temperature of the lab varied throughout the day the temperature of the test liquid, and its viscosity, varied too. In order to remove the temperature dependence from the analysis, the viscosity of the test liquid at the test conditions was used in the analysis. To determine the viscosity at a particular set of test conditions, the simple shear flow properties of the fluids were measured at 20°, 23°, and 25° C. The steady shear viscosity of the fluids was found to obey an Arenhius relationship with temperature. The viscosity of the test liquid at a particular condition could be calculated by multiplying a reference viscosity with the magnitude of a shifting function $H(T)$ defined as:

$$\eta(T) = H(T)\eta(\dot{\gamma}) \tag{3.2}$$

where $H(T)$ followed an Arhenius expression:

$$H(T) = \exp\left[a\left(\frac{1}{T - T_o} - \frac{1}{T_a - T_o}\right)\right] \tag{3.3}.$$

In Equation 3.3, T_o is a reference temperature, -273.15° C, a is the ratio of the activation energy to the perfect gas constant, and T_a is the temperature for which $H(T)=1$. The values of the Arhenius parameter a are given in Table 3.3.

Table 3.3 Arhenius temperature function parameters

Test Fluids				a
Silicone Oil				
1000 cst		10,000 cst		
0.86		0.14		1410
Boger Fluids				
PIB	PB 320	PB 750	K	
0.0012	0.3720	0.558	0.0697	5880
0.0024	0.3710	0.557	0.0696	5379
0.0036	0.3709	0.556	0.0695	5339
Elastic, Shear-thinning Fluids				
PIB	PB 320	PB 750	K	
0.0045	0.556	0.370	0.0695	4280
0.0062	0.5191	0.3461	0.1286	4733

3.2.2 Apparatus

The bench top roll coating apparatus is pictured in the schematic in Figure 2.2. It consists of two rolls: one a rigid steel tube and the other a solid roll but with a deformable cover. Each roll is independently driven by a servomotor and drive. The covered roll is mounted on low friction slide tables and can be loaded against the rigid roll by pneumatic actuators. Precision regulators control the applied load. A PC based data acquisition system is used to change the roll speeds and collect information from the various sensors.

A capacitance gauging technique is used to monitor the wet film thickness as well as the actual gap between the roll surfaces. The fluid pressure profile in the nip is monitored with a piezoelectric pressure transducer. The applied load is measured on either end of the shaft of the deformable roll by force transducers.

3.2.3 Procedure

The run-out of the roll surfaces caused each experiment to consist of a preliminary run and a test run. Air was the test medium in the preliminary run which was used to establish the distance between the probe face and the target at various points around the circumferences of the rolls. The test liquid was then added to the system in the test run and the output voltage from the probes was obtained at the same points around the circumference of the roll or shaft. The minimum gap, and the wet film thickness of the test liquid, is proportional to the voltage difference between the baseline run and the run with the test liquid. The procedure is presented schematically in Figure 2.5. After the measurements were obtained, the roll speed was increased and more fluid was added to the system.

3.3 Theoretical Investigation

A commercially available finite element software package, POLYFLOW (Fluent Inc., Lebanon, NH) was used to study the flow of viscoelastic fluids in a rigid roll coating geometry. An initial attempt at incorporating an Oldroyd-B fluid model in the Newtonian lubrication model was made, but with limited success. Due to the limitations of the boundary conditions available in the commercial software, the flow domain had to be modeled as a fixed position, rigid roll system. Two non-Newtonian fluid models were used in the study. The Oldroyd-B model was used to study purely elastic behavior and a Giesekus model was used to study the combined effects of viscoelasticity and shear thinning. The governing momentum equation, excluding gravitational effect but including inertial terms is:

$$\rho \frac{D\mathbf{v}}{Dt} = \nabla \cdot \tau \tag{3.4}$$

where $\frac{D\mathbf{v}}{Dt} = \frac{\partial \mathbf{v}}{\partial t} + \mathbf{v} \cdot \nabla \mathbf{v}$ is material derivative of the velocity, $\mathbf{v}$ following the motion. τ is the total stress tensor for the fluid, which is composed of pressure and viscous stress as:

$$\tau = -p\mathbf{I} + \mathbf{T} \tag{3.5}$$

where p is the pressure, $\mathbf{I}$ is the unit tensor, and $\mathbf{T}$ is the extra, viscous stress tensor. Mass conservation is represented by the incompressible, continuity equation is:

$$\nabla \cdot \mathbf{v} = 0 \tag{3.6}.$$

The two fluid models are constitutive relations for the extra stress tensor $\mathbf{T}$. The extra viscous stress can be thought of as the sum of both the polymer and solvent contributions to the stress of the solution. $\mathbf{T}_1$ is the polymer contribution and $\mathbf{T}_2$ is the purely viscous solvent contribution. The total extra stress is given by:

$$\mathbf{T} = \mathbf{T}_1 + \mathbf{T}_2 \tag{3.7}$$

where $\mathbf{T}_1$ depends on the fluid model and $\mathbf{T}_2$ is computed from:

$$\mathbf{T}_2 = 2\eta_2 \mathbf{D} \tag{3.8}.$$

In Equation 3.8, η_2 is the viscosity of the solvent and $\mathbf{D}$ is the rate of deformation tensor. The viscosity ratio η_r indicates the influence of the polymer on the total solution viscosity and is defined as:

$$\eta_r = \frac{\eta_2}{\eta_1 + \eta_2} \tag{3.9}.$$

The polymer contribution to the total extra stress constitutive relation for the Oldroyd-B model is defined as:

$$\mathbf{T}_1 + \lambda \overset{\nabla}{\mathbf{T}}_1 = 2\eta_1 \mathbf{D} \tag{3.10}$$

where λ is a relaxation time constant of the material and the upper convected time derivative of the viscoelastic extra stress and it is defined as:

$$\overset{\nabla}{\mathbf{T}}_1 = \frac{D\mathbf{T}_1}{Dt} - \mathbf{T}_1 \cdot \nabla\mathbf{v} - \nabla\mathbf{v}^T \cdot \mathbf{T}_1 \tag{3.11}$$

The constitutive relation for the viscoelastic extra stress in the Giesekus model is given by:

$$\left(\mathbf{I} + \frac{\alpha\lambda}{\eta_1}\mathbf{T}_1\right) \cdot \mathbf{T}_1 + \lambda \overset{\nabla}{\mathbf{T}}_1 = 2\eta_1\mathbf{D} \tag{3.12}$$

where α is a material constant related to the interaction between polymer molecules.

The values for the material parameters and the components of the test fluids by weight percent, at T = 23° C, are presented in Table 3.4. The total solution viscosity and the solvent viscosity were measured on the Bohlin CVO-50 constant stress rheometer. The values for α and λ were determined by fitting the fluid models to the steady shear and dynamic oscillatory measurements. The fitting algorithm, which minimizes the difference between the measured value and fitted value, is described in the POLYMAT user guide. The information for the zero-shear viscosity and the solvent viscosity were fixed as parameters. An initial guess for the relaxation time, equal to the inverse of the frequency where the elastic and viscous moduli were equal, was used to begin the iterations. It should be noted that the relaxation times listed in Table 3.4 are fitted values and not measured directly.

Table 3.4 Fitted model parameters for the viscoelastic test fluids

Test Fluids				η_r	η (Pas)	η_2 (Pas)	λ (s)	α
Boger Fluids								
PIB	PB 320	PB 750	K					
0.0012	0.3720	0.558	0.0697	0.5	0.69	0.35	0.01	
0.0024	0.3710	0.557	0.0696	0.4	0.86	0.35	0.04	
0.0036	0.3709	0.556	0.0695	0.26	1.38	0.35	0.96	
Elastic, Shear-thinning Fluids								
PIB	PB 320	PB 750	K					
0.0045	0.556	0.370	0.0695	0.18	0.84	0.15	0.94	0.0003
0.0062	0.5191	0.3461	0.1286	0.095	0.92	0.09	1.63	0.0003

The Galerkin finite element method was used to solve the governing system of equations for the two-dimensional, free surface flow problem. The flow domain is shown in Figure 3.4 along with the boundary conditions. Because the roll speeds were equal, a symmetry boundary condition could be imposed on the mid-plane between the two rolls and saving computation time. The POLYFLOW code had difficulty obtaining a stable solution when an incoming film to the nip was used. Therefore, the inlet was assumed to be flooded and a zero pressure condition was imposed far upstream. Zero pressure was also imposed at the outlet of the flow domain, which was far down-stream of the nip and film-split. A free surface condition was also used. The domain appears distorted in Figure 3.4 because the length scale in the Y direction is exaggerated by 5 times the length scale in the X direction.

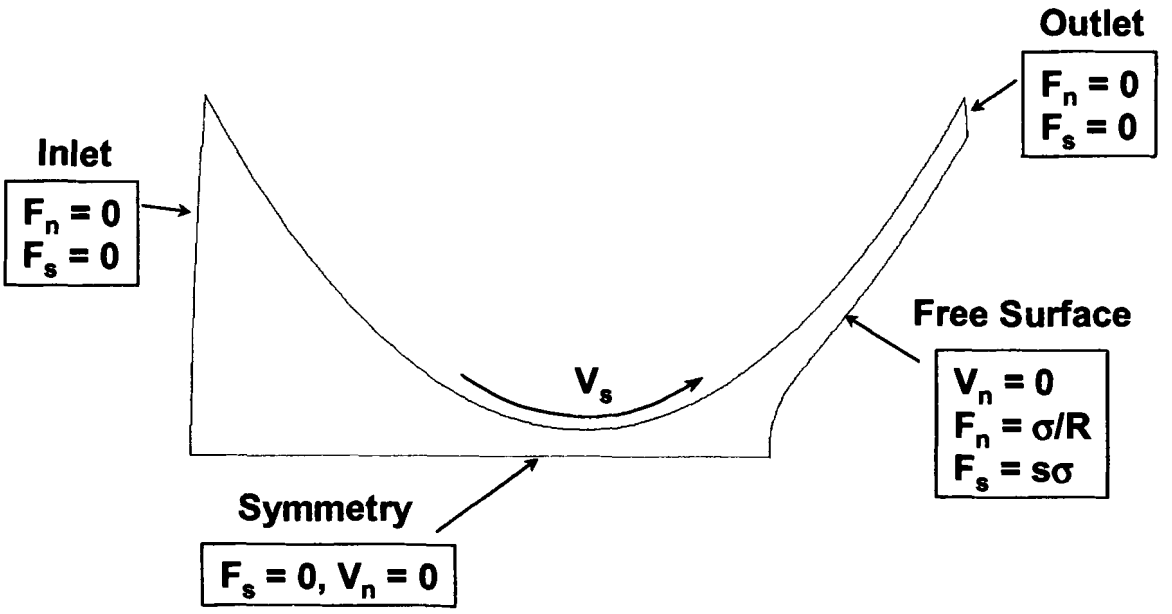

Figure 3.4 Flow domain

The domain was broken down into a mesh of quadrilateral elements, Figure 3.5. The mesh was generated with the commercial package, Gambit (Fluent Inc., Lebanon, NH). The mesh required 1200 elements before significant changes in the calculated fields were eliminated.

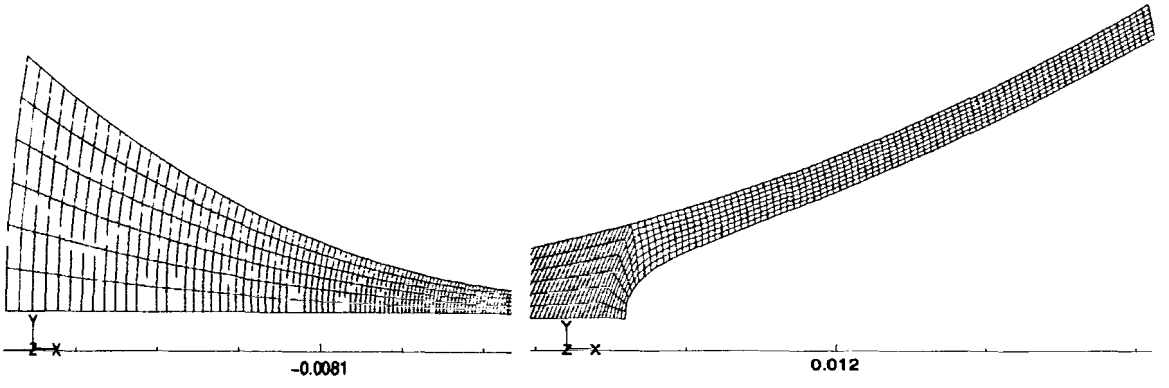

Figure 3.5 Typical finite element mesh

The coupled system of extra stress, velocity, pressure, and the free surface was solved simultaneously. Both the velocity and free surface coordinates used quadratic interpolation functions and linear, continuous functions were used for the pressure. The

extra stress tensor used a 4x4 bilinear interpolation with streamline up-winding to improve the stability (Debbaut *et al.* (1988), Marchal *et al.* (1987)). Please refer to the POLYFLOW User Guide for more information regarding the interpolation functions. The Thompson transformation remeshing method was used in the calculations; further information regarding POLYFLOW's implementation of this technique can be found in the POLYFLOW User Guide. The solution to a series of elliptic partial differential equations is required to translate the mesh nodes. This remeshing scheme is robust for large mesh deformations. Convergence was determined by the relative error between the modifications at each node between two successive iterations to the maximum value of the field at the current iteration. When this value reached 0.0001, the solution was considered converged.

Because free surface and viscoelastic flows are highly nonlinear problems, it is very difficult to obtain converged solutions. In order to facilitate this, the problem was solved for the Newtonian base case first and this solution was used as the initial guess for the viscoelastic problem. Viscoelastic effects were then gradually introduced through an evolution scheme via the relaxation time.

3.4 Results and Discussion

The next set of six figures present the measured gap width, scaled with the effective roll radius, as a function of the elasticity number Ne and the load parameter Nw for the three constant viscosity elastic test fluids. Each point on the graph is the average of ten measurements with deviations from the mean of less than 1 μm. Even though the Boger fluids showed a small dependence on the shear rate, $n < 1$, the viscosity used in the analysis was considered as a constant under the operating conditions. The experimental operating

conditions are presented in Table 3.5. Measurements for the 0.12% PIB test fluid are presented in Figures 3.6 and 3.7.

Table 3.5 Experimental operating conditions

Parameter	Dimensional	Dimensionless
σ (N/m)	0.021 - 0.029	
μ (Pas)	0.2 - 1.38	
ρ (kg/m)	845 - 977	
$\overline{V}$ (m/s)	0.1-1.4	
W (N/m)	900-8700	
b (m)	0.006	
E_e (Pa)	39478879	
R_e (m)	0.03175	
H (μm)	6 - 160	
ν		0.49
Ne		$0.02 - 0.1 \times 10^{-6}$
Nw		$0.8 - 6.9 \times 10^{-3}$
g_3		2.5 - 22
Ca		>> 1
Re		<< 1

Figure 3.6 shows behavior similar to the Newtonian base case in that as the roll speed increased, so did the measured gap width. However, a slight difference in the sensitivity to the elasticity parameter was observed; the slope increased from 0.55 to 0.59. Figure 3.7 plots the dimensionless gap as a function of the load parameter. The most notable feature is that the measured gap is much more sensitive to the applied load compared to the Newtonian base case; the slope changed from -0.39 to -48. The measured gap width data for the 0.12% solution can be fit to the empirical relation:

$$\frac{H}{R} = 0.60 N_e^{0.59} N_w^{-0.48} \qquad (3.13).$$

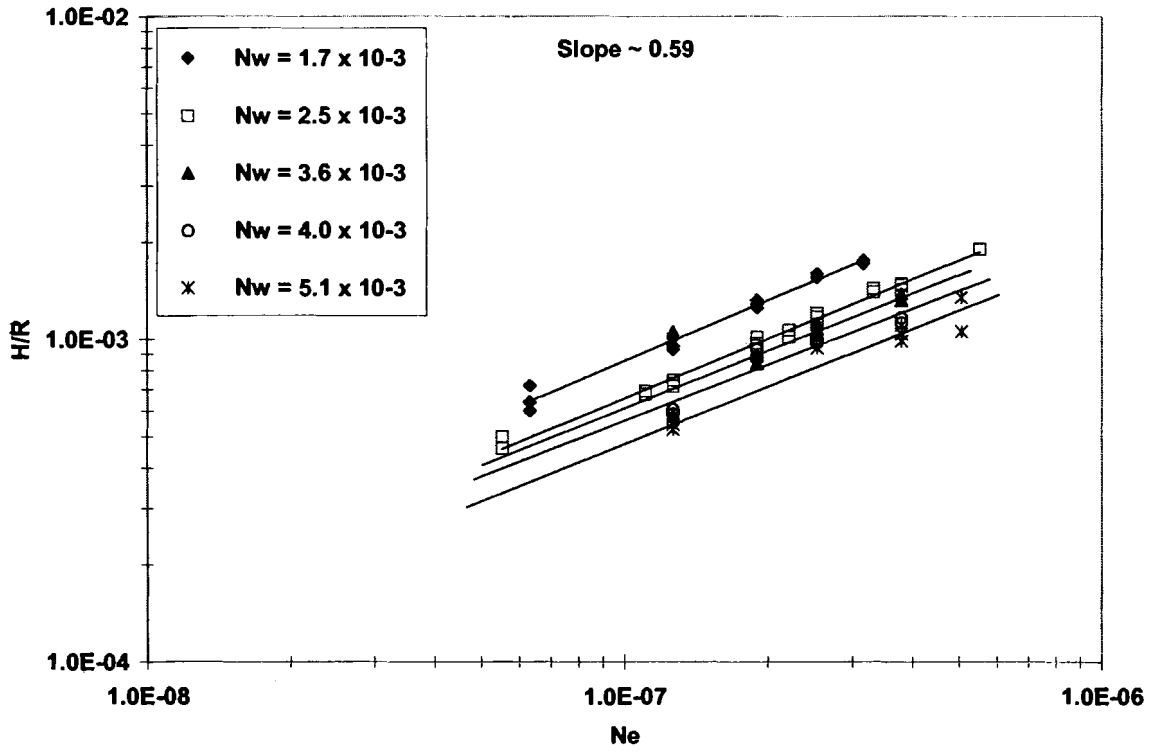

Figure 3.6 Dimensionless gap vs. elasticity parameter for 0.12% PIB

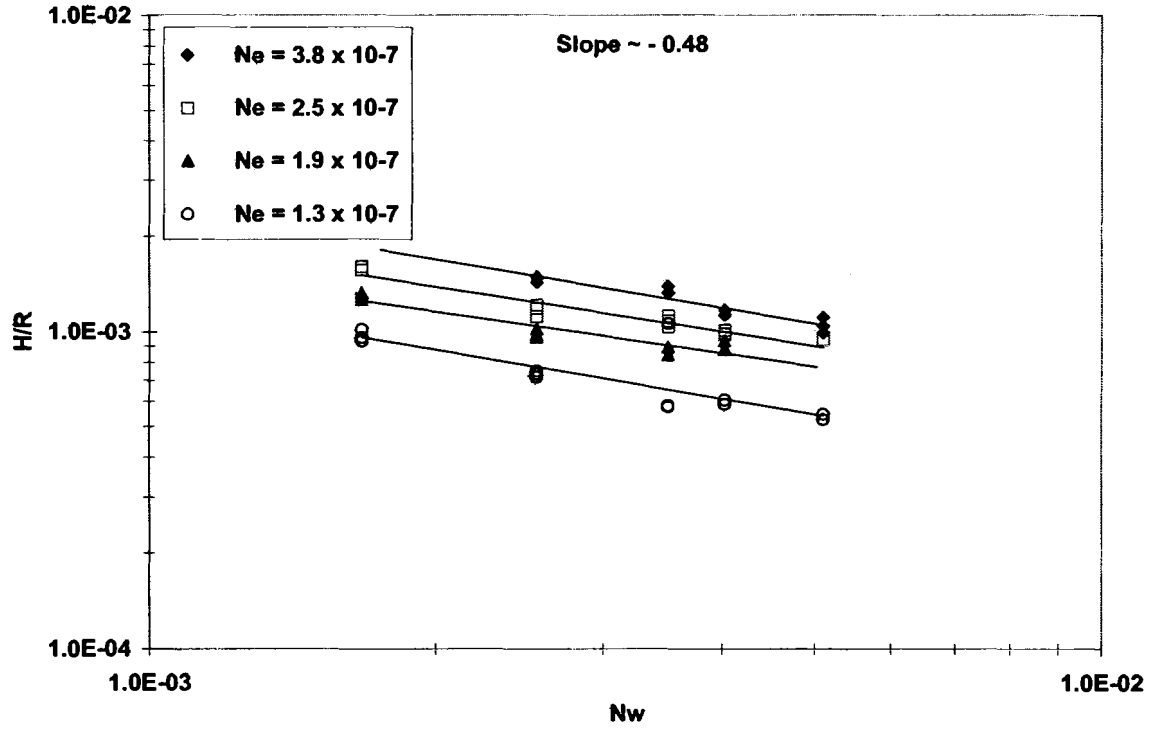

Figure 3.7 Dimensionless gap vs. the load parameter for 0.12% PIB

The measured gap as a function of the elasticity and load numbers for the 0.24% PIB solution are presented next. In Figure 3.8, doubling the concentration of polymer caused the sensitivity to roll speed to increase further; the slope increased from 0.59 to 0.63. Sensitivity to the applied load also increased as shown in Figure 3.9; the slope decreased from a value of -0.48 to a slope of -0.58. The measured gap width data for the 0.24% solution can be fit to the empirical relation:

$$\frac{H}{R} = 0.42 N_e^{0.63} N_w^{-0.58} \qquad (3.14).$$

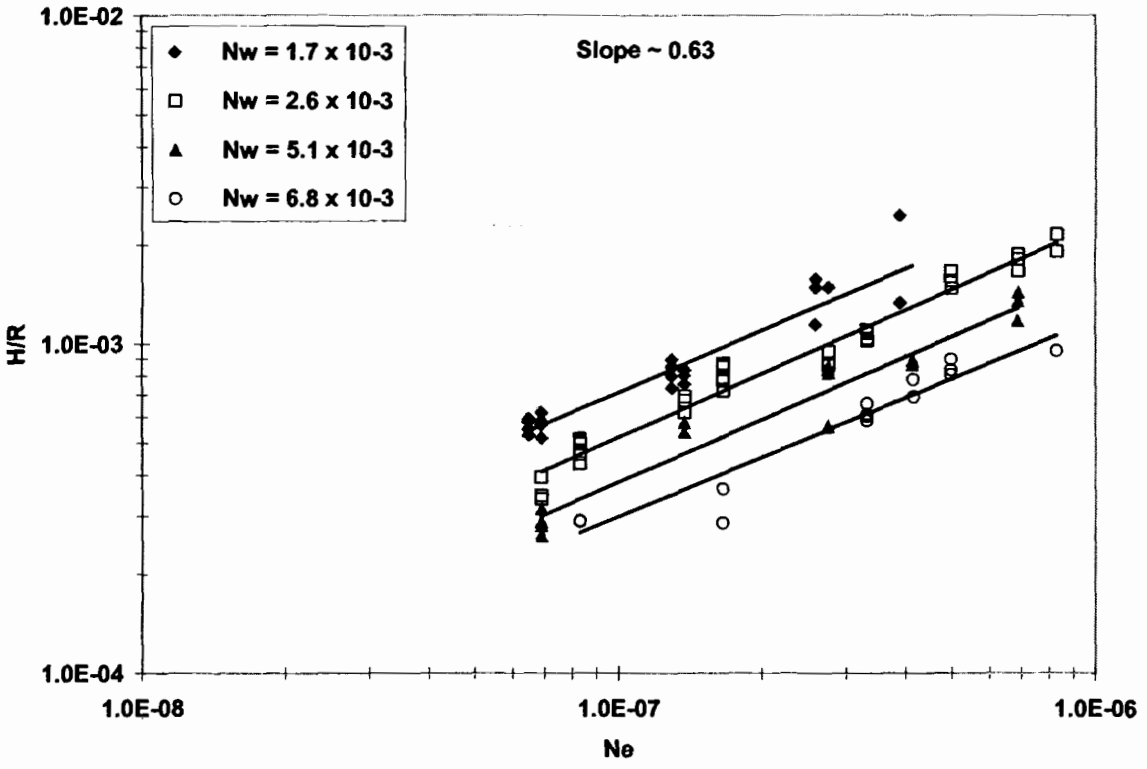

Figure 3.8 Dimensionless gap vs. elasticity parameter for 0.24% PIB

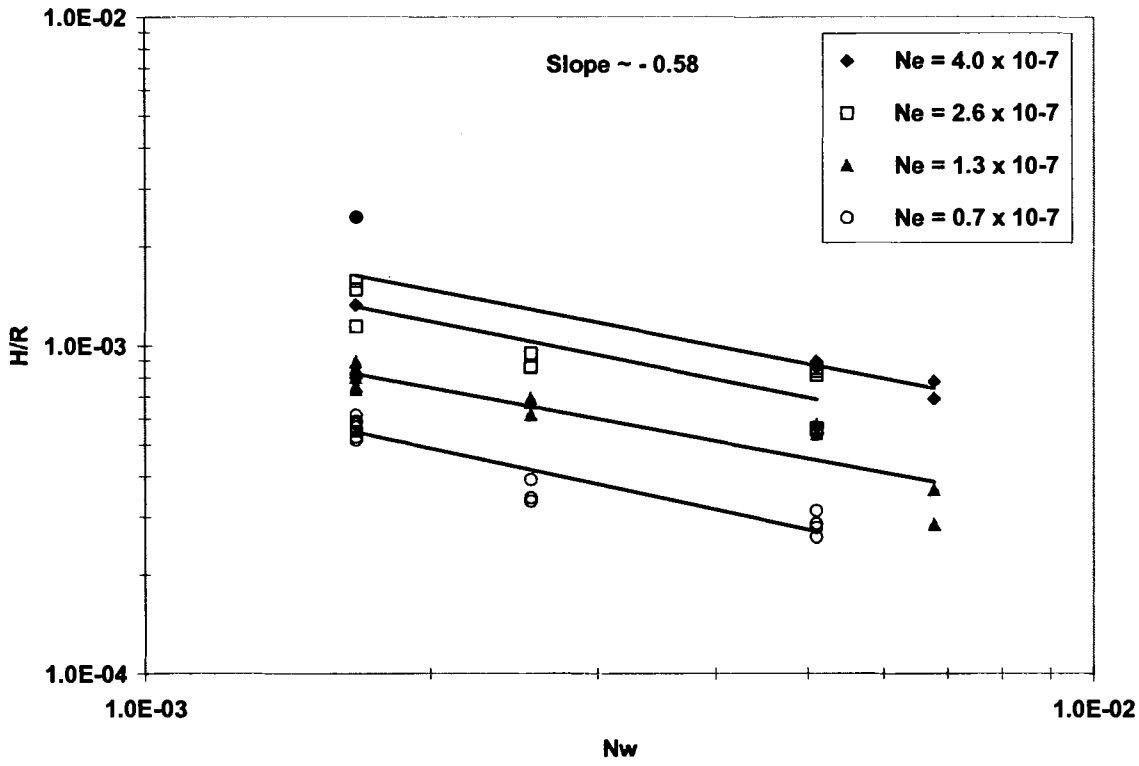

Figure 3.9 Dimensionless gap vs. the load parameter for 0.24% PIB

Figures 3.10 and 3.11 show the results for the 0.36% PIB solution. Adding more polymer to the solution did not produce a detectible change in the sensitivity to the roll speed, compared to the 0.24% PIB solution. However, the sensitivity to the applied load continued to increase from –0.58 to –1.05. This result indicated that higher levels of fluid elasticity are changing the relationship between the load and gap. The measured gap width for the 0.36% solution can be fit to the empirical relation:

$$\frac{H}{R} = 0.036 N_e^{0.62} N_w^{-1.05} \qquad (3.15).$$

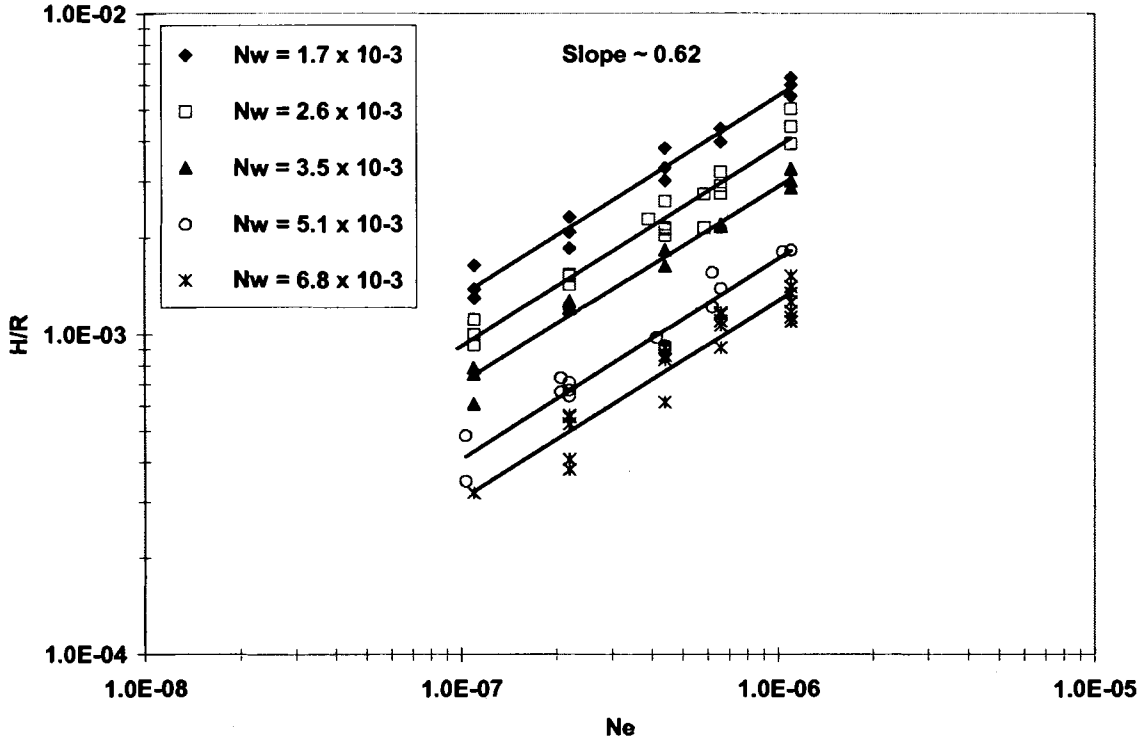

Figure 3.10 Dimensionless gap vs. the elasticity parameter for 0.36% PIB

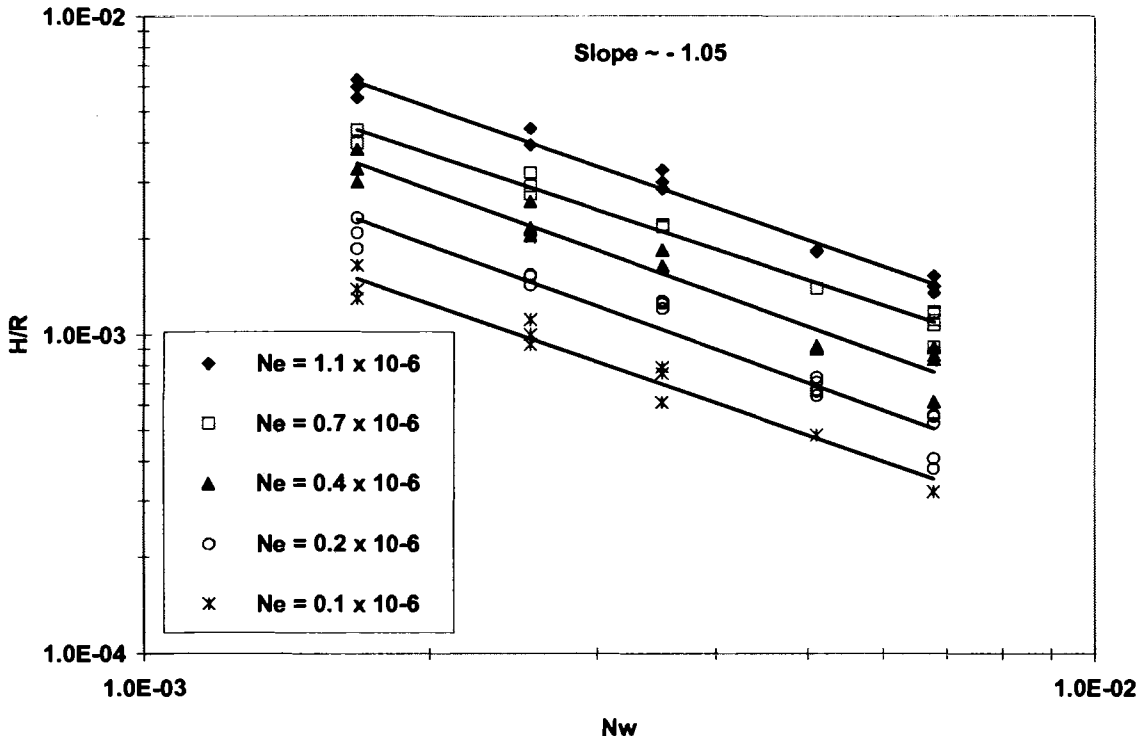

Figure 3.11 Dimensionless gap vs. the load parameter for 0.36% PIB

It should be noted that only one value of roll radius and elastic modulus were used throughout the experiments and in the fitting procedure. Therefore, it cannot be confirmed that the indicated dependencies on these two quantities are absolute. However, dimensional analysis indicates that these three dimensionless groups, H/R, Ne, and Nw should fully describe the system unless some other important parameter, that is not included, is influencing the system. The empirical correlation is compared with the experimental data in Figure 3.12.

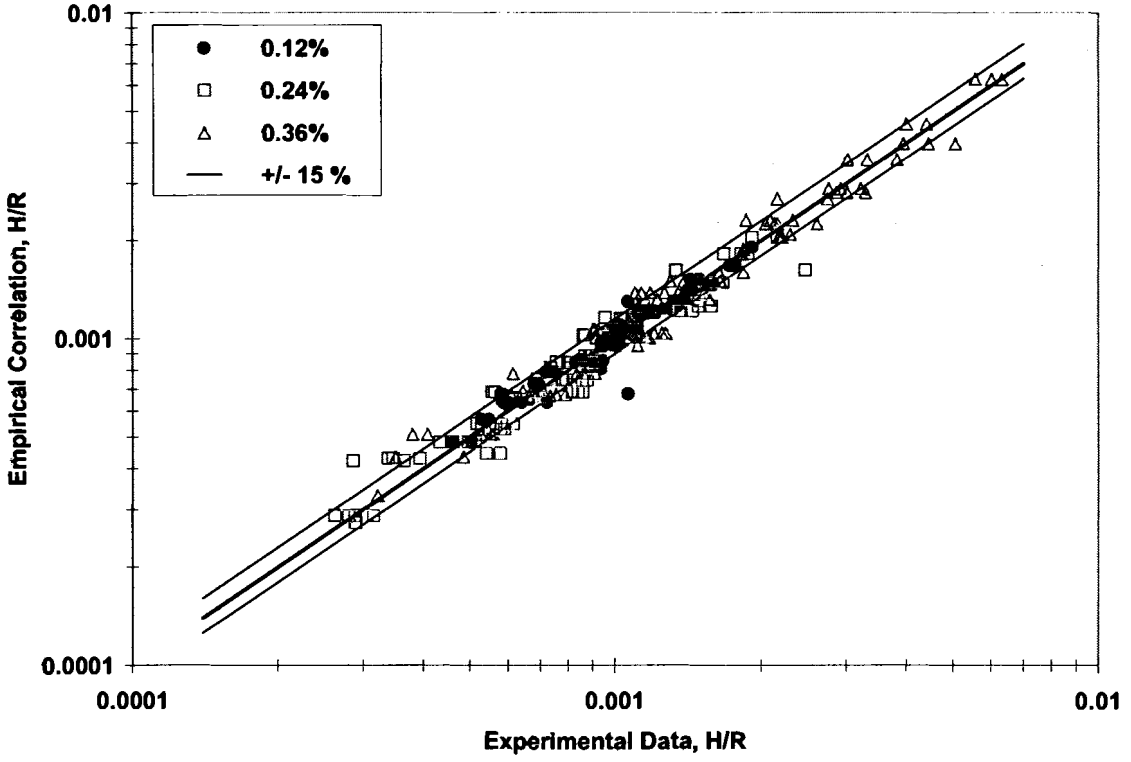

Figure 3.12 Comparison of empirical relations with measured gap

The effects of elasticity on the flow can be resolved by comparing the empirical relations to the Newtonian base case. In the next set of figures, a modified load number,

$\frac{H}{R} N_w^{0.39}$, is plotted as a function of the elasticity number. Figure 3.13 shows the behavior at relatively low loads, Nw = 0.001.

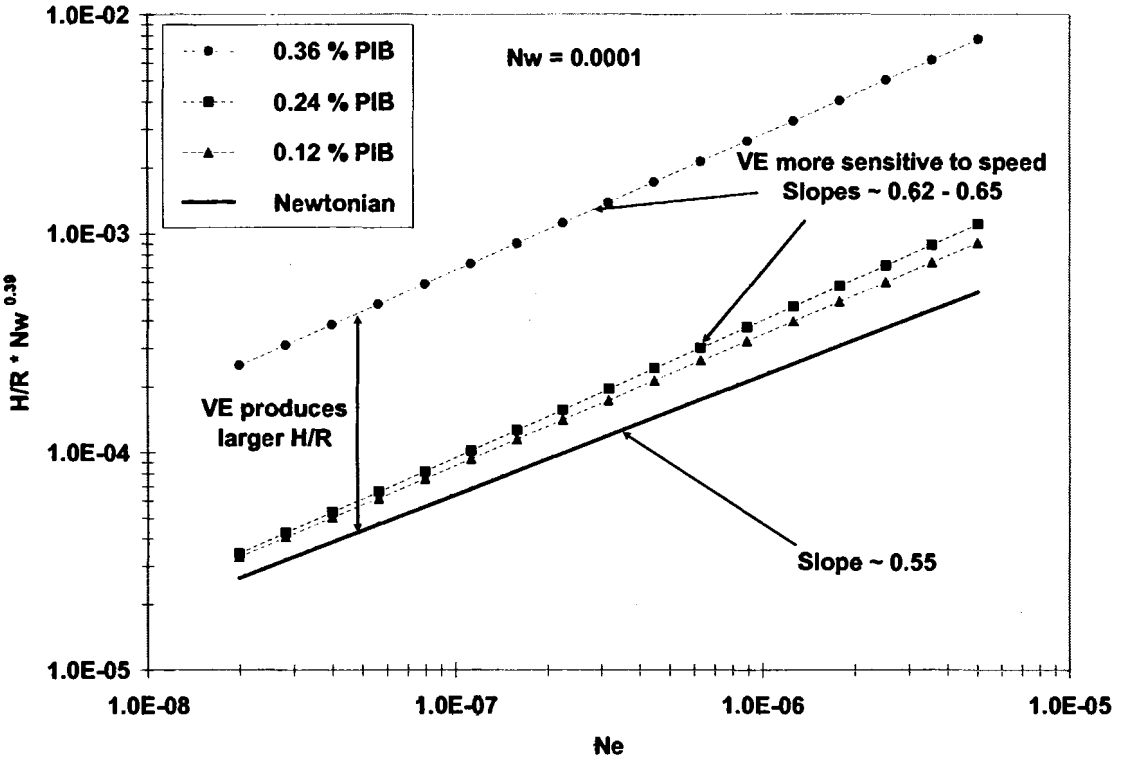

Figure 3.13 Comparison between elastic fluids at low load

The viscoelastic fluids are more sensitive to roll speed. At low applied load, the shear stresses are small but the normal stress generated is large enough to separate the roll surfaces beyond what is expected for an equivalent Newtonian fluid. This behavior is similar to the increased load bearing capacity observed by Williamson *et al.* (1997) in their journal bearing studies. Kang, Lee, and Liu (1991) observed increased flow rate in their experiments with viscoelastic liquids in a fixed engagement deformable roll coating flow study. Figure 3.14 shows the behavior at intermediate loading.

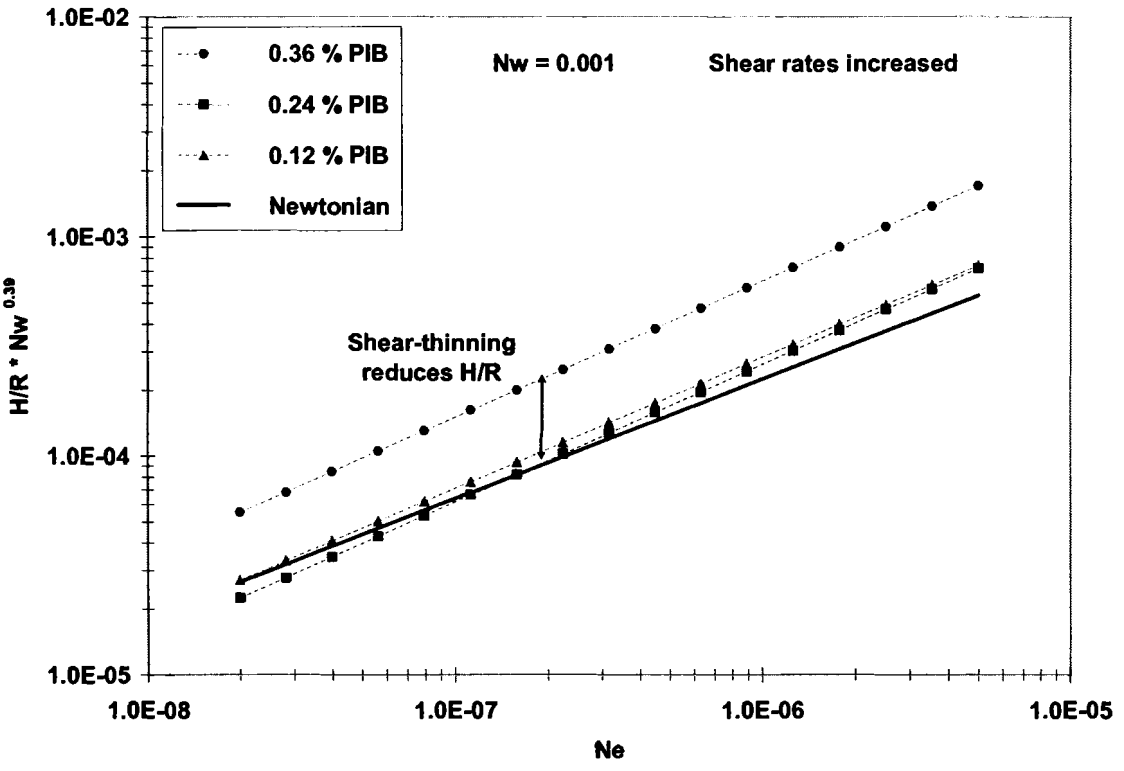

Figure 3.14 Comparison of elastic fluids at intermediate load

At intermediate loads shear stress increased. The higher concentration fluid still produced larger H/R compared to the Newtonian case but the overall magnitude decreased. For the lower concentration liquids at low speeds, the shear stress overcomes the normal stress and the measured gap is equivalent to the Newtonian case; at higher speeds wider gaps are observed. The behavior at high loads is plotted in Figure 3.15.

At high loads the shear stress is quite large. It is likely that shear-thinning effects have overcome the roll separating forces. However, the fluid with the weakest dependence on shear rate produced enough extra roll separating force at high speeds to create larger H/R than the Newtonian case.

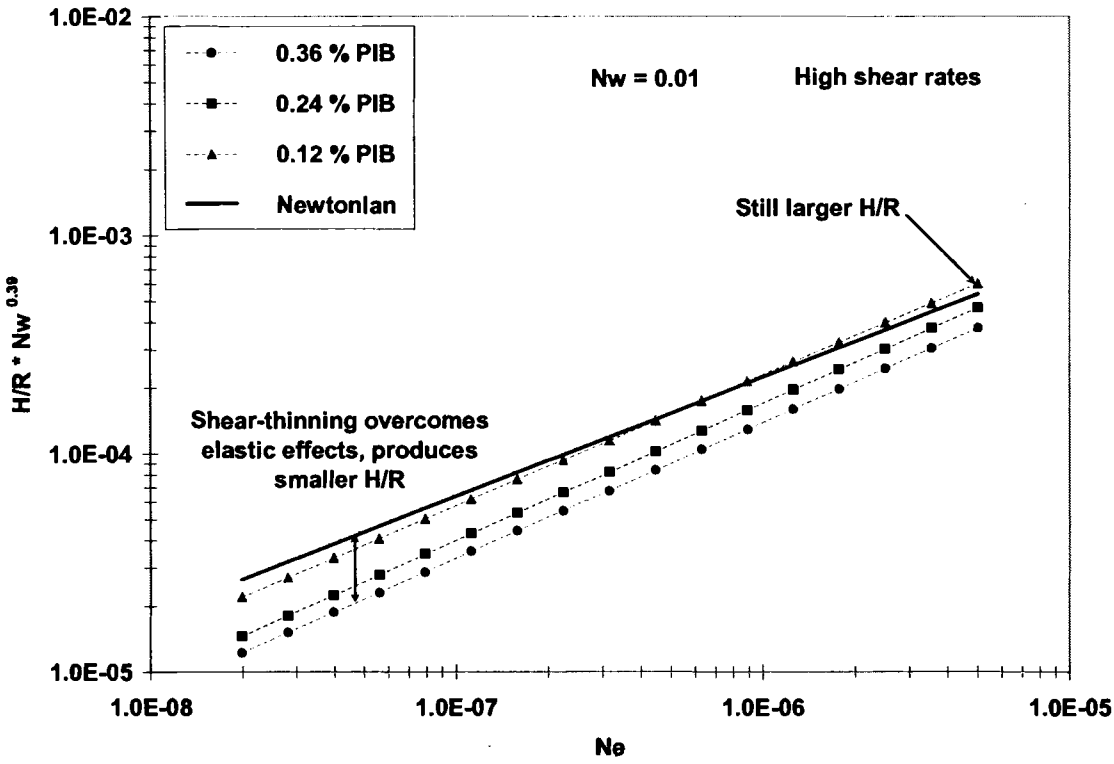

Figure 3.15 Comparison of elastic fluids at high load

Examples of the measured pressure profiles are shown in Figure 3.16. The measured pressure has been scaled with the roll cover thickness, b, effective roll radius R, and the effective elastic modulus, E, of the cover. The pressure was scaled with the thickness of the cover because of the observations of previous workers that indicate the cover thickness influences the film thickness. The measured profiles have been shifted so that the maximum pressure occurs at x/R = 0. The profiles of the 0.12% PIB solution are very similar to the Newtonian base case except for the behavior at the film-split. At the nip exit, it was observed that the minimum pressure was larger than the Newtonian base case over the range of applied loads tested. Also, the magnitude of the minimum pressure was much less sensitive to changes in the applied load compared to the Newtonian case. This behavior was exhibited by all three of the constant viscosity elastic liquids over the range of roll speeds shown in Figure 3.17.

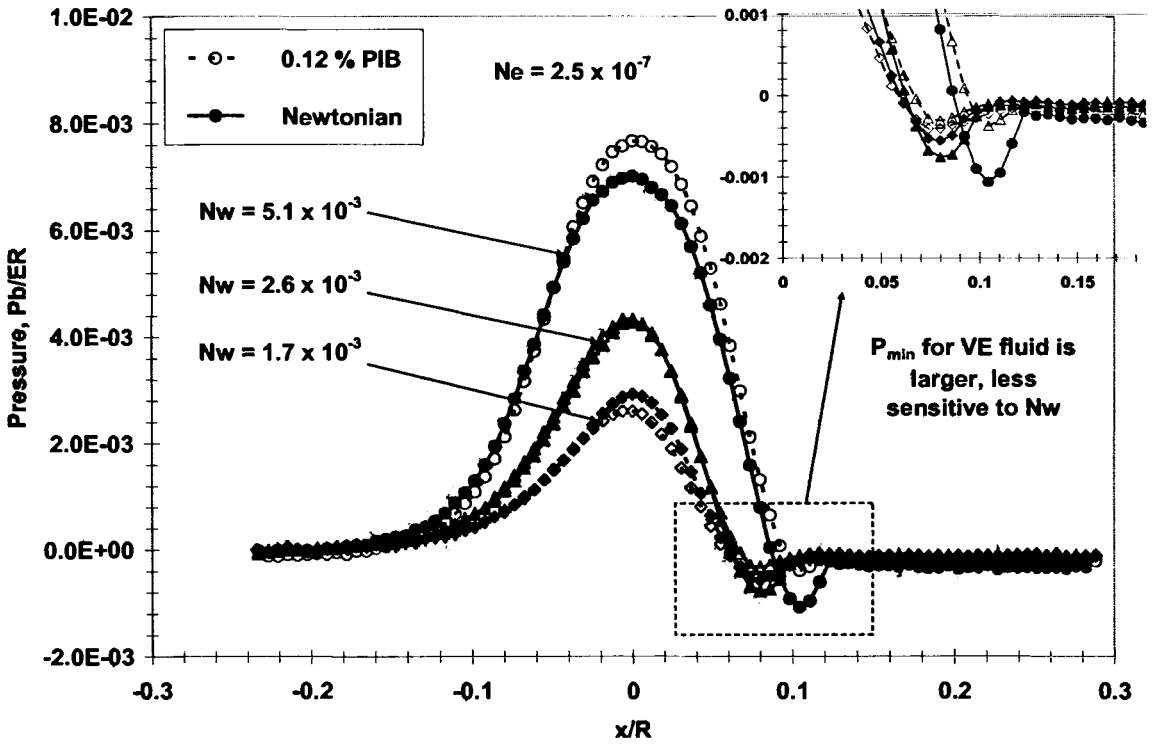

Figure 3.16 Pressure profiles for the 0.12% PIB fluid

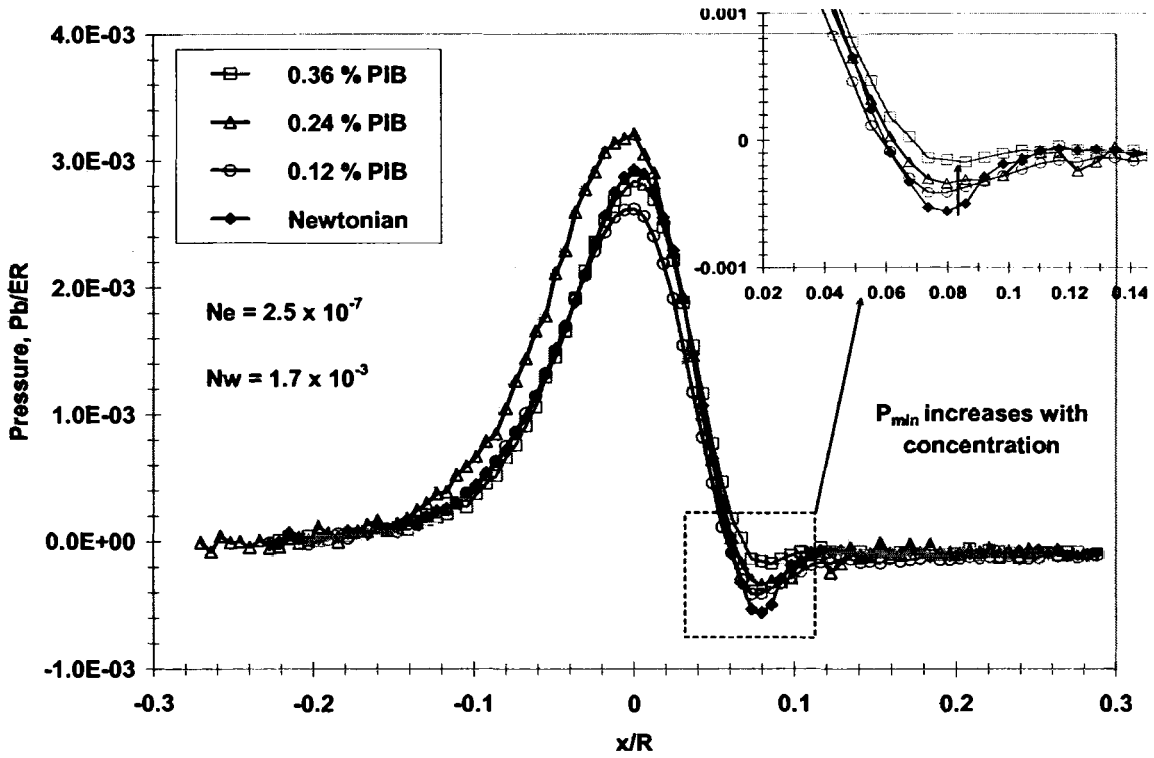

Figure 3.17 Pressure profiles of the constant viscosity elastic fluids

The measured gap width for the viscoelastic, shear-thinning liquids are plotted next. The shear-thinning fluids were analyzed with a viscosity that corresponded to an estimated shear rate in the nip and the fit to the Carreau viscosity model. The shear rate in the nip was calculated from the roll speed and measured gap width:

$$\dot{\gamma} = \frac{\overline{V}}{H} \tag{3.16}.$$

Figure 3.18 shows the measured gap as a function of the elasticity parameter at several applied loads for the 0.45% PIB solution. Even though this solution has a significantly different power-law index, n = 0.88, compared to the previous liquids, the sensitivity to the elasticity parameter is nearly equivalent. The sensitivity to the elasticity number remained relatively constant when compared to the 0.24% and 0.36% PIB solutions. The measured gap as a function of applied load is plotted in Figure 3.19. The sensitivity to the applied load did not change relative to the 0.36% PIB solution, however, the gap width is still much more sensitive to the applied load than the Newtonian base case.

The measured gap as a function of the elasticity parameter for the 0.62% PIB solution is shown in Figure 3.20. The relationship for the load number is in Figure 3.21. Further increase in polymer concentration did not produce a detectable change in the sensitivity to the roll speed or load. In some way, the shear-thinning behavior balances the increase in normal force. There must be some aspect of this polymer-solvent system when the influence of the polymer comes to some steady behavior.

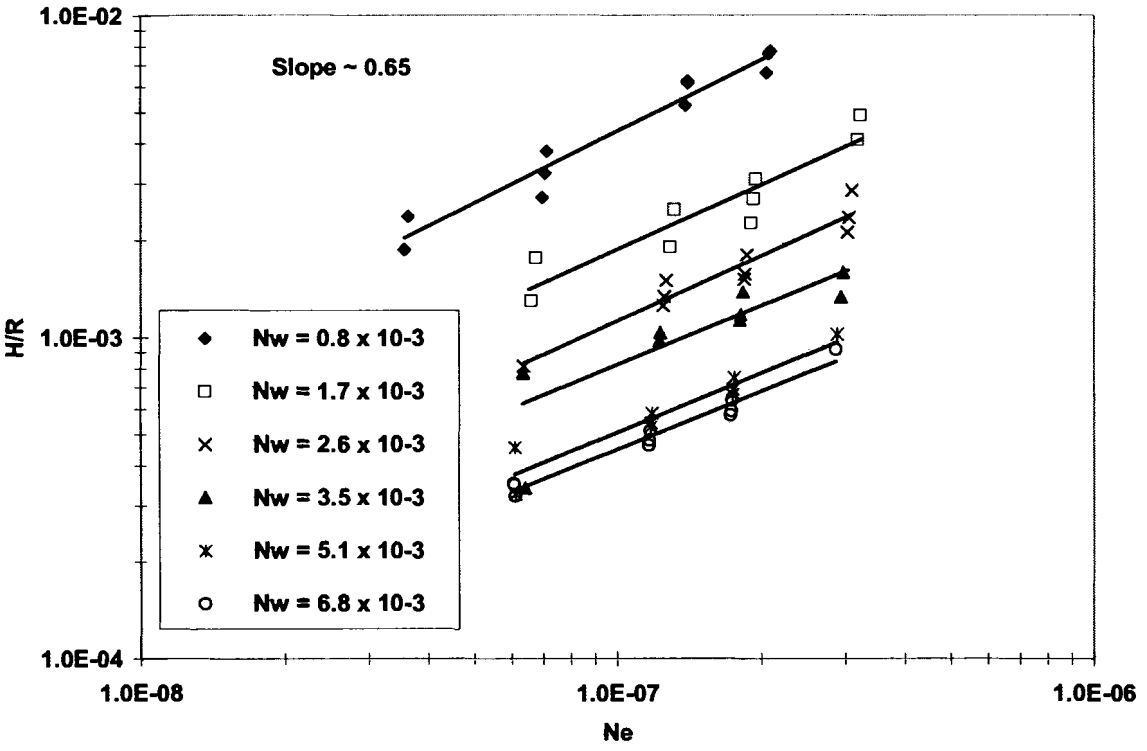

Figure 3.18 Dimensionless gap vs. the elasticity parameter for 0.45% PIB

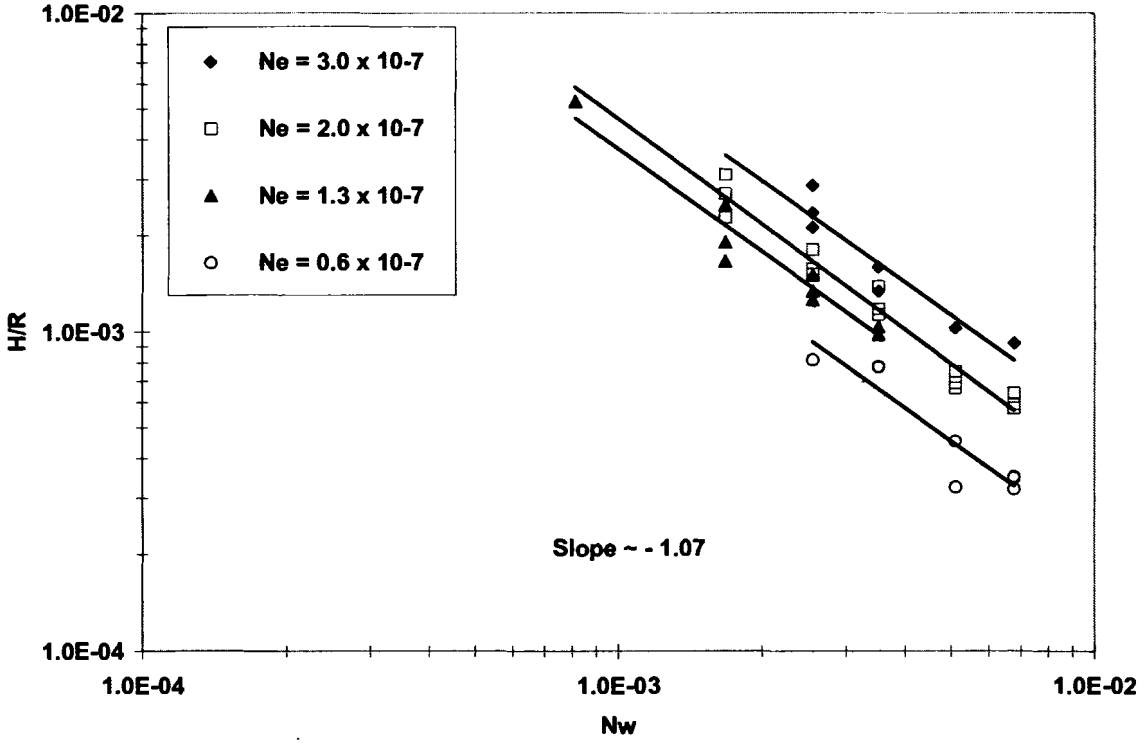

Figure 3.19 Measured gap vs. the load parameter for 0.45% PIB solution

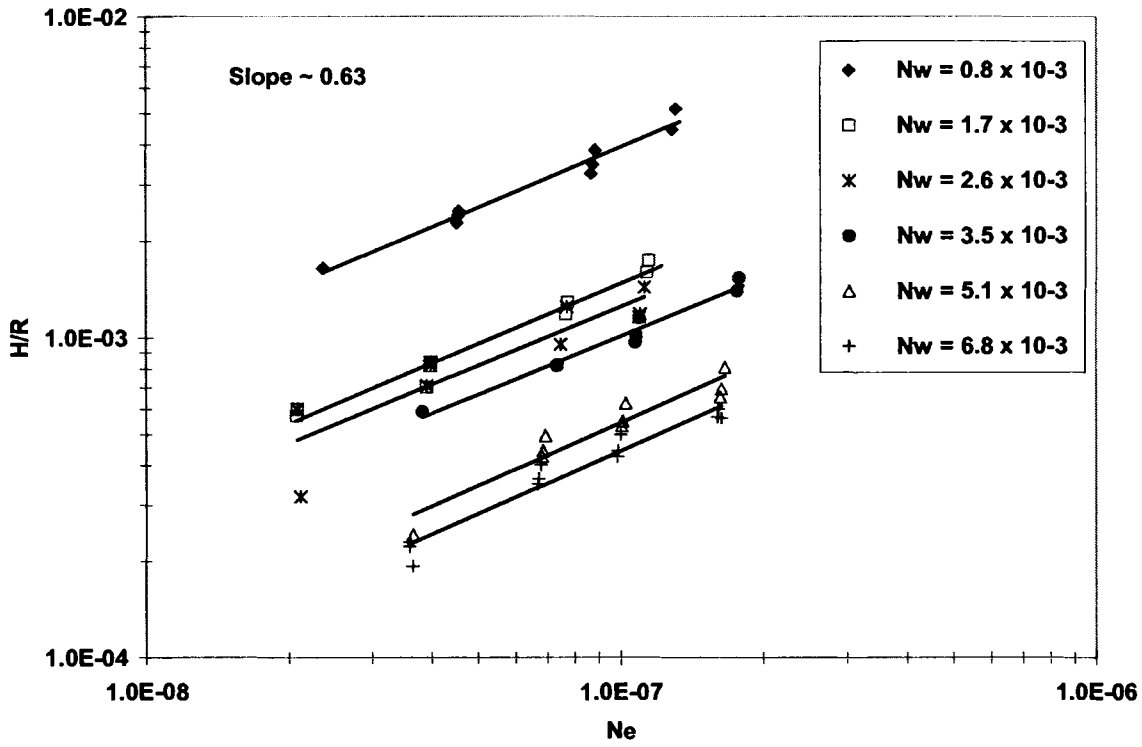

Figure 3.20 Measured gap as a function of elasticity number for 0.62% PIB

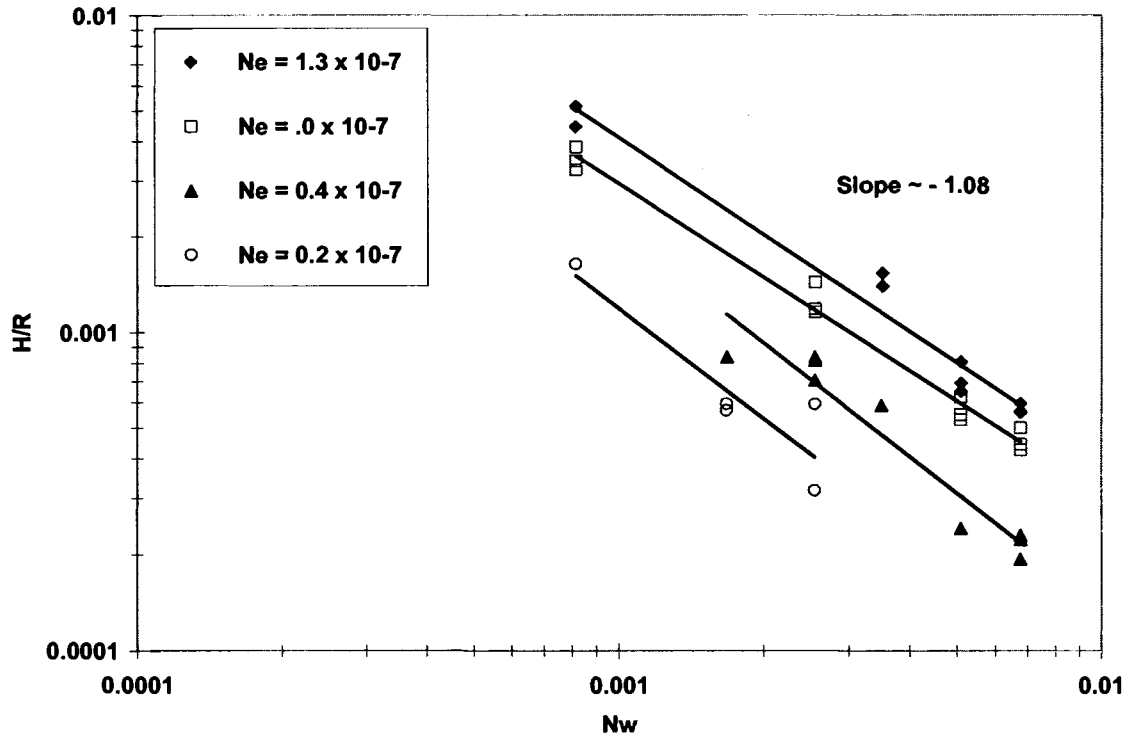

Figure 3.21 Measured gap as a function of load parameter for the 0.62% PIB solution

The measured gap width data was correlated with the elasticity and load parameters for the range of operating conditions tested. This set of data produced more scatter than the previous data sets. However, the correlation produced a fit to within +/- 5% for 95% of the measured data points, Figure 3.22. The measured gap width is correlated with the elasticity and load parameters in the following empirical relations. The 0.45% PIB solution follows:

$$\frac{H}{R} = 0.065 N_e^{0.65} N_w^{-1.07} \tag{3.17}$$

and the 0.62% PIB solution follows:

$$\frac{H}{R} = 0.048 N_e^{0.63} N_w^{-1.08} \tag{3.18}.$$

The data are more scattered compared to the previous data sets as shown in Figure 3.19. The empirical correlations are summarized in Table 3.6 in terms of the operating variables with inputs in MKS units.

The measured gap widths for the test conditions are summarized in Figures 3.23-3.25. The behavior of the shear-thinning fluids can be compared to the Newtonian base case by plotting the modified load number $\frac{H}{R} N_w^{0.39}$ versus the elasticity parameter Ne. The data for the 0.36% fluid has been included as an additional comparator. Figure 3.23 compares the behavior at low applied load. At low loads and the resulting low shear rate, the shear-thinning elastic fluids produced an increase in the measured gap between the roll surfaces, compared to the constant viscosity elastic fluids. The sensitivity to the roll speed increased from the Newtonian case but remained relatively consistent with the 0.24% and 0.36% PIB solutions. The measuring system could barely detect a difference in the measured gap, between the two shear-thinning fluids.

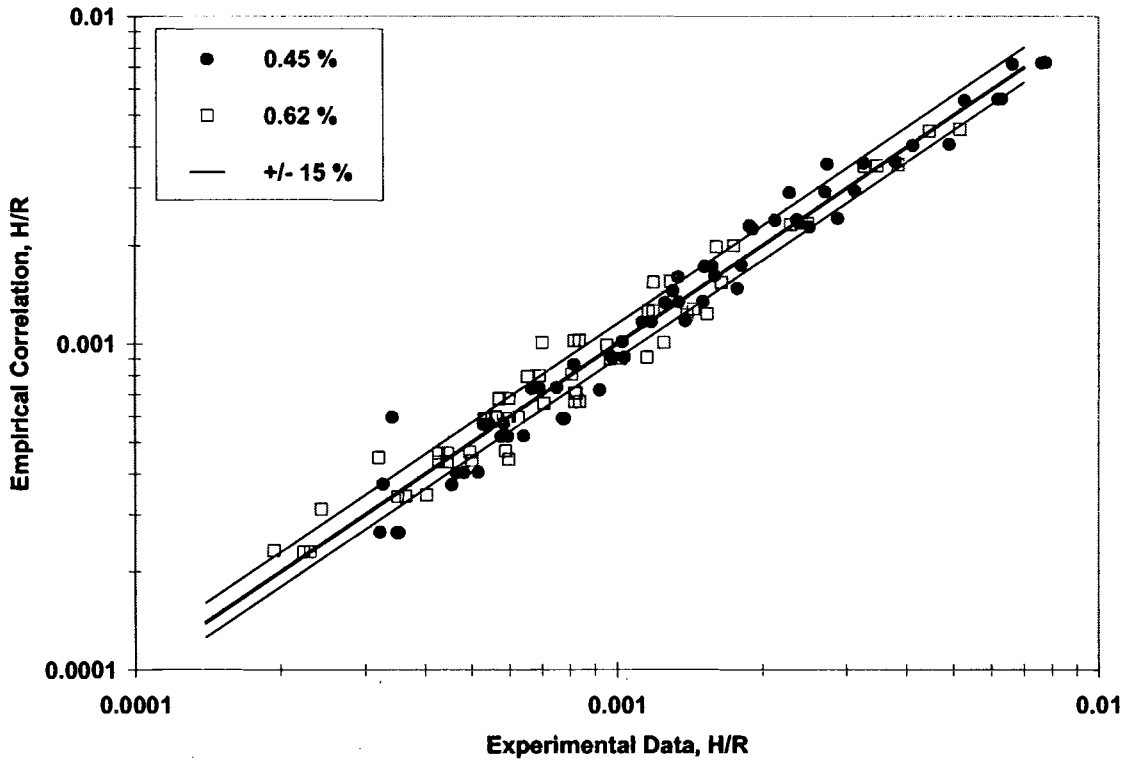

Figure 3.22 Best fit of the empirical correlations with the measured data

Table 3.6 Summary of empirical correlations

H	$H = k\mu^a \overline{V}^b W^c E^d R^e$					
	k	a	b	c	d	e
Newtonian	0.42	0.55	0.55	-0.39	-0.16	0.84
0.12% PIB	0.60	0.59	0.59	-0.48	-0.11	0.89
0.24% PIB	0.42	0.63	0.63	-0.58	-0.05	0.95
0.36% PIB	0.036	0.62	0.62	-1.05	-0.43	1.43
0.45% PIB	0.065	0.65	0.65	-1.07	-0.42	1.42
0.62% PIB	0.048	0.63	0.63	-1.08	-0.45	1.45

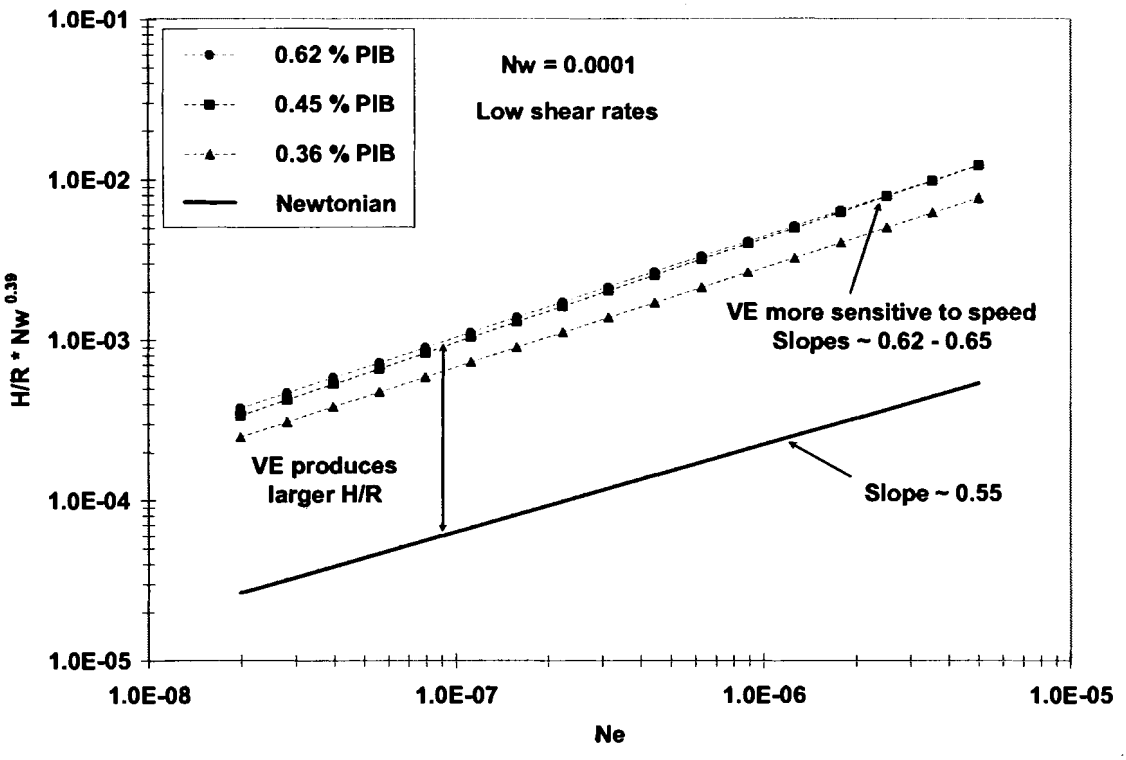

Figure 3.23 Gap as a function of Ne at low load

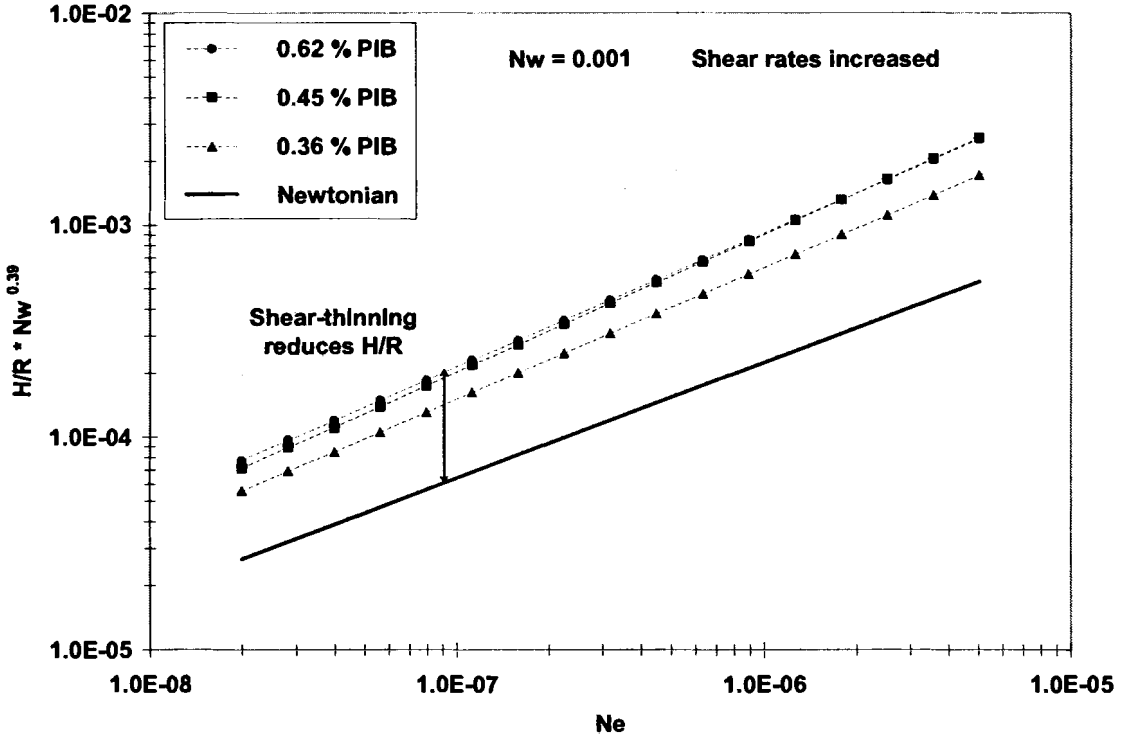

Figure 3.24 Gap as a function of Ne at intermediate load

As the applied load is increased, as reported in Figure 3.24, the measured gap width of the shear-thinning fluids decreased significantly. A further increase in the applied load, by another order of magnitude, produced further decreases in the measured gap. At high loads, shown in Figure 3.25, the measured gap of the shear-thinning fluids was much less than the Newtonian base case and less than the constant viscosity elastic test liquids. This indicates that the shear-thinning behavior can overcome the normal stress produced by the dissolved polymer. This result was expected because the Newtonian component no longer dominates the solution at such high concentrations. Also, at low speeds, even though the gap between the rolls is small, the shear rate is also small. Published measurements of the first normal stress indicate that normal stress effects grow with shear rate for PIB solutions. This result was observed by Davies and Walters (1973) who showed for elastic, shear-thinning liquids, the ratio of the first normal stress difference to the shear stress, had to be large in order for extra load bearing capacity to occur.

The dimensionless, measured pressure profiles of the shear-thinning liquids are shown in Figure 3.26 for an intermediate load. The pressure profiles for the viscoelastic liquids are very similar to the Newtonian case. Increasing the polymer content of the solution caused the minimum pressure at the nip exit to increase relative to the Newtonian case. Even at higher loads, the minimum pressure of the Newtonian fluid, at the nip exit, is consistently less than the viscoelastic fluids Figure 3.27. This result seems to contradict the results of measurements of ink "tack" measured in printing press nips. However, "tack" has been shown to be quite dependent on the thickness of the ink layer in the nip. The gap in the tack tests is no known. Here, the gap increases with increasing polymer concentration.

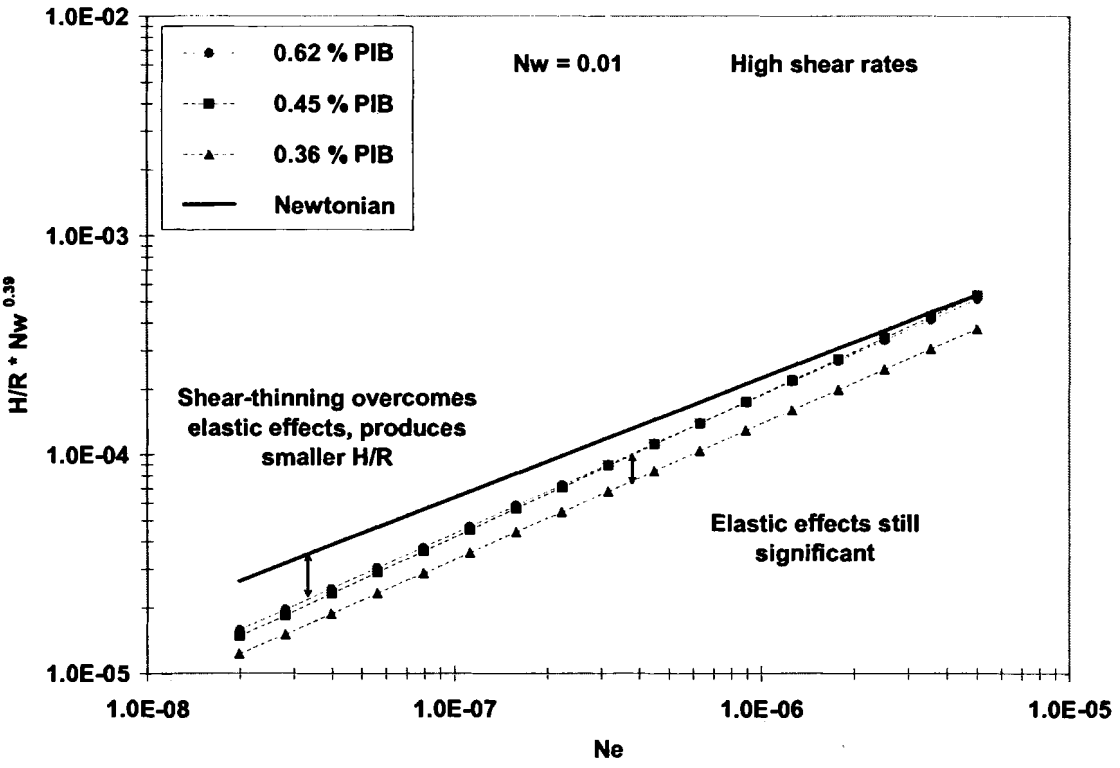

Figure 3.25 Gap as a function of Ne at high load

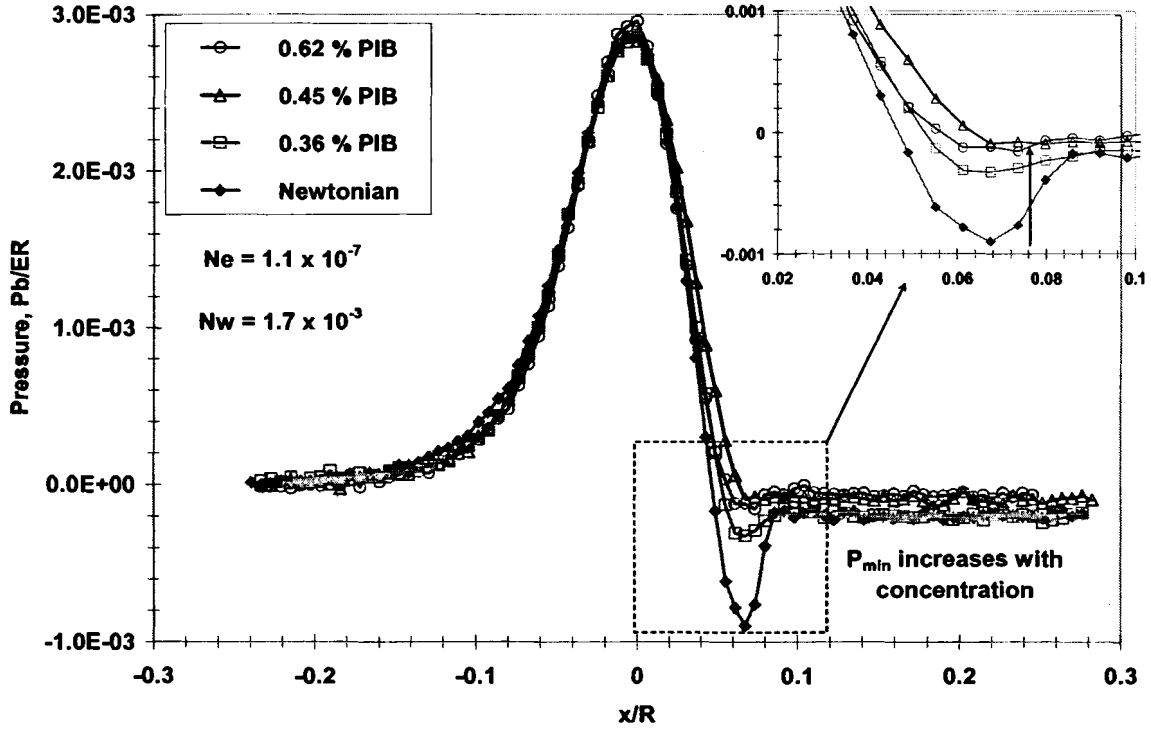

Figure 3.26 Pressure profiles of the shear-thinning elastic liquids

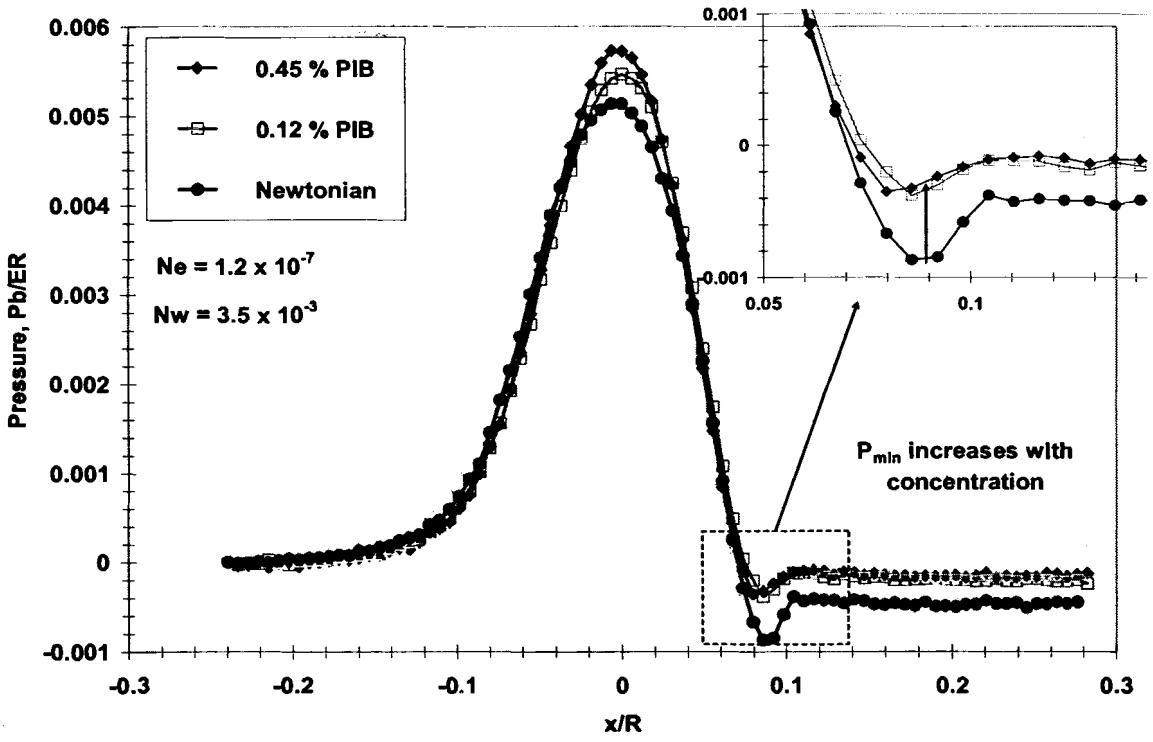

Figure 3.27 Pressure profiles for shear-thinning and elastic liquids

Even though comparing the results from the finite element calculations directly to the experimental measurements is not possible because the flow systems are fundamentally different, the calculations reveal interesting features of the viscoelastic flow that have not been shown in the literature. The finite element calculations were used to study the competing effects of elasticity and shear thinning in a symmetric, rigid roll, forward coating system.

The simulations were run to as high Weissenberg number, We, as possible where We indicates the effect of elasticity and is defined as:

$$We = \lambda \frac{\overline{V}}{H} \tag{3.19}$$

where $\overline{V}$ is the average roll speed, H is the measured gap between the rolls, and λ is a characteristic relaxation time of the test fluid. The capillary number, Ca, was used as another

dimensionless group to characterize the viscous and surface tension forces in the system and is given by:

$$Ca = \frac{\eta_o \bar{V}}{\sigma} \tag{3.20}$$

where η_o is the zero-shear viscosity and σ is the surface tension of the liquid. Above We = 5.0, the mesh became distorted at the domain exit. Even though the simulation converged, these results were not plotted because of the unnatural shape of the free surface at the domain exit. Typical streamlines for the Newtonian and Oldroyd-B fluids are compared in Figure 3.28. The model parameters for the results presented in the following contour plots are presented in Table 3.7.

Table 3.7 Model parameters used in the flow simulations

Parameter	Oldroyd-B	Giesekus
H (m)	0.0005	0.0005
R (m)	0.05	0.05
$\bar{V}$ (m/s)	0.004, 0.5	0.004, 0.5
σ (N/m)	0.02	0.02
ρ (kg/m^3)	1000	1000
η_o (Pas)	0.5	0.5
η_r	0.1	0.1
λ (s)	0 - 0.005	0 - 0.005
α		0.1

The streamlines of the viscoelastic flow are similar to the Newtonian flow, however, the film-split point in the viscoelastic model is shifted down-stream slightly at moderate We, compared to the Newtonian model.

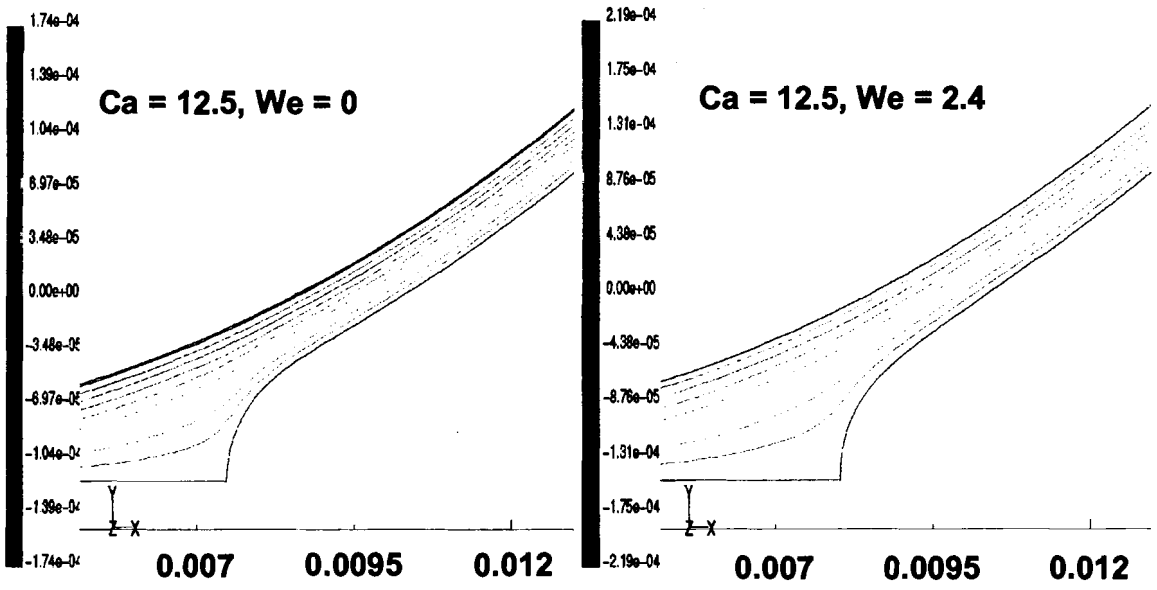

Figure 3.28 Streamlines for Newtonian and Oldroyd-B models

The contours of the first normal stress component of the total extra stress, $\mathbf{T}_{11}$, are shown in Figure 3.29. There is a large normal stress build-up at the point of high extension in the Newtonian base case. This stress concentration transforms into a sort of stress boundary layer that is attached to the free surface downstream from the split point in the viscoelastic flow. There are two explanations for the appearance of the stress layer. The first is that it may be an artifact of the Oldroyd-B model. The extension rate in the area where the boundary layer appears is quite large and may be in the range of where the extensional viscosity of the Oldroyd-B fluid becomes unbounded. Unbounded extensional viscosity would produce errors near the surface. However, the error would decrease as the extension rate in the flow decreased and this is indicated by the decreasing gradient of the stress contours toward the roll surface.

The other explanation is that the boundary layer is a genuine effect of a viscoelastic fluid in the roll coating geometry. If this is the case, the stress boundary layer may influence the behavior of the polymer molecules in the area and may indicate the presence of a purely

elastic instability mechanism. It is difficult to obtain any information regarding stability from the results available from the POLYFLOW package. However, finite element calculations and experimental observations of the recirculation flows of constant viscosity elastic fluids have linked the stretching of polymer molecules, in areas of high extension, to purely elastic instabilities (Shaqfeh *et al.* (1996)).

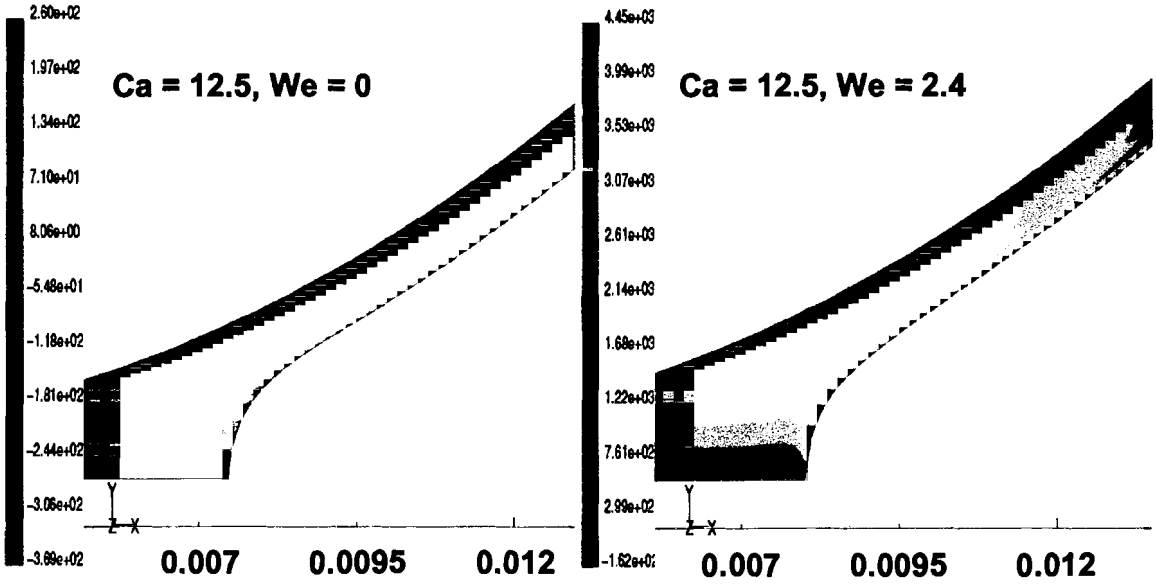

Figure 3.29 Contours of the first normal stress

The contours of the shear stress component, $\mathbf{T}_{12}$, of the total extra stress are plotted in Figure 3.30. Shear stress increased in the viscoelastic flow model, however, the gradient of the shear stress throughout the domain decreased. The contours of the second normal stress component, $\mathbf{T}_{22}$, of the total extra stress are plotted in Figure 3.31. The second normal stress also increased throughout the domain and a stress boundary layer formed at the surface of the meniscus.

When the Capillary number was decreased, a recirculation appeared on the downstream side of the nip, as shown in the streamlines plotted in Figure 3.32. Again, at low Ca, the film-split position was shifted slightly downstream at moderate We.

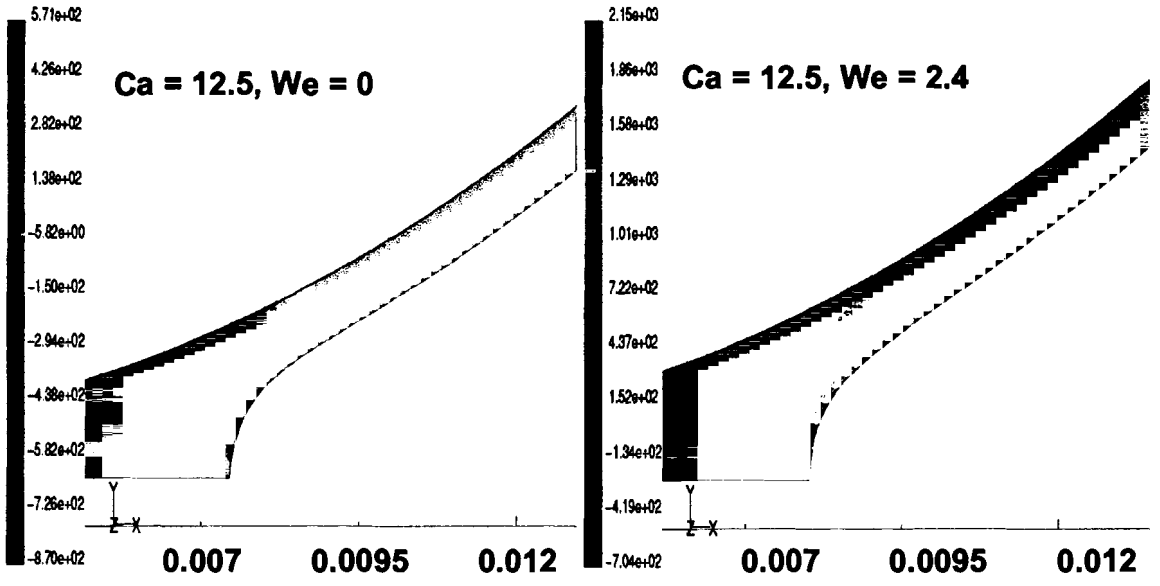

Figure 3.30 Contours of the shear stress

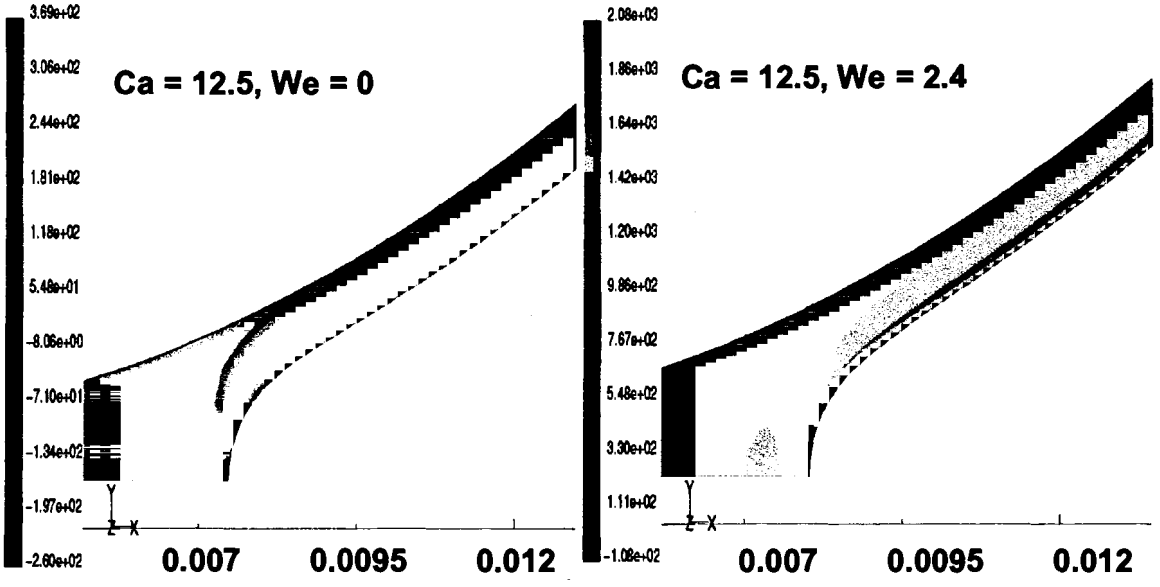

Figure 3.31 Contours of the second normal stress

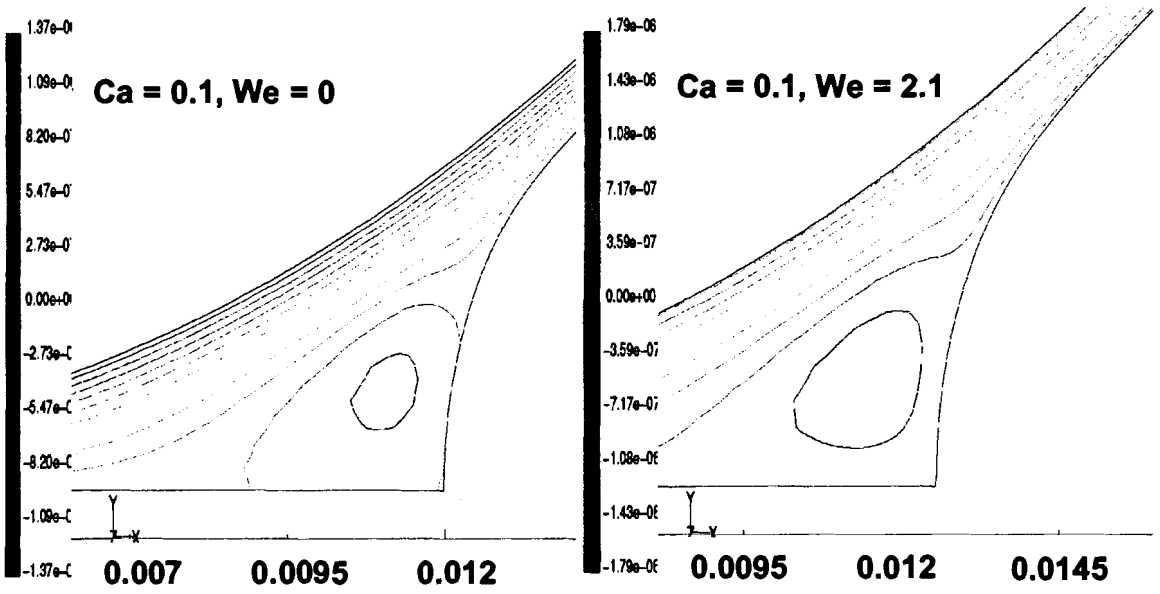

Figure 3.32 Streamlines for low Ca flow

Contours of the first normal stress at high and low Ca are compared in Figure 3.33. The stress boundary layer at the free surface does not appear in the low Ca flow at similar levels of elasticity. At low Ca, the extension rate along the free surface is reduced compared to the high Ca flow. This suggests that the observed stress boundary layer may be an artifact of the unbounded extensional viscosity of the Oldroyd-B model used in the calculations.

Contours of the second normal stress are shown in Figure 3.34. At low Ca, there appears to be a high stress concentration near the roll surface, downstream of the split point. At, large Ca, the stress concentration shifts to the free surface at the film-split. It should be noted that the magnitudes of the second normal stresses observed at low and high Ca differ by three orders of magnitude.

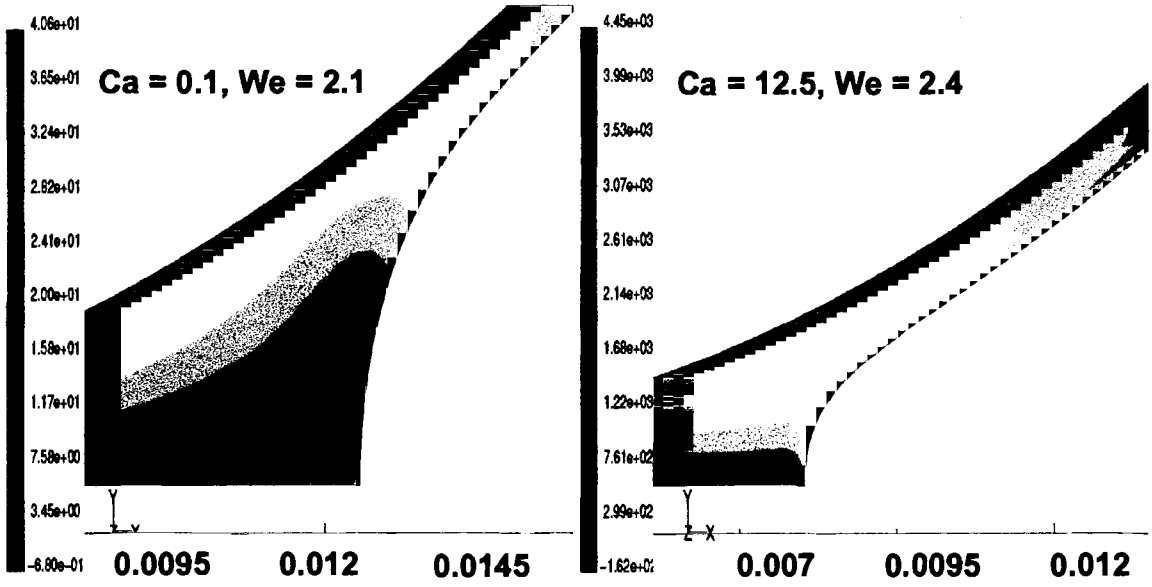

Figure 3.33 Contours of the first normal stress at low and high Ca

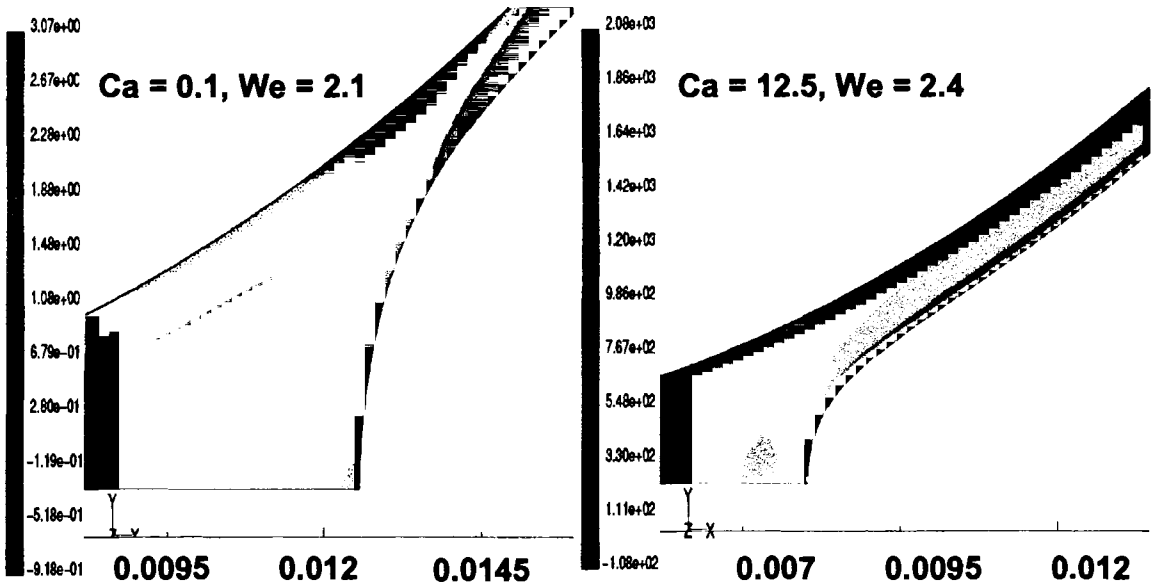

Figure 3.34 Contours of the second normal stress for low and high Ca

The next set of figures reveals the effects of shear-thinning viscosity on the viscoelastic flow through the Giesekus fluid model. Streamlines are plotted in Figure 3.35. The Giesekus model, for similar operating parameters, has shifted the split-point much further downstream. This observation may be explained by the large amount of shear thinning produced by the model with the parameters used in the calculations; the power law index is approximately 0.46. Coyle *et al.* (1987) observed a downstream shift of the film-split meniscus in finite element simulations of purely viscous shear-thinning fluids in a forward roll coating geometry.

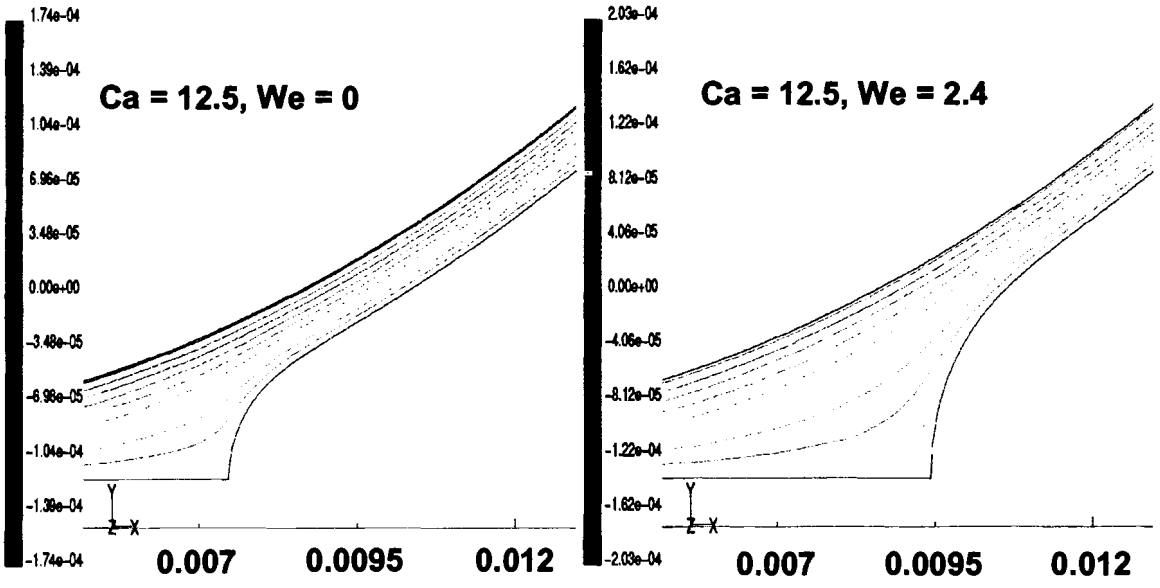

Figure 3.35 Streamlines for the Giesekus model

Contours of the first normal stress, for both the Oldroyd-B and Giesekus models, are compared in Figure 3.36. The stress boundary layer has disappeared in the Giesekus model flow. The Giesekus fluid model has a bounded extensional viscosity and the results from the simulations further point to the unbounded extensional viscosity of the Oldroyd-B model as the cause of the appearance of the stress boundary layer at the free surface. It should be noted, however, that the Ca used in the comparisons, is based on the zero shear

viscosity of the fluid. Because of the presence of shear-thinning, a modified Ca that accounts for decreasing viscosity, may need to be used before quantitative comparisons can be made between the two models.

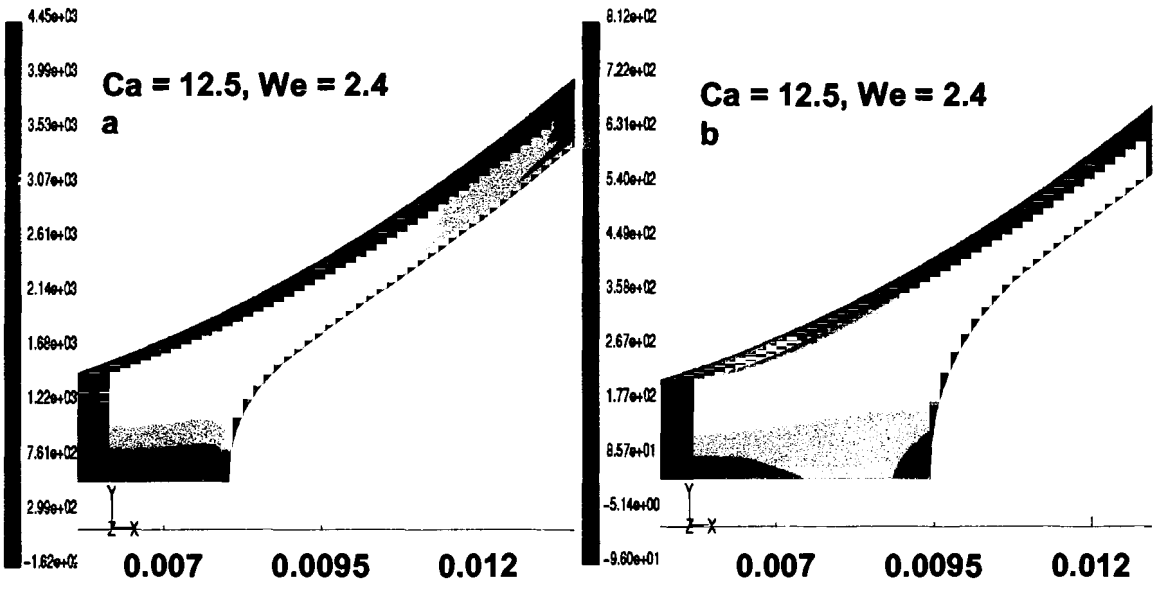

Figure 3.36 Contours of the first normal stess for Oldroyd-B (a) and Giesekus (b)

The magnitudes of the second normal stress are dramatically reduced by the presence of shear thinning as shown in Figure 3.37b. It is possible to make a cautious estimate of some effects of viscoelasticity on the stability of the flow from Figure 3.36 and 3.37. If the stability of the flow is influenced by the appearance of the stress boundary layer, then adding shear thinning had a stabilizing effect on the flow. Gutoff and Kendrick (1982) observed a stabilizing effect on the slide-coating bead when they added small amounts of polymer to their test fluid.

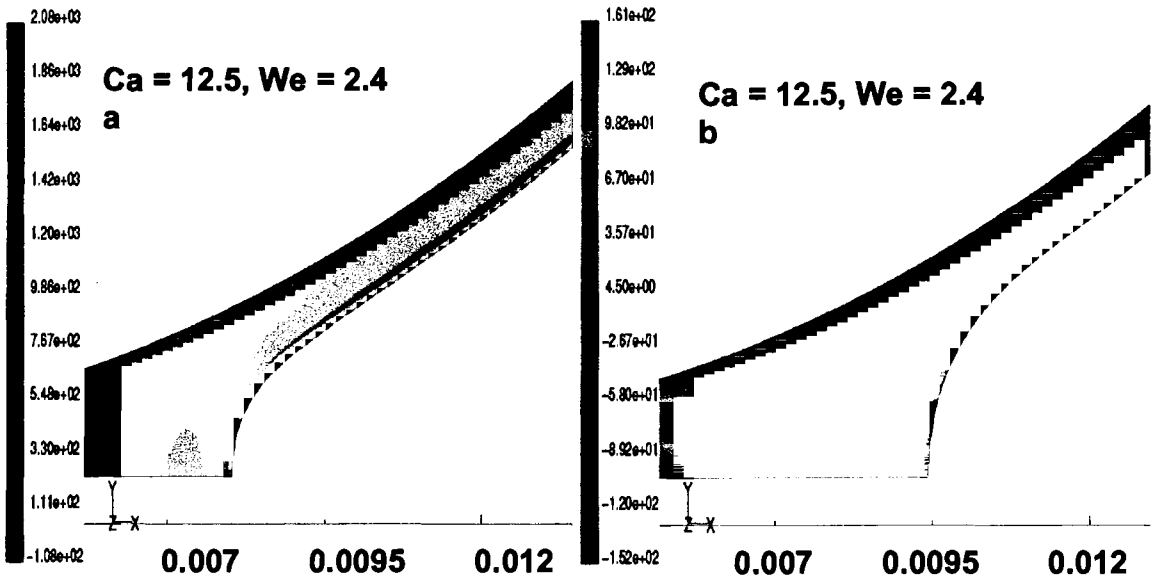

Figure 3.37 Contours of the second normal stress for Oldroyd-B (a) and Giesekus (b)

Examples of the pressure profiles are plotted in Figure 3.38. Increasing the level of elasticity, We, had a much larger influence on both the maximum and minimum pressure for the Giesekus fluid. At high We, the pressure gradient at the film-split was much less than at low We, indicating that it may have a significant effect on the ribbing instability mechanism. It appears that the pressure gradient for the purely elastic fluid increased as elastic effects increased.

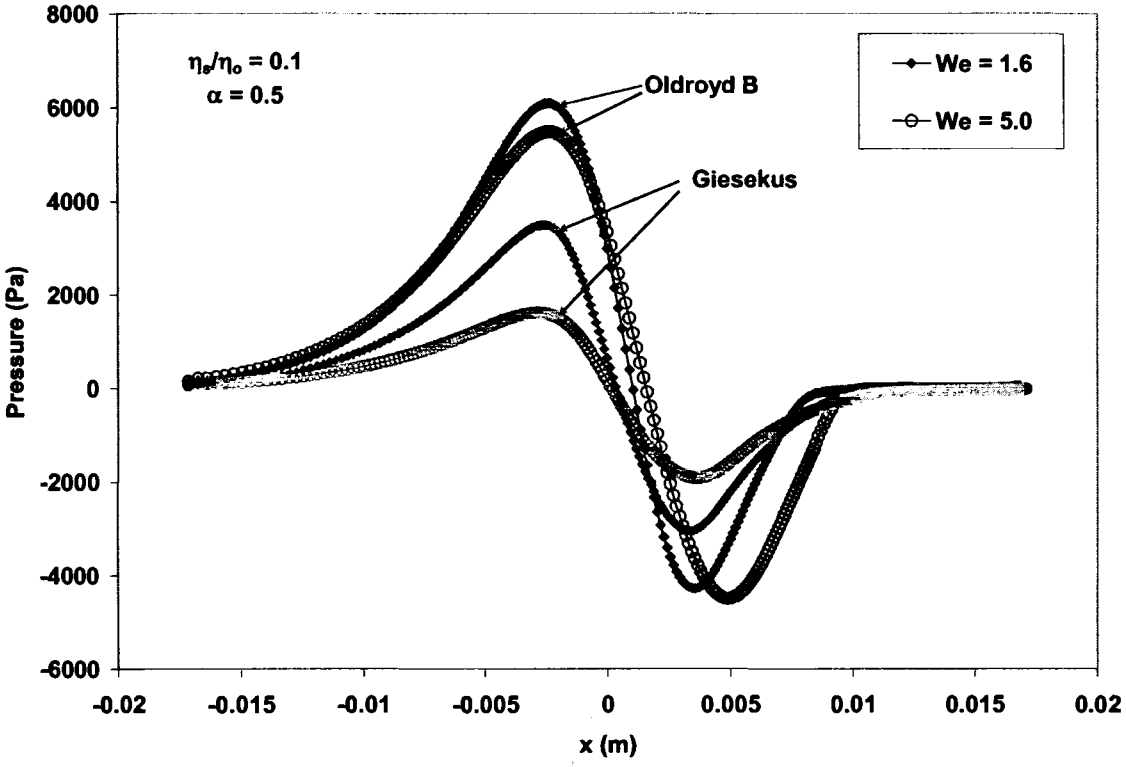

Figure 3.38 Pressure profiles

The pressure profiles can be integrated to study the roll separating force and are plotted in Figure 3.39. Decreasing the viscosity ratio increased the roll separating force in the Oldroyd-B flow up to a We = 1.6 and maintained increased separating force as We increased further. Increasing the viscosity ratio in the Giesekus model reduced the roll separating force and continued the reduction as We increased.

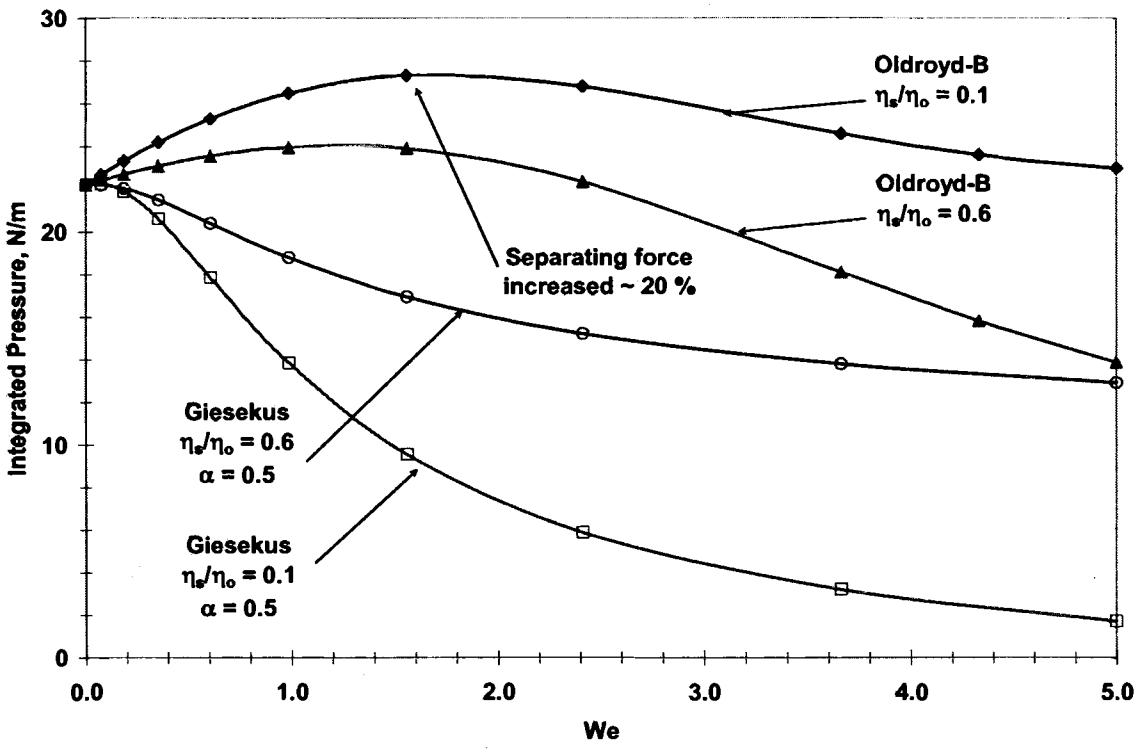

Figure 3.39 Integrated pressure profiles

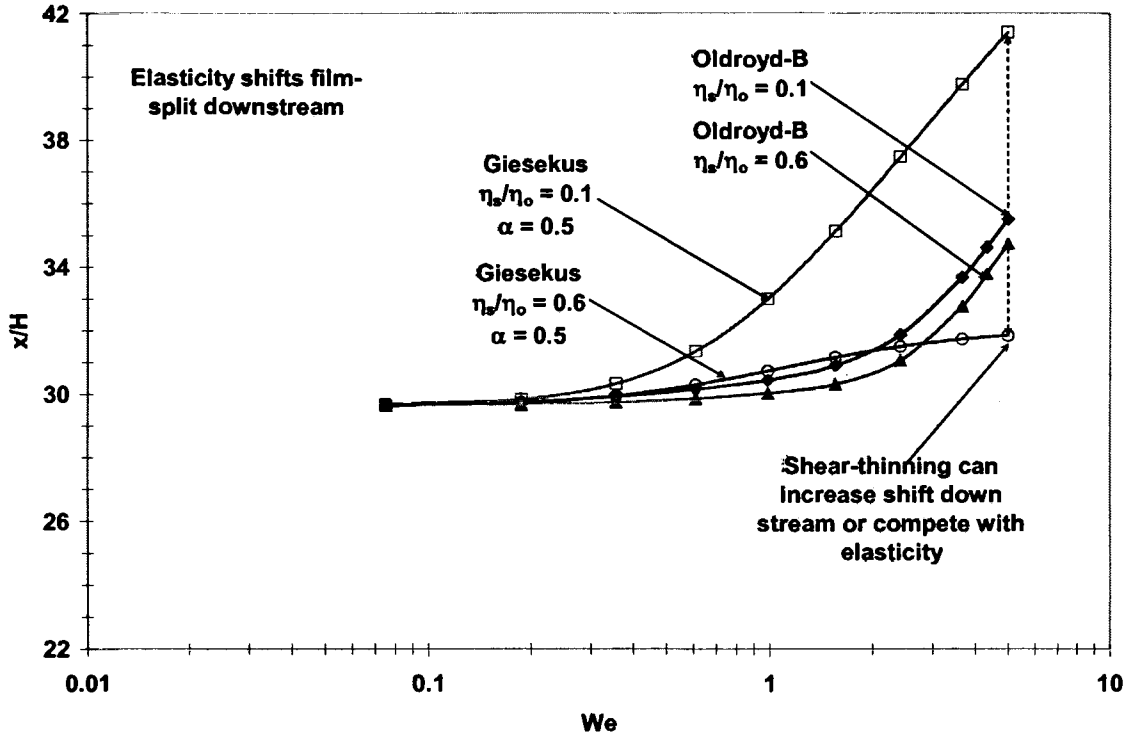

Figure 3.40 Film split position

Figure 3.40 reveals that elasticity shifts the film-split downstream. Also, increasing the polymer effect, by decreasing the viscosity ratio, had a large impact on the film-split position with the Giesekus fluid. This behavior is commonly observed in calculations with purely viscous shear-thinning fluids (Coyle *et al.* 1987). Coyle *et al.* (1987) and Benkreira *et al.* (1981) showed that the film-split recedes into the nip as the Ca of the flow increases. At equal roll speeds and gaps, a shear-thinning liquid has a lower viscosity and thus a lower Ca, which translates into a downstream shift of the split point. Figure 3.40 also shows that for an equivalent level of polymer contribution to the solution, the purely elastic fluid has a split point located further downstream than the shear-thinning fluid. Elasticity is definitely changing the relationship between the film split location and the Ca of the flow. The dimensionless flow rate for both models is plotted in Figure 3.41. Increasing elasticity increased the flow rate of the Oldroyd-B fluid much more than the Giesekus fluid. In both cases, increasing the polymer contribution produced a significant increase in dimensionless flow rate. Keep in mind that the gap is held constant. Elasticity seems to be able to pull more fluid through the nip, possibly because of the large extensional stresses in the flow.

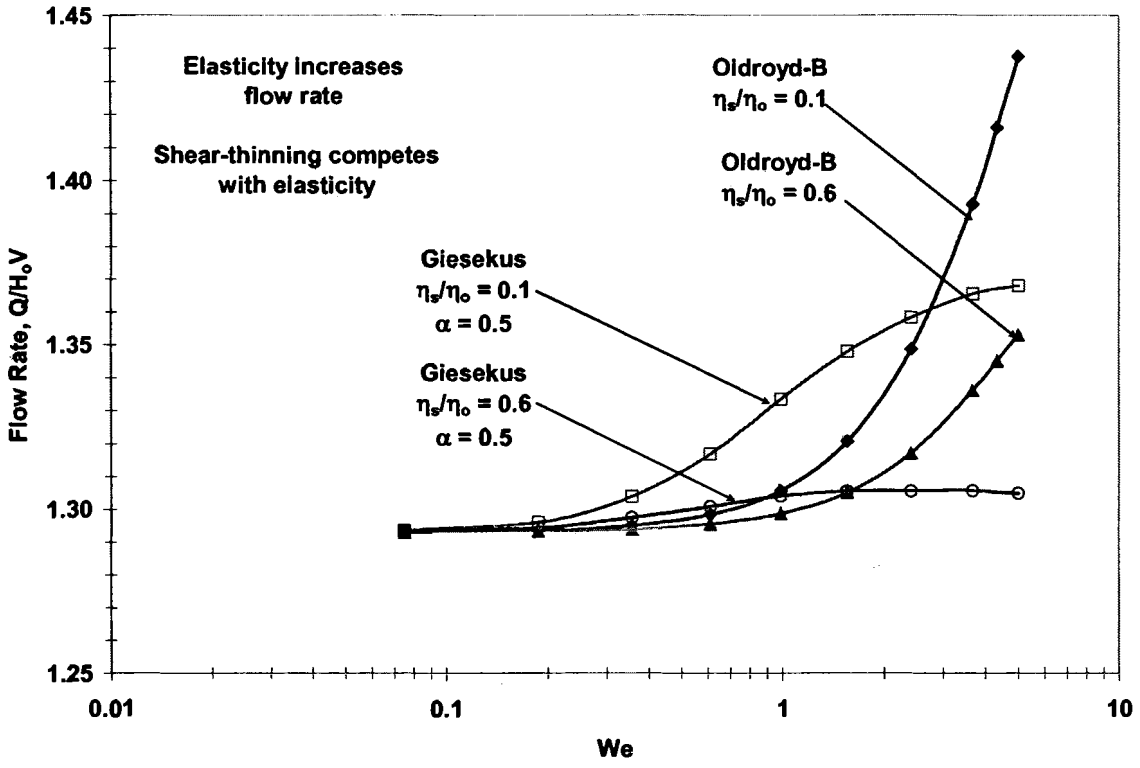

Figure 3.41 Dimensionless flow rate for the viscoelastic flows

3.5 Summary

Results and conclusions from chapter 3 are summarized as follows:

- Five characterized model fluids were used to study the effects of elasticity and shear-thinning elastic behavior on the forward, deformable roll coating system with a load controlled gap.
- The constant viscosity elastic fluids showed increased sensitivity of the measured gap to roll speed and applied load compared to the Newtonian base case. At, low and intermediate loads at moderate roll speeds, the normal stresses generated in the nip caused the gap between the roll surfaces to increase compared to the Newtonian case.

- Elastic shear-thinning fluids showed increased sensitivity of the measured gap to both roll speed and applied load compared to the Newtonian base case. At low and intermediate loads at high speeds, the normal stress generated in the nip increased the gap between the roll surfaces further from the Newtonian case.
- Increased gap is consistent with experimental observations of increased flow rate in a fixed engagement deformable roll system and it is consistent with observed increase in load bearing capacity in a journal bearing flow system.
- The Galerkin finite element method was used to study the two-dimensional, free surface, viscoelastic flow between to fixed, rigid rolls with symmetric roll speeds. A purely elastic fluid model revealed the presence of a first normal stress boundary layer downstream of the film split at high Ca and moderate We.
- An elastic, shear-thinning fluid model showed that the presence of shear thinning delayed the appearance of the first normal stress boundary layer.
- The pressure gradient in the flow of a purely elastic liquid increased with We indicating that the flow became unstable. Adding shear thinning decreased the pressure gradient indicating that the flow became more stable.

4 SUMMARY

4.1 Summary of Chapter 2

- A bench-top apparatus was constructed to study elasto-hydrodynamic forward roll coating flows.
- A technique was developed and applied to measure the gap between the roll surfaces. Measurements of the gap corresponded with the expected value at the point of maximum fluid pressure within the nip and the measured wet film thickness.
- The measured gap and its sensitivity to the external load and roll speed were consistent with published experimental data and theoretical analyses.
- There was some evidence of increasing sensitivity to the applied load caused by the influence of the thin, deformable roll cover used in the experiments.
- A model of the deformable roll coating system was developed based on the lubrication approximation with non-Hertzian deformation of the roll cover and a visco-capillary boundary condition at the film-split.
- The lubrication model reproduced the magnitude and shape of the measured pressure, for low external loads, after values of the negative pressure below –100 kPa were removed from the calculations.

4.2 Summary of Chapter 3

Results and conclusions from chapter 3 are summarized as follows:

- Five characterized model fluids were used to study the effects of elasticity and shear-thinning elastic behavior on the forward, deformable roll coating system with a load controlled gap.
- The constant viscosity elastic fluids showed increased sensitivity of the measured gap to roll speed and applied load compared to the Newtonian base case. At, low and intermediate loads at moderate roll speeds, the normal stresses generated in the nip caused the gap between the roll surfaces to increase compared to the Newtonian case.
- Elastic shear-thinning fluids showed increased sensitivity of the measured gap to both roll speed and applied load compared to the Newtonian base case. At low and intermediate loads at high speeds, the normal stress generated in the nip increased the gap between the roll surfaces further from the Newtonian case.
- Increased gap is consistent with experimental observations of increased flow rate in a fixed engagement deformable roll system and it is consistent with observed increase in load bearing capacity in a journal bearing flow system.
- The Galerkin finite element method was used to study the two-dimensional, free surface, viscoelastic flow between to fixed, rigid rolls with symmetric roll speeds. A purely elastic fluid model revealed the presence of a first normal stress boundary layer downstream of the film split at high Ca and moderate We.
- An elastic, shear-thinning fluid model showed that the presence of shear thinning delayed the appearance of the first normal stress boundary layer.

- The pressure gradient in the flow of a purely elastic liquid increased with We indicating that the flow became unstable. Adding shear thinning decreased the pressure gradient indicating that the flow became more stable.

4.3 Recommendations for Future Work

- A significant factor contributing to the uncertainty in the measurements was the extent of the eccentricity of the rolls and bearings. The first step in future experiments should include a rebuild of the rolls and bearing so that the total runout for each roll is less than 10 μm. Including split pillow blocks or bearing mounts would enable quick change over to study different roll diameters or roll covers.
- The lack of safety measures on the device should be addressed. At the minimum, and emergency stop switch should be installed in the form of a cable encircling the entire apparatus so that the rolls can be stopped. An improvement would be to include a means of opening the nip when the E-stop was triggered.
- Permanently fixing the drive for the deformable roll to the base plate would decrease the error in the applied load significantly by removing the extra inertia. Using a Schmitt coupling to connect the drive shaft to the roll would accomplish this task.
- A means of fixing the gap, and setting a precise gap, should also be installed. This would allow more types of roll coating flows to be studied.
- There was also some problem with the convolution of the pressure data with the nip length. Increasing the diameter of the rolls to 20 cm would increase the nip length and reduce the convolution. A larger diameter roll would also reduce the error in the capacitance probe measurements. If a larger diameter roll is installed, it would be

important to include gear reducers between the drive shaft and the rolls so that the drives could continue to operate within their limits at low speed conditions. Gear reducers would also increase the resolution from the pressure and capacitance transducers.

- Increasing the thickness of the roll cover would facilitate comparison to other published data and decreases its influence on the flow through the nip.
- Some information regarding the test fluids was unavailable, including: extensional viscosity, normal stress, and relaxation time measurements.
- Previous work has shown contradictory observations of the sensitivity to roll speed differential. Future experiments should study the speed differential to examine the effects of increased shear on flow of viscoelastic liquids.
- The reverse roll coating flow of viscoelastic fluids also should be investigated.
- Finite element models of the two-dimensional, viscoelastic roll coating flow should continue to be explored over a wider range of capillary number. Much information could be gained without including the effects of a deformable roll cover.

REFERENCES

Adachi, K.; Tamura, T., and Nakamura, R. Coating flows in a nip region and various critical phenomena. AIChE Journal. 1988; 34(3):456-464.

Alonso, S. and Tanguy, P. A. Hydrodynamic instabilities in the metering nip of a film coater. TAPPI Journal. 2001; 84(5):1-20.

Aspler, J. S. and Taylor, S. Tack development in water-based inks. Nordic Pulp and Paper Research Journal. 1991; 6(1):4-7.

Bapat, C. N. and Batra, R. C. Finite plane strain deformations of nonlinear viscoelastic rubber-covered rolls. International Journal for Numerical Methods in Engineering. 1984; 20(1):1911-1927.

Bauman, T.; Sullivan, T., and Middleman, S. Ribbing instability in coating flows: effect of polymer additives. Chemical Engineering Communications. 1982; 14:35-46.

Benjamin, D. F. Roll Coating Flows and Multiple Roll Systems. Minneapolis, MN: University of Minnesota; 1994.

Benjamin, D. F.; Anderson, T. J., and Scriven, L. E. Multiple roll systems: steady-state operation. AIChE Journal. 1995; 41(5):1045-1060.

Benjamin, D. F.; Carvalho, M. S.; Anderson, T. J., and Scriven, L. E. Forward roll film-splitting: theory and experiment. TAPPI Coating Conference Proceedings; 1994: 109-123.

Benkreira, H.; Edwards, M. F., and Wilkinson, W. L. Roll coating of purely viscous liquids. Chemical Engineering Science. 1981; 36:429-434.

Beris, A. N.; Armstrong, R. C., and Brown, R. A. Perturbation theory for viscoelastic fluids between eccentric rotating cylinders. Journal of Non-Newtonian Fluid Mechanics. 1983; 13(1):109-148.

---. Finite element calculation of viscoelastic flow in a journal bearing: II. Moderate viscosity. Journal of Non-Newtonian Fluid Mechanics. 1986; 19:323-347.

Blayo, A.; Fang, S. W.; Gandini, A., and Le Nest, J. F. Study of ink misting phenomena. American Ink Maker. 1998; 76(5):54-61.

Bohan, M. F. J.; Claypole, T. C., and Gethin, D. T. Dynamic measurement of ink film thickness, pressure and temperature in rolling contacts. Technical Association of Graphic Arts Proceedings. Bookcrafters, Inc. Chelsea, MI; 2001: pgs 111-124.

Bohan, M. F. J.; Claypole, T. C., and Grethin, D. T. The application of roughness model to a soft EHL contact. International Journal of Numerical Methods for Heat & Fluid Flow. 2002; 12(4):356-374.

Bohan, M. F. J.; Lim, C. H.; Korochkina, T. V.; Claypole, T. C.; Gethin, D. T., and Roylance, B. J. An investigation of the hydrodyanmic and mechanical behavior of a soft nip rolling contact. Proc Instn. Mech. Engrs. 1997; 211(J):37-49.

Booth, G. L. *Coating Equipment and Processes.* New York, NY: Lockwood Publishing Company; 1970.

Cameron, A. *Basic Lubrication Theory.* New York, NY: John Wiley & Sons; 1976.

Carvalho, M. S. and Scriven, L. E. Effect of deformable roll cover on roll coating. TAPPI Journal. 1994; 77(5):201-208.

---. Deformable roll coating flows: steady state and linear perturbation analysis. Journal of Fluid Mechanics. 1997a; 339:143-172.

---. Flows in forward deformable roll coating gaps: comparison between spring and plane-strain models of roll cover. Journal of Computational Physics. 1997b; 138:449-479.

Christiansen, S. Resins are gaining weight. American Ink Maker. 1995; 73(10):14-60.

Cohu, O. and Benkreira, H. Air entrainment in angled dip coating. Chemical Engineering Science. 1998; 53(1):533.

Cohu, O. and Magnin, A. Forward roll coating of Newtonian fluids with deformable rolls: an experimental investigation. Chemical Engineering Science. 1997; 52(8):1339-1347.

Coyle, D. J. Experimental Studies of Flow Between Deformable Rolls. AIChE Spring National Meeting; New Orleans, LA. 1988a.

---. Forward roll coating with deformable rolls: a simple one-dimensional elastohydrodynamic model. Chemical Engineering Science. 1988b; 43(10):2673-2684.

---. Nonlinear Theory of squeeze-roll coating. AIChE Spring National Meeting; Orlando, FL. 1990.

---. Roll Coating. In: *Modern Coating and Drying Technology.* Cohen, E. D.; Gutoff, E. B. (eds). New York, NY: VCH Publishers; 1992; pp. 63-116.

---. Knife and Roll Coating. In: *Liquid Film Coating.* Kistler, S. F.; Schweizer, P. M. (eds). London: Chapman & Hall; 1997; pp. 539-571.

Coyle, D. J.; Macosko, C. W., and Scriven, L. E. Film-splitting flows of shear-thinning liquids in forward roll coating. AIChE Journal. 1987; 33(5):741-746.

Crook, A. W. The lubrication of rollers. Philosophical Transactions of the Royal Society of London, Series A, Mathematical and Physical Sciences. 1958; 250(A):387-409.

Davies, M. J. and Walters, K. The Behavior of Non-Newtonian Lubricants in Journal Bearings- A Theoretical Study. In: *Rheology of Lubricants.* Davenport, T. C., (ed.)New York, NY: John Wiley & Sons; 1973; pp. 65-80.

Dobbels, F. and Mewis, J. Analysis of nip flow operations involving a viscoelastic roller. Chemical Engineering Science. 1978; 33:493-500.

Dontula, P.; Macosko, C. W., and Scriven, L. E. Model elastic liquids with water-soluble polymers. AIChE Journal. 1998; 44(6):1247-1255.

Dontula, P.; Pasquali, M.; Macosko, C. W., and Scriven, L. E. Viscoelastic effects in forward-roll coating flows, Ait-Kadi, A.; Dealy, J. M.; James, D. F., and Williams, M. C., (eds). Proc. XIIth Int. Congr. on Rheology; Quebec City, Quebec, Canada. Canadian Rheology Group; 1996: 709-710.

Doremus, P. and Piau, J. Viscoelastic elongational lubrication. Journal of Non-Newtonian Fluid Mechanics. 1981; 9:389-400.

Doremus, P. and Piau. J. Experimental study of viscoelastic effects in a cylinder-plane lubricated contact. Journal of Non-Newtonian Fluid Mechanics. 1983; 13:79-91.

Dowson, D. and Higginson, H. G. *Elasto-Hydrodynamic Lubrication.* New York, NY: Pergamon Press; 1966.

Elrod, H. G. A cavitation algorithm. Journal of Lubrication Technology. 1981; 103(1):350-354.

Fernando, R. H. and Glass, J. E. Dynamic uniaxial extensional viscosity (DUEV) effects in roll application II. Polymer blend studies. Journal of Rheology. 1988; 32(2):199-213.

Fetsko, J. M.; Schaeffer, W. D., and Zettlemoyer, A. C. Sources of differences in picking results among presses. TAPPI Journal. 1963; 46(3):157-162.

Gaskell, P. H.; Innes, G. E., and Savage, M. D. An experimental investigation of meniscus roll coating. Journal of Fluid Mechanics. 1998; 355:17-44.

Gaskell, P. H.; Savage, M. D.; Summers, J. L., and Thompson, H. M. Modeling and analysis of meniscus roll coating. Journal of Fluid Mechanics. 1995; 298(1):113-137.

Glass, J. E. Dynamics of roll spatter and tracking Part 1: commercial latex trade paints. Journal of Coatings Technology. 1978a; 50(640):53-60.

---. Dynamics of roll spatter and tracking Part 2: Formulation effects in experimental paints. Journal of Coatings Technology. 1978b; 50(640):61-68.

---. Dynamics of roll spatter and tracking Part 3: Importance of extensional viscosities. Journal of Coatings Technology. 1978c; 50(641):56-71.

---. Dynamics of roll spatter and tracking Part 4: Importance of G* recovery and N1 tracking. Journal of Coatings Technology. 1978d; 50(641):72-78.

Glass, J. E. and Prud'homme, R. K. Coating Rheology: component influence on the rheological response and performance of water-borne coatings in roll applications. Schweizer, P. M. and Kistler, S. F., (eds.). *Liquid Film Coating.* Cambridge UK: Chapman & Hall; 1997; pp. 137-182.

Greener, J. and Middleman S. A theory of roll coating of viscous and viscoelastic fluids. Polymer Engineering and Science. 1975; 15(1):1-10.

Greener, J.; Sullivan, T.; Turner, B., and Middleman, S. Ribbing instability of a two-roll coater: Newtonian fluids. Chemical Engineering Communications. 1980; 5(1):73-83.

Grön, J.; Sunde, H., and Nikula, E. Runnability aspects in high-speed film transfer coating. TAPPI Journal. 1998; 81(2):157-165.

Gutoff, E. B. and Kendrick, C. E. Low flow limits of coatability on a slide coater. AIChE Journal. 1987; 33(1):141-145.

Hall, R. W. and Savage, M. D. Two-dimensional elastohydrodynamic lubrication Part 1: the associated dry contact problem. Proc Instn. Mech. Engrs. 1988; 202(C5):347-353.

Herrebrugh, K. Solving the incompressible and isothermal problem in elastohydrodynamic lubrication through an integral equation. Journal of Lubrication Technology. 1968; 90(1):262-270.

Higgins, B. G. Coating Methods. In: *Encyclopedia of Polymer Science and Technology.* 1st ed. New York, NY: John Wiley; 1965; pp. 765-807.

Hooke, C. J. The elastohydrodynamic lubrication of a cylinder on an elastomeric layer. Wear. 1986; 111:83-99.

Johnson, K. L. Regimes of Elastohydrodynamic lubrication. Journal of Mechanical Engineering Science. 1970; 12(1):9-16.

---. *Contact Mechanics.* Cambridge, UK: Cambridge University Press; 1985.

Jorgensen, G. W. and Lavi, A. *Lithographic Pressman's Handbook.* GATF; 1973.

Kang, Y.; Lee, K., and Liu, T. The effect of polymer additive on the performance of a two-roll coater. Journal of Applied Polymer Science. 1991; 43:1187-1195.

Lopez, F.V., Pauchard, L., Rosen, M., and Rabaud, M. Non-Newtonian effects on ribbing instability threshold. Journal of Non-Newtonian Fluid Mechanics. 2002; 103:123-139

MacPhee, J. A unified view of the film splitting process. American Ink Maker. 1997; 75(1):42-50.

Mewis, J. and Dobbles, F. Nip flow and tack of printing inks. Industrial and Engineering Chemistry Product Research and Development. 1981; 20:515-519.

Mill, C. C. and South, G. R. Formation of ribs on rotating rollers. Journal of Fluid Mechanics. 1967; 28:523-529.

Miller, J. C. and Myers, R. R. A Photographic Study of Liquid Flow in a Roll Nip. Transactions of the Society of Rheology. 1958; 2:77-93.

Myers, R. R. and Hoffman, R. D. The Distribution of Pressure in the Roll Application of Newtonian Fluids. Transactions of the Society of Rheology. 1961; 5:317-328.

Myers, R. R.; Miller, J. C., and Zettlemoyer, A. C. The splitting of thin liquid films. Kinematics. Journal of Colloid Science. 1959; 14:287-299.

Nguyen, D.A. and Sridhar, T. Preparation and some properties of M1 and its constituents. Journal of Non-Newtonian Fluid Mechanics. 1990; 35:pp 93-104.

Patel, N. and Dealy, J. M. Measurement of tensile stress at the exit of a printing nip. Journal of Non-Newtonian Fluid Mechanics. 1987; 22:245-252.

Pitts, E. and Greiller, J. The flow of thin liquid films between rollers. Journal of Fluid Mechanics. 1961; 11:33-50.

POLYFLOW User Guide. Fluent Inc., Lebanon, NH, 2002.

Poranen, J.; Kataja, M.; Niemisto, A., and Grön, J. A method for measuring and controlling the pressure in the metering nip of a metering size press coating process. Nordic Pulp and Paper Research Journal. 2000; 15(5):486-493.

Pranckh, F. R. and Coyle, D. J. Elastohydrodynamic Coating Systems. In: *Liquid Film Coating.* Kistler, S. F.; Schweizer, P. M. (eds). London: Chapman & Hall; 1997; pp. 599-635.

Prilutski, G., Gupta, K., Sridhar, T., and Ryan, M.E. Model viscoelastic liquids. Journal of Non-Newtonian Fluid Mechanics. 1983; 12:pp 233-241.

Reglat, O. and Tanguy, P. A. Experimental study of the flow in the metering nip of a metering-size press. AIChE Journal. 1997; 43(11):2911-2920.

Roper, J. A.; Bousfield, D. W.; Urscheler, R., and Salminen, P. Observations and proposed mechanisms of misting on high-speed metered size press coaters. TAPPI Coating Conference Proceedings; 1997: 1-14.

Roper, J. A.; Salminen, P.; Urscheler, R., and Bousfield, D. W. Studies of orange peel formation in high-speed film coating. TAPPI Journal. 1999; 82(1):231-238.

Satas, D. *Web Processing and Converting Technology and Equipment.* New York, NY: Van Nostrand Reinhold; 1984.

Savage, M. D. Mathematical models for coating processes. Journal of Fluid Mechanics. 1982; 117:443-455.

Shaqfeh, E. S. G. Purely elastic instabilities in viscometric flows. Annual Review of Fluid Mechanics. 1996; 28:129-185.

Smith, J. W. and Maloney, J. D. Flow of fluids between rotating rollers. TAPPI Journal. 1966; 49(11):63A-66A.

Soules, D. A.; Fernando, R. H., and Glass, J. E. Dynamic uniaxial extensional viscosity (DUEV) effects in roll application I. Rib and web growth in commercial coatings. Journal of Rheology. 1988; 32(2):181-198.

Spiers, R. P.; Subbaraman, C. V., and Wilkinson, W. L. Chemical Engineering Science. 1974; 29(1):389.

Sridhar, T. An overview of the M1 project. Journal of Non-Newtonian Fluid Mechanics. 1990; 35:pp 85-92.

Swales, P. D.; Dowson, D., and Latham, J. L. Theoretical and experimental observations of the behavior of soft elastic materials under elastohydrodynamic conditions. Proceedings of the Institution of Mechanical Engineers 1972 Symposium on Elastohydrodynamic Lubrication ; 1972: 22-28.

Taylor, J. H. and Zettlemoyer, A. C. Hypothesis on the mechanism of ink splitting during printing. TAPPI Journal. 1958; 41(12):749-757.

Tharmalingam, S. and Wilkinson, W. L. The coating of Newtonian liquids onto a roll rotating at low speeds. Polymer Engineering and Science. 1978; 18(15):1155-1159.

---. The coating of Newtonian liquids onto a rotating roll. Chemical Engineering Science. 1978; 33:1481-1487.

Triantafillopoulos N. G. *Paper Coating Viscoelasticity and its Significance in Blade Coating.* Atlanta, GA: TAPPI Press; 1996.

Varnam, C. J. and Hooke. C. J. Non-Hertzian elastohydrodynamic contacts: an experimental investigation. Journal of Mechanical Engineering Science. 1977; 19(5):189-192.

Voet, A. Ink misting and its prevention. American Ink Maker. 1956; 34(2):32.

Yih, C. S. Instability of a rotating liquid film with a free surface. Philosophical Transactions of the Royal Society of London, Series A, Mathematical and Physical Sciences. 1960; 258(1):63-89.

Zang, Y. H.; Aspler, J. S.; Boluk, M. Y., and De Grace, J. H. Direct measurement of tensile stress ("tack") in thin ink films. Journal of Rheology. 1991; 35(3):345-361.

Zink, S. C. Coating Processes. In: *Encyclopedia of Chemical Technology.* 3rd ed. New York, NY: Wiley; 1979; pp. 386-426.

APPENDIX

Table A. 1 Silicone oil, W = 1020 N/m

Silicone Oil							
Dimensional					Dimensionless		
W (N/m)	V (m/s)	μ (Pas)	h_{Film} (μm)	H (μm)	μV/ER	W/ER	H/R
1020	0.10	1.37	17.31	34.62	1.1E-07	8.1E-04	1.1E-03
1020	0.20	1.37	26.85	53.70	2.2E-07	8.1E-04	1.7E-03
1020	0.40	1.37	42.87		4.4E-07	8.1E-04	
1020	1.00	1.37	60.04	120.08	1.1E-06	8.1E-04	3.8E-03
1020	0.10	1.37	16.84	33.68	1.1E-07	8.1E-04	1.1E-03
1020	0.20	1.37	26.01	52.02	2.2E-07	8.1E-04	1.6E-03
1020	0.40	1.37	39.35	78.70	4.4E-07	8.1E-04	2.5E-03
1020	1.00	1.37	60.27	120.54	1.1E-06	8.1E-04	3.8E-03
1020	0.10	1.37	16.55	33.10	1.1E-07	8.1E-04	1.0E-03
1020	0.20	1.37	25.40	50.80	2.2E-07	8.1E-04	1.6E-03
1020	0.40	1.37	38.65	77.30	4.4E-07	8.1E-04	2.4E-03
1020	1.00	1.37	59.98	119.96	1.1E-06	8.1E-04	3.8E-03

Table A. 2 Silicone oil, W = 2100 N/m

Silicone Oil							
Dimensional					Dimensionless		
W (N/m)	V (m/s)	μ (Pas)	h_{Film} (μm)	H (μm)	μV/ER	W/ER	H/R
2100	0.10	1.37	14.95	28.27	1.1E-07	1.7E-03	8.9E-04
2100	0.20	1.37	20.74	41.48	2.2E-07	1.7E-03	1.3E-03
2100	0.40	1.37	33.67	67.34	4.4E-07	1.7E-03	2.1E-03
2100	1.00	1.37	50.67	101.34	1.1E-06	1.7E-03	3.2E-03
2100	0.10	1.37	14.80	29.60	1.1E-07	1.7E-03	9.3E-04
2100	0.20	1.37	20.46	40.92	2.2E-07	1.7E-03	1.3E-03
2100	0.40	1.37	32.61	65.22	4.4E-07	1.7E-03	2.1E-03
2100	1.00	1.37	47.87	95.74	1.1E-06	1.7E-03	3.0E-03
2100	0.10	1.37	14.63	29.26	1.1E-07	1.7E-03	9.2E-04
2100	0.20	1.37	20.02	40.04	2.2E-07	1.7E-03	1.3E-03
2100	0.40	1.37	31.88	63.76	4.4E-07	1.7E-03	2.0E-03
2100	1.00	1.37	47.49	94.98	1.1E-06	1.7E-03	3.0E-03

Table A. 3 Silicone oil, W = 3200 N/m

Silicone Oil							
Dimensional					Dimensionless		
W (N/m)	V (m/s)	μ (Pas)	h_{Film} (μm)	H (μm)	μV/ER	W/ER	H/R
3200	0.10	1.37	12.24	24.48	1.1E-07	2.6E-03	7.7E-04
3200	0.20	1.37	16.53	33.06	2.2E-07	2.6E-03	1.0E-03
3200	0.40	1.37	25.30	50.60	4.4E-07	2.6E-03	1.6E-03
3200	1.00	1.37	40.13	80.26	1.1E-06	2.6E-03	2.5E-03
3200	0.10	1.37	12.03	24.06	1.1E-07	2.6E-03	7.6E-04
3200	0.20	1.37	16.62	33.24	2.2E-07	2.6E-03	1.0E-03
3200	0.40	1.37	24.71	49.42	4.4E-07	2.6E-03	1.6E-03
3200	1.00	1.37	36.87	83.09	1.1E-06	2.6E-03	2.6E-03
3200	0.10	1.37	12.02	24.04	1.1E-07	2.6E-03	7.6E-04
3200	0.20	1.37	16.31	32.62	2.2E-07	2.6E-03	1.0E-03
3200	0.40	1.37	24.26	48.52	4.4E-07	2.6E-03	1.5E-03
3200	1.00	1.37	36.95	83.97	1.1E-06	2.6E-03	2.6E-03

Table A. 4 Silicone oil, W = 4400 N/m

Silicone Oil							
Dimensional					Dimensionless		
W (N/m)	V (m/s)	μ (Pas)	h_{Film} (μm)	H (μm)	μV/ER	W/ER	H/R
4400	0.10	1.37	10.67	21.34	1.1E-07	3.5E-03	6.7E-04
4400	0.20	1.37	13.42	26.84	2.2E-07	3.5E-03	8.5E-04
4400	0.40	1.37	21.50	43.00	4.4E-07	3.5E-03	1.4E-03
4400	1.00	1.37	34.13	68.26	1.1E-06	3.5E-03	2.1E-03
4400	0.10	1.37	10.57	21.14	1.1E-07	3.5E-03	6.7E-04
4400	0.20	1.37	13.54	27.08	2.2E-07	3.5E-03	8.5E-04
4400	0.40	1.37	21.13	42.26	4.4E-07	3.5E-03	1.3E-03
4400	1.00	1.37	33.60	78.13	1.1E-06	3.5E-03	2.5E-03
4400	0.10	1.37	10.36	20.72	1.1E-07	3.5E-03	6.5E-04
4400	0.20	1.37	13.32	26.64	2.2E-07	3.5E-03	8.4E-04
4400	0.40	1.37	20.84	41.68	4.4E-07	3.5E-03	1.3E-03
4400	1.00	1.37	32.97	65.94	1.1E-06	3.5E-03	2.1E-03

Table A. 5 Silicone oil, W = 6400 N/m

Silicone Oil							
Dimensional					Dimensionless		
W (N/m)	V (m/s)	μ (Pas)	h_{Film} (μm)	H (μm)	μV/ER	W/ER	H/R
6400	0.20	1.37	11.97	23.94	2.2E-07	5.1E-03	7.5E-04
6400	0.40	1.37	18.55	37.10	4.4E-07	5.1E-03	1.2E-03
6400	0.80	1.37	26.50	53.00	8.8E-07	5.1E-03	1.7E-03
6400	1.20	1.37	34.61			5.1E-03	
6400	0.20	1.37	11.91			5.1E-03	
6400	0.40	1.37	18.21	36.42	4.4E-07	5.1E-03	1.1E-03
6400	0.80	1.37	25.83	51.66	8.8E-07	5.1E-03	1.6E-03
6400	1.20	1.37	35.03			5.1E-03	
6400	0.20	1.37	11.86			5.1E-03	
6400	0.40	1.37	18.15	36.30	4.4E-07	5.1E-03	1.1E-03
6400	0.80	1.37	26.16	52.32	8.8E-07	5.1E-03	1.6E-03
6400	1.20	1.37	35.36			5.1E-03	

Table A. 6 Silicone oil, W = 8500 N/m

Silicone Oil							
Dimensional					Dimensionless		
W (N/m)	V (m/s)	μ (Pas)	h_{Film} (μm)	H (μm)	μV/ER	W/ER	H/R
8500	0.20	1.37	11.59			6.8E-03	
8500	0.40	1.37	17.73	33.29	4.4E-07	6.8E-03	1.0E-03
8500	0.80	1.37	24.85	45.36	8.8E-07	6.8E-03	1.4E-03
8500	1.20	1.37	27.80	55.60	1.3E-06	6.8E-03	1.8E-03
8500	0.20	1.37	11.33			6.8E-03	
8500	0.40	1.37	17.48	31.73	4.4E-07	6.8E-03	1.0E-03
8500	0.80	1.37	25.14	45.46	8.8E-07	6.8E-03	1.4E-03
8500	1.20	1.37	31.72	63.44	1.3E-06	6.8E-03	2.0E-03
8500	0.20	1.37	11.25			6.8E-03	
8500	0.40	1.37	17.29	30.49	4.4E-07	6.8E-03	9.6E-04
8500	0.80	1.37	25.11	44.74	8.8E-07	6.8E-03	1.4E-03
8500	1.20	1.37	30.78			6.8E-03	

Table A. 7 0.12% PIB, W = 2100 N/m

0.12% PIB							
Dimensional					Dimensionless		
W (N/m)	V (m/s)	μ (Pas)	h_{Film} (μm)	H (μm)	μV/ER	W/ER	H/R
2100	0.10	0.79	11.01	20.38	6.3E-08	1.7E-03	6.4E-04
2100	0.20	0.79	14.84	29.68	1.3E-07	1.7E-03	9.3E-04
2100	0.30	0.79	21.07	42.14	1.9E-07	1.7E-03	1.3E-03
2100	0.40	0.79	26.03		2.5E-07	1.7E-03	
2100	0.50	0.79	28.84		3.2E-07	1.7E-03	
2100	0.10	0.79	11.52	19.14	6.3E-08	1.7E-03	6.0E-04
2100	0.20	0.79	14.74	32.33	1.3E-07	1.7E-03	1.0E-03
2100	0.30	0.79	20.54	41.08	1.9E-07	1.7E-03	1.3E-03
2100	0.40	0.79	25.43	50.86	2.5E-07	1.7E-03	1.6E-03
2100	0.50	0.79	28.07	56.14	3.2E-07	1.7E-03	1.8E-03
2100	0.10	0.79	11.48	22.96	6.3E-08	1.7E-03	7.2E-04
2100	0.20	0.79	14.71	30.47	1.3E-07	1.7E-03	9.6E-04
2100	0.30	0.79	20.03	40.06	1.9E-07	1.7E-03	1.3E-03
2100	0.40	0.79	24.80	49.60	2.5E-07	1.7E-03	1.6E-03
2100	0.50	0.79	27.37	54.74	3.2E-07	1.7E-03	1.7E-03

Table A. 8 0.12% PIB, W = 3200 N/m

0.12% PIB							
Dimensional					Dimensionless		
W (N/m)	V (m/s)	μ (Pas)	h_{Film} (μm)	H (μm)	μV/ER	W/ER	H/R
3200	0.10	0.79	10.48		6.3E-08	2.6E-03	
3200	0.20	0.79	11.66	23.32	1.3E-07	2.6E-03	7.3E-04
3200	0.30	0.79	17.17	31.02	1.9E-07	2.6E-03	9.8E-04
3200	0.40	0.79	20.06	35.44	2.5E-07	2.6E-03	1.1E-03
3200	0.60	0.79	23.78	47.36	3.8E-07	2.6E-03	1.5E-03
3200	0.10	0.69	8.83	15.93	5.5E-08	2.6E-03	5.0E-04
3200	0.20	0.69	12.74	21.57	1.1E-07	2.6E-03	6.8E-04
3200	0.40	0.69	16.21	32.42	2.2E-07	2.6E-03	1.0E-03
3200	0.60	0.69	22.41	44.82	3.3E-07	2.6E-03	1.4E-03
3200	1.00	0.69	28.82	60.75	5.5E-07	2.6E-03	1.9E-03
3200	0.10	0.69	9.46	14.62	5.5E-08	2.6E-03	4.6E-04
3200	0.20	0.69	13.52	22.03	1.1E-07	2.6E-03	6.9E-04
3200	0.40	0.69	17.01	34.02	2.2E-07	2.6E-03	1.1E-03
3200	0.60	0.69	22.99	45.98	3.3E-07	2.6E-03	1.4E-03
3200	1.00	0.69	30.39	60.78	5.5E-07	2.6E-03	1.9E-03

Table A. 9 0.12% PIB, W = 4400 N/m

0.12% PIB							
Dimensional					Dimensionless		
W (N/m)	V (m/s)	μ (Pas)	h_{Film} (μm)	H (μm)	μV/ER	W/ER	H/R
4400	0.10	0.79	8.88		6.3E-08	3.5E-03	
4400	0.20	0.79	9.12	33.77	1.3E-07	3.5E-03	1.1E-03
4400	0.30	0.79	13.52	26.84	1.9E-07	3.5E-03	8.5E-04
4400	0.40	0.79	16.98	34.34	2.5E-07	3.5E-03	1.1E-03
4400	0.60	0.79	18.94	42.27	3.8E-07	3.5E-03	1.3E-03
4400	0.10	0.79	9.22		6.3E-08	3.5E-03	
4400	0.20	0.79	9.21	18.43	1.3E-07	3.5E-03	5.8E-04
4400	0.30	0.79	14.20	28.40	1.9E-07	3.5E-03	8.9E-04
4400	0.40	0.79	16.44	32.88	2.5E-07	3.5E-03	1.0E-03
4400	0.60	0.79	17.95	44.20	3.8E-07	3.5E-03	1.4E-03
4400	0.10	0.79	8.65		6.3E-08	3.5E-03	
4400	0.20	0.79	9.29	18.58	1.3E-07	3.5E-03	5.9E-04
4400	0.30	0.79	14.22	28.44	1.9E-07	3.5E-03	9.0E-04
4400	0.40	0.79	16.23	35.67	2.5E-07	3.5E-03	1.1E-03
4400	0.60	0.79	17.98	42.04	3.8E-07	3.5E-03	1.3E-03

Table A. 10 0.12% PIB, W = 5050 N/m

0.12% PIB							
Dimensional					Dimensionless		
W (N/m)	V (m/s)	μ (Pas)	h_{Film} (μm)	H (μm)	μV/ER	W/ER	H/R
5050	0.10	0.79	10.99		6.3E-08	4.0E-03	
5050	0.20	0.79	10.75	19.33	1.3E-07	4.0E-03	6.1E-04
5050	0.30	0.79	14.07	28.14	1.9E-07	4.0E-03	8.9E-04
5050	0.40	0.79	16.03	32.06	2.5E-07	4.0E-03	1.0E-03
5050	0.60	0.79	18.59	37.18	3.8E-07	4.0E-03	1.2E-03
5050	0.10	0.79	11.00		6.3E-08	4.0E-03	
5050	0.20	0.79	9.39	18.79	1.3E-07	4.0E-03	5.9E-04
5050	0.30	0.79	14.86	29.72	1.9E-07	4.0E-03	9.4E-04
5050	0.40	0.79	15.64	31.28	2.5E-07	4.0E-03	9.9E-04
5050	0.60	0.79	17.94	35.88	3.8E-07	4.0E-03	1.1E-03
5050	0.10	0.79	10.99		6.3E-08	4.0E-03	
5050	0.20	0.79	9.37	18.75	1.3E-07	4.0E-03	5.9E-04
5050	0.30	0.79	13.94	27.88	1.9E-07	4.0E-03	8.8E-04
5050	0.40	0.79	15.56	31.12	2.5E-07	4.0E-03	9.8E-04
5050	0.60	0.79	17.93	35.86	3.8E-07	4.0E-03	1.1E-03

Table A. 11 0.12% PIB, W = 6400 N/m

0.12% PIB							
Dimensional					Dimensionless		
W (N/m)	V (m/s)	μ (Pas)	h_{Film} (μm)	H (μm)	μV/ER	W/ER	H/R
6400	0.20	0.79	8.70	17.40	1.3E-07	5.1E-03	5.5E-04
6400	0.40	0.79	15.59		2.5E-07	5.1E-03	
6400	0.60	0.79	17.65	35.30	3.8E-07	5.1E-03	1.1E-03
6400	0.80	0.79	26.00		5.1E-07	5.1E-03	
6400	0.20	0.79	8.39	16.77	1.3E-07	5.1E-03	5.3E-04
6400	0.40	0.79	14.97	29.94	2.5E-07	5.1E-03	9.4E-04
6400	0.60	0.79	16.57	33.14	3.8E-07	5.1E-03	1.0E-03
6400	0.80	0.79	21.50	43.00	5.1E-07	5.1E-03	1.4E-03
6400	0.20	0.79	8.39	16.78	1.3E-07	5.1E-03	5.3E-04
6400	0.40	0.79	15.20		2.5E-07	5.1E-03	
6400	0.60	0.79	15.75	31.50	3.8E-07	5.1E-03	9.9E-04
6400	0.80	0.79	16.87	33.74	5.1E-07	5.1E-03	1.1E-03

Table A. 12 0.24% PIB, W = 2100 N/m

0.24% PIB							
Dimensional					Dimensionless		
W (N/m)	V (m/s)	μ (Pas)	h_{Film} (μm)	H (μm)	μV/ER	W/ER	H/R
2100	0.10	0.81	9.10	18.41	6.5E-08	1.7E-03	5.8E-04
2100	0.20	0.81	14.78	23.37	1.3E-07	1.7E-03	7.4E-04
2100	0.40	0.81	23.56	47.12	2.6E-07	1.7E-03	1.5E-03
2100	0.60	0.81	42.58		3.9E-07	1.7E-03	
2100	0.10	0.81			6.5E-08	1.7E-03	
2100	0.20	0.81	26.37	27.25	1.3E-07	1.7E-03	8.6E-04
2100	0.40	0.81	32.83		2.6E-07	1.7E-03	
2100	0.60	0.81	48.02	42.44	3.9E-07	1.7E-03	1.3E-03
2100	0.10	0.81	11.60	17.45	6.5E-08	1.7E-03	5.5E-04
2100	0.20	0.81	18.28	28.50	1.3E-07	1.7E-03	9.0E-04
2100	0.40	0.81	25.09	50.18	2.6E-07	1.7E-03	1.6E-03
2100	0.60	0.81	39.19	78.38	3.9E-07	1.7E-03	2.5E-03
2100	0.10	0.81	47.38	18.74	6.5E-08	1.7E-03	5.9E-04
2100	0.20	0.81	50.53	25.45	1.3E-07	1.7E-03	8.0E-04
2100	0.40	0.81	55.42	36.39	2.6E-07	1.7E-03	1.1E-03
2100	0.60	0.81	65.21	42.37	3.9E-07	1.7E-03	1.3E-03

Table A. 13 0.24% PIB, W = 3200 N/m

0.24% PIB							
Dimensional					Dimensionless		
W (N/m)	V (m/s)	μ (Pas)	h_{Film} (μm)	H (μm)	μV/ER	W/ER	H/R
3200	0.10	1.04	149.30	15.73	8.3E-08	2.6E-03	5.0E-04
3200	0.20	1.04	147.30	27.76	1.7E-07	2.6E-03	8.7E-04
3200	0.40	1.04	128.60	34.44	3.3E-07	2.6E-03	1.1E-03
3200	1.00	1.04	105.20	68.57	8.3E-07	2.6E-03	2.2E-03
3200	0.10	1.04	128.80	16.30	8.3E-08	2.6E-03	5.1E-04
3200	0.20	1.04	124.40	22.93	1.7E-07	2.6E-03	7.2E-04
3200	0.40	1.04	109.50	32.60	3.3E-07	2.6E-03	1.0E-03
3200	1.00	1.04	93.06	60.86	8.3E-07	2.6E-03	1.9E-03
3200	0.10	1.04	5.47	13.73	8.3E-08	2.6E-03	4.3E-04
3200	0.20	1.04	10.38	25.13	1.7E-07	2.6E-03	7.9E-04
3200	0.40	1.04	14.69	33.06	3.3E-07	2.6E-03	1.0E-03
3200	0.60	1.04	21.45	49.57	5.0E-07	2.6E-03	1.6E-03
3200	0.10	1.04	8.10	14.61	8.3E-08	2.6E-03	4.6E-04
3200	0.20	1.04	12.89	27.16	1.7E-07	2.6E-03	8.6E-04
3200	0.40	1.04	17.21	34.58	3.3E-07	2.6E-03	1.1E-03
3200	0.60	1.04	24.15	53.00	5.0E-07	2.6E-03	1.7E-03

Table A. 14 0.24% PIB, W = 6400 N/m

0.24% PIB							
Dimensional					Dimensionless		
W (N/m)	V (m/s)	μ (Pas)	h_{Film} (μm)	H (μm)	μV/ER	W/ER	H/R
6400	0.10	0.86	13.45	8.32	6.9E-08	5.1E-03	2.6E-04
6400	0.20	0.86	18.49	18.35	1.4E-07	5.1E-03	5.8E-04
6400	0.40	0.86	19.54	25.90	2.8E-07	5.1E-03	8.2E-04
6400	1.00	0.86	24.05	43.13	6.9E-07	5.1E-03	1.4E-03
6400	0.10	0.86	10.09		6.9E-08	5.1E-03	
6400	0.20	0.86	15.66		1.4E-07	5.1E-03	
6400	0.40	0.86	15.93	26.62	2.8E-07	5.1E-03	8.4E-04
6400	1.00	0.86	15.78	37.41	6.9E-07	5.1E-03	1.2E-03
6400	0.10	0.86	11.26	9.14	6.9E-08	5.1E-03	2.9E-04
6400	0.20	0.86	15.92		1.4E-07	5.1E-03	
6400	0.40	0.86	15.35	27.20	2.8E-07	5.1E-03	8.6E-04
6400	1.00	0.86	22.91	45.82	6.9E-07	5.1E-03	1.4E-03
6400	0.10	0.86	4.68	10.01	6.9E-08	5.1E-03	3.2E-04
6400	0.20	0.86	10.25		1.4E-07	5.1E-03	
6400	0.40	0.86	10.39	17.88	2.8E-07	5.1E-03	5.6E-04
6400	0.60	0.86	14.39	28.13	4.1E-07	5.1E-03	8.9E-04

Table A. 15 0.24% PIB, W = 8500 N/m

0.24% PIB							
Dimensional					Dimensionless		
W (N/m)	V (m/s)	μ (Pas)	h_{Film} (μm)	H (μm)	μV/ER	W/ER	H/R
8500	1.00	1.04	34.29	30.28	8.3E-07	6.8E-03	9.5E-04
8500	0.50	1.04	13.15	21.92	4.1E-07	6.8E-03	6.9E-04
8500	0.50	1.04	12.38	24.76	4.1E-07	6.8E-03	7.8E-04
8500	0.10	1.04	4.79	9.20	8.3E-08	6.8E-03	2.9E-04
8500	0.40	1.04	10.47	20.94	3.3E-07	6.8E-03	6.6E-04
8500	0.60	1.04	14.27	28.54	5.0E-07	6.8E-03	9.0E-04
8500	0.20	1.04	9.48	11.58	1.7E-07	6.8E-03	3.6E-04
8500	0.40	1.04	9.56	19.11	3.3E-07	6.8E-03	6.0E-04
8500	0.10	1.04	4.57	9.14	8.3E-08	6.8E-03	2.9E-04
8500	0.20	1.04	9.32		1.7E-07	6.8E-03	
8500	0.40	1.04	9.28	18.56	3.3E-07	6.8E-03	5.8E-04
8500	0.60	1.04	12.84	25.68	5.0E-07	6.8E-03	8.1E-04
8500	0.10	1.04	4.57	9.14	8.3E-08	6.8E-03	2.9E-04
8500	0.20	1.04	9.23	9.08	1.7E-07	6.8E-03	2.9E-04
8500	0.40	1.04	9.83	19.43	3.3E-07	6.8E-03	6.1E-04
8500	0.60	1.04	13.26	26.52	5.0E-07	6.8E-03	8.4E-04

Table A. 16 0.36% PIB, W = 2100 N/m

0.36% PIB							
Dimensional					Dimensionless		
W (N/m)	V (m/s)	μ (Pas)	h_{Film} (μm)	H (μm)	μV/ER	W/ER	H/R
2100	0.10	1.38	15.21	52.41	1.1E-07	1.7E-03	1.7E-03
2100	0.20	1.38	18.25	73.93	2.2E-07	1.7E-03	2.3E-03
2100	0.40	1.38	41.68	121.30	4.4E-07	1.7E-03	3.8E-03
2100	0.60	1.38	90.54	139.60	6.6E-07	1.7E-03	4.4E-03
2100	1.00	1.38	117.50	200.60	1.1E-06	1.7E-03	6.3E-03
2100	0.10	1.38	14.12	44.11	1.1E-07	1.7E-03	1.4E-03
2100	0.20	1.38	16.64	66.37	2.2E-07	1.7E-03	2.1E-03
2100	0.40	1.38	38.94	105.30	4.4E-07	1.7E-03	3.3E-03
2100	0.60	1.38	94.82	139.60	6.6E-07	1.7E-03	4.4E-03
2100	1.00	1.38	138.70	190.90	1.1E-06	1.7E-03	6.0E-03
2100	0.10	1.38	13.60	41.29	1.1E-07	1.7E-03	1.3E-03
2100	0.20	1.38	16.04	59.17	2.2E-07	1.7E-03	1.9E-03
2100	0.40	1.38	35.25	95.87	4.4E-07	1.7E-03	3.0E-03
2100	0.60	1.38	100.90	126.80	6.6E-07	1.7E-03	4.0E-03
2100	1.00	1.38	133.50	176.40	1.1E-06	1.7E-03	5.6E-03

Table A. 17 0.36% PIB, W = 3200 N/m

0.36% PIB							
Dimensional					Dimensionless		
W (N/m)	V (m/s)	μ (Pas)	h_{Film} (μm)	H (μm)	μV/ER	W/ER	H/R
3200	0.10	1.38	10.06	35.37	1.1E-07	2.6E-03	1.1E-03
3200	0.20	1.38	11.31	48.43	2.2E-07	2.6E-03	1.5E-03
3200	0.40	1.38	21.63	68.74	4.4E-07	2.6E-03	2.2E-03
3200	0.60	1.38	35.90	102.20	6.6E-07	2.6E-03	3.2E-03
3200	1.00	1.38	100.20	160.50	1.1E-06	2.6E-03	5.1E-03
3200	0.10	1.38	9.78	31.76	1.1E-07	2.6E-03	1.0E-03
3200	0.20	1.38	11.31	48.96	2.2E-07	2.6E-03	1.5E-03
3200	0.40	1.38	20.46	67.72	4.4E-07	2.6E-03	2.1E-03
3200	0.60	1.38	38.45	92.74	6.6E-07	2.6E-03	2.9E-03
3200	1.00	1.38	159.80	141.10	1.1E-06	2.6E-03	4.4E-03
3200	0.10	1.38	9.80	29.54	1.1E-07	2.6E-03	9.3E-04
3200	0.20	1.38	10.78	45.48	2.2E-07	2.6E-03	1.4E-03
3200	0.40	1.38	19.82	64.86	4.4E-07	2.6E-03	2.0E-03
3200	0.60	1.38	41.41	87.72	6.6E-07	2.6E-03	2.8E-03
3200	1.00	1.38	161.60	125.00	1.1E-06	2.6E-03	3.9E-03

Table A. 18 0.36% PIB, W = 4400 N/m

0.36% PIB							
Dimensional					Dimensionless		
W (N/m)	V (m/s)	μ (Pas)	h_{Film} (μm)	H (μm)	μV/ER	W/ER	H/R
4400	0.10	1.38	9.69	19.39	1.1E-07	3.5E-03	6.1E-04
4400	0.20	1.38	10.02	40.44	2.2E-07	3.5E-03	1.3E-03
4400	0.40	1.38	17.68	58.39	4.4E-07	3.5E-03	1.8E-03
4400	0.60	1.38	20.50	70.01	6.6E-07	3.5E-03	2.2E-03
4400	1.00	1.38	35.42	104.50	1.1E-06	3.5E-03	3.3E-03
4400	0.10	1.38	9.62	25.05	1.1E-07	3.5E-03	7.9E-04
4400	0.20	1.38	10.29	38.26	2.2E-07	3.5E-03	1.2E-03
4400	0.40	1.38	17.51	52.05	4.4E-07	3.5E-03	1.6E-03
4400	0.60	1.38	19.53	70.30	6.6E-07	3.5E-03	2.2E-03
4400	1.00	1.38	37.03	95.72	1.1E-06	3.5E-03	3.0E-03
4400	0.10	1.38	9.68	23.98	1.1E-07	3.5E-03	7.6E-04
4400	0.20	1.38	9.70	39.69	2.2E-07	3.5E-03	1.3E-03
4400	0.40	1.38	17.34		4.4E-07	3.5E-03	
4400	0.60	1.38	19.24	69.12	6.6E-07	3.5E-03	2.2E-03
4400	1.00	1.38	37.31	91.07	1.1E-06	3.5E-03	2.9E-03

Table A. 19 0.36% PIB, W = 6400 N/m

0.36% PIB							
Dimensional					Dimensionless		
W (N/m)	V (m/s)	μ (Pas)	h_{Film} (μm)	H (μm)	μV/ER	W/ER	H/R
6400	0.20	1.38	8.51	22.53	2.2E-07	5.1E-03	7.1E-04
6400	0.40	1.38	14.71	28.63	4.4E-07	5.1E-03	9.0E-04
6400	0.60	1.38	15.46		6.6E-07	5.1E-03	
6400	1.00	1.38	44.09		1.1E-06	5.1E-03	
6400	0.20	1.38	8.72	21.32	2.2E-07	5.1E-03	6.7E-04
6400	0.40	1.38	14.41	28.82	4.4E-07	5.1E-03	9.1E-04
6400	0.60	1.38	15.48		6.6E-07	5.1E-03	
6400	1.00	1.38	55.26		1.1E-06	5.1E-03	
6400	0.20	1.38	8.75		2.2E-07	5.1E-03	6.4E-04
6400	0.40	1.38	14.66	29.32	4.4E-07	5.1E-03	9.2E-04
6400	0.60	1.38	14.41	44.31	6.6E-07	5.1E-03	1.4E-03
6400	1.00	1.38	63.92	58.35	1.1E-06	5.1E-03	1.8E-03

Table A. 20 0.36% PIB, W = 8500 N/m

0.36% PIB							
Dimensional					Dimensionless		
W (N/m)	V (m/s)	μ (Pas)	h_{Film} (μm)	H (μm)	μV/ER	W/ER	H/R
8500	0.20	1.38	8.37	16.74	2.2E-07	6.8E-03	5.3E-04
8500	0.40	1.38	13.66	28.84	4.4E-07	6.8E-03	9.1E-04
8500	0.60	1.38	14.84	37.37	6.6E-07	6.8E-03	1.2E-03
8500	1.00	1.38	24.45	48.44	1.1E-06	6.8E-03	1.5E-03
8500	0.20	1.38	8.90	17.79	2.2E-07	6.8E-03	5.6E-04
8500	0.40	1.38	13.56	27.27	4.4E-07	6.8E-03	8.6E-04
8500	0.60	1.38	15.81	35.16	6.6E-07	6.8E-03	1.1E-03
8500	1.00	1.38	49.18	44.87	1.1E-06	6.8E-03	1.4E-03
8500	0.20	1.38	8.80	17.59	2.2E-07	6.8E-03	5.5E-04
8500	0.40	1.38	13.57	26.50	4.4E-07	6.8E-03	8.3E-04
8500	0.60	1.38	15.92	34.02	6.6E-07	6.8E-03	1.1E-03
8500	1.00	1.38	94.73	45.02	1.1E-06	6.8E-03	1.4E-03

Table A. 21 0.45% PIB, W = 1020 N/m

0.45 % PIB							
Dimensional					Dimensionless		
W (N/m)	V (m/s)	μ (Pas)	h_{Film} (μm)	H (μm)	μV/ER	W/ER	H/R
1020	0.10	0.47	18.98		3.7E-08	8.1E-04	
1020	0.20	0.45	53.21	120.50	7.1E-08	8.1E-04	3.8E-03
1020	0.40	0.44	88.46	196.80	1.4E-07	8.1E-04	6.2E-03
1020	0.60	0.44	123.30	246.60	2.1E-07	8.1E-04	7.8E-03
1020	0.10	0.46	13.42	76.01	3.6E-08	8.1E-04	2.4E-03
1020	0.20	0.44	51.99	103.30	7.1E-08	8.1E-04	3.3E-03
1020	0.40	0.44	85.28	199.70	1.4E-07	8.1E-04	6.3E-03
1020	0.60	0.43	107.20	242.20	2.1E-07	8.1E-04	7.6E-03
1020	0.10	0.45	10.77	59.81	3.6E-08	8.1E-04	1.9E-03
1020	0.20	0.44	49.47	86.85	7.0E-08	8.1E-04	2.7E-03
1020	0.40	0.44	83.58	167.70	1.4E-07	8.1E-04	5.3E-03
1020	0.60	0.43	114.80	210.60	2.1E-07	8.1E-04	6.6E-03

Table A. 22 0.45% PIB, W = 2100 N/m

0.45 % PIB							
Dimensional					Dimensionless		
W (N/m)	V (m/s)	μ (Pas)	h_{Film} (μm)	H (μm)	μV/ER	W/ER	H/R
2100	0.20	0.42	8.24	56.40	6.7E-08	1.7E-03	1.8E-03
2100	0.40	0.41	15.75	79.54	1.3E-07	1.7E-03	2.5E-03
2100	0.60	0.41	16.71	99.01	1.9E-07	1.7E-03	3.1E-03
2100	1.00	0.41	53.77		3.2E-07	1.7E-03	
2100	0.20	0.41	7.68	41.49	6.6E-08	1.7E-03	1.3E-03
2100	0.40	0.40	14.94	60.60	1.3E-07	1.7E-03	1.9E-03
2100	0.60	0.40	18.56	85.92	1.9E-07	1.7E-03	2.7E-03
2100	1.00	0.40	73.30	155.80	3.2E-07	1.7E-03	4.9E-03
2100	0.20	0.41	7.38		6.5E-08	1.7E-03	
2100	0.40	0.40	14.02		1.3E-07	1.7E-03	
2100	0.60	0.40	16.66	72.43	1.9E-07	1.7E-03	2.3E-03
2100	1.00	0.40	77.36	130.90	3.2E-07	1.7E-03	4.1E-03

Table A. 23 0.45% PIB, W = 3200 N/m

0.45 % PIB							
Dimensional					Dimensionless		
W (N/m)	V (m/s)	μ (Pas)	h_{Film} (μm)	H (μm)	μV/ER	W/ER	H/R
3200	0.20	0.41	5.60		6.5E-08	2.6E-03	
3200	0.40	0.40	10.59	47.91	1.3E-07	2.6E-03	1.5E-03
3200	0.60	0.39	11.05	57.45	1.9E-07	2.6E-03	1.8E-03
3200	1.00	0.39	19.04	91.20	3.1E-07	2.6E-03	2.9E-03
3200	0.20	0.41	5.55		6.5E-08	2.6E-03	
3200	0.40	0.39	10.71	42.72	1.3E-07	2.6E-03	1.3E-03
3200	0.60	0.39	11.84	50.03	1.8E-07	2.6E-03	1.6E-03
3200	1.00	0.38	18.64	74.99	3.1E-07	2.6E-03	2.4E-03
3200	0.20	0.40	5.41	25.93	6.4E-08	2.6E-03	8.2E-04
3200	0.40	0.39	10.33	40.04	1.2E-07	2.6E-03	1.3E-03
3200	0.60	0.39	11.36	48.25	1.8E-07	2.6E-03	1.5E-03
3200	1.00	0.38	17.66	67.59	3.0E-07	2.6E-03	2.1E-03

Table A. 24 0.45% PIB, W = 4400 N/m

0.45 % PIB							
Dimensional					Dimensionless		
W (N/m)	V (m/s)	μ (Pas)	h_{Film} (μm)	H (μm)	μV/ER	W/ER	H/R
4400	0.20	0.40	5.42	10.83	6.4E-08	3.5E-03	3.4E-04
4400	0.40	0.39	11.06	32.96	1.2E-07	3.5E-03	1.0E-03
4400	0.60	0.38	10.12	44.04	1.8E-07	3.5E-03	1.4E-03
4400	1.00	0.38	14.17		3.0E-07	3.5E-03	
4400	0.20	0.40	5.39	24.76	6.3E-08	3.5E-03	7.8E-04
4400	0.40	0.38	10.72	31.16	1.2E-07	3.5E-03	9.8E-04
4400	0.60	0.38	10.44	37.48	1.8E-07	3.5E-03	1.2E-03
4400	1.00	0.37	15.62	50.69	3.0E-07	3.5E-03	1.6E-03
4400	0.20	0.40	5.46	24.54	6.3E-08	3.5E-03	7.7E-04
4400	0.40	0.39	10.53	32.90	1.2E-07	3.5E-03	1.0E-03
4400	0.60	0.38	10.35	35.93	1.8E-07	3.5E-03	1.1E-03
4400	1.00	0.37	15.66	42.57	2.9E-07	3.5E-03	1.3E-03

Table A. 25 0.45% PIB, W = 6400 N/m

0.45 % PIB							
Dimensional					Dimensionless		
W (N/m)	V (m/s)	μ (Pas)	h_{Film} (μm)	H (μm)	μV/ER	W/ER	H/R
6400	0.20	0.39	4.94		6.2E-08	5.1E-03	
6400	0.40	0.37	9.63	18.52	1.2E-07	5.1E-03	5.8E-04
6400	0.60	0.37	9.23	23.88	1.8E-07	5.1E-03	7.5E-04
6400	1.00	0.36	12.13	32.64	2.9E-07	5.1E-03	1.0E-03
6400	0.20	0.38	5.18	10.36	6.1E-08	5.1E-03	3.3E-04
6400	0.40	0.37	9.92	17.32	1.2E-07	5.1E-03	5.5E-04
6400	0.60	0.36	9.63	21.95	1.7E-07	5.1E-03	6.9E-04
6400	1.00	0.36	13.60		2.9E-07	5.1E-03	
6400	0.20	0.38	5.16	14.45	6.1E-08	5.1E-03	4.6E-04
6400	0.40	0.37	9.68	16.78	1.2E-07	5.1E-03	5.3E-04
6400	0.60	0.36	9.57	21.18	1.7E-07	5.1E-03	6.7E-04
6400	1.00	0.36	6.36		2.8E-07	5.1E-03	

Table A. 26 0.45% PIB, W = 8500 N/m

0.45 % PIB							
Dimensional					Dimensionless		
W (N/m)	V (m/s)	μ (Pas)	h_{Film} (μm)	H (μm)	μV/ER	W/ER	H/R
8500	0.20	0.38	5.12	10.23	6.1E-08	6.8E-03	3.2E-04
8500	0.40	0.37	9.00	16.37	1.2E-07	6.8E-03	5.2E-04
8500	0.60	0.36	9.37	20.37	1.7E-07	6.8E-03	6.4E-04
8500	1.00	0.36	11.69	29.30	2.9E-07	6.8E-03	9.2E-04
8500	0.20	0.38	5.54	11.09	6.1E-08	6.8E-03	3.5E-04
8500	0.40	0.37	8.86	15.31	1.2E-07	6.8E-03	4.8E-04
8500	0.60	0.36	9.82	18.88	1.7E-07	6.8E-03	5.9E-04
8500	1.00	0.35	9.40		2.8E-07	6.8E-03	
8500	0.20	0.38	5.59	11.18	6.1E-08	6.8E-03	3.5E-04
8500	0.40	0.37	8.86	14.75	1.2E-07	6.8E-03	4.6E-04
8500	0.60	0.36	9.73	18.31	1.7E-07	6.8E-03	5.8E-04
8500	1.00	0.33	4.54		2.7E-07	6.8E-03	

Table A. 27 0.62% PIB, W = 1020 N/m

0.62 % PIB							
Dimensional					Dimensionless		
W (N/m)	V (m/s)	μ (Pas)	h_{Film} (μm)	H (μm)	μV/ER	W/ER	H/R
1020	0.10	0.32	22.66		2.6E-08	8.1E-04	
1020	0.20	0.29	24.99	76.52	4.6E-08	8.1E-04	2.4E-03
1020	0.40	0.27	69.31	110.40	8.7E-08	8.1E-04	3.5E-03
1020	0.60	0.27	112.50	141.60	1.3E-07	8.1E-04	4.5E-03
1020	0.10	0.31	15.58		2.5E-08	8.1E-04	
1020	0.20	0.29	20.16	79.03	4.6E-08	8.1E-04	2.5E-03
1020	0.40	0.27	69.06	103.50	8.7E-08	8.1E-04	3.3E-03
1020	0.60	0.27	112.90	164.00	1.3E-07	8.1E-04	5.2E-03
1020	0.10	0.30	12.71	52.30	2.4E-08	8.1E-04	1.6E-03
1020	0.20	0.28	17.76	72.78	4.5E-08	8.1E-04	2.3E-03
1020	0.40	0.28	61.48	122.10	8.8E-08	8.1E-04	3.8E-03
1020	0.60	0.28	106.10		1.3E-07	8.1E-04	

Table A. 28 0.62% PIB, W = 2100 N/m

0.62 % PIB							
Dimensional					Dimensionless		
W (N/m)	V (m/s)	μ (Pas)	h_{Film} (μm)	H (μm)	μV/ER	W/ER	H/R
2100	0.10	0.27	6.63		2.1E-08	1.7E-03	
2100	0.20	0.25	5.85	26.59	4.0E-08	1.7E-03	8.4E-04
2100	0.40	0.25	11.66		8.0E-08	1.7E-03	
2100	0.60	0.25	13.94		1.2E-07	1.7E-03	
2100	0.10	0.26	6.35	19.00	2.1E-08	1.7E-03	6.0E-04
2100	0.20	0.25	5.25	25.91	4.0E-08	1.7E-03	8.2E-04
2100	0.40	0.24	10.69	41.02	7.7E-08	1.7E-03	1.3E-03
2100	0.60	0.24	11.91	55.43	1.1E-07	1.7E-03	1.7E-03
2100	0.10	0.26	6.22	18.12	2.1E-08	1.7E-03	5.7E-04
2100	0.20	0.25	5.15	22.24	3.9E-08	1.7E-03	7.0E-04
2100	0.40	0.24	10.06	37.78	7.7E-08	1.7E-03	1.2E-03
2100	0.60	0.24	11.06	50.98	1.1E-07	1.7E-03	1.6E-03

Table A. 29 0.62% PIB, W = 3200 N/m

0.62 % PIB							
Dimensional					Dimensionless		
W (N/m)	V (m/s)	μ (Pas)	h_{Film} (μm)	H (μm)	μV/ER	W/ER	H/R
3200	0.10						
3200	0.20	0.25	3.50	26.62	4.0E-08	2.6E-03	8.4E-04
3200	0.40	0.24	8.91	39.75	7.7E-08	2.6E-03	1.3E-03
3200	0.60	0.23	8.12	45.78	1.1E-07	2.6E-03	1.4E-03
3200	0.10	0.27	4.57		2.1E-08	2.6E-03	
3200	0.20	0.25	3.40	26.02	4.0E-08	2.6E-03	8.2E-04
3200	0.40	0.23	9.08	30.34	7.5E-08	2.6E-03	9.6E-04
3200	0.60	0.23	8.64	37.79	1.1E-07	2.6E-03	1.2E-03
3200	0.10	0.26	4.85	19.00	2.1E-08	2.6E-03	6.0E-04
3200	0.20	0.25	3.78	22.49	3.9E-08	2.6E-03	7.1E-04
3200	0.40	0.23	8.97		7.4E-08	2.6E-03	
3200	0.60	0.23	8.20	36.93	1.1E-07	2.6E-03	1.2E-03

Table A. 30 0.62% PIB, W = 4400 N/m

0.62 % PIB							
Dimensional					Dimensionless		
W (N/m)	V (m/s)	μ (Pas)	h_{Film} (μm)	H (μm)	μV/ER	W/ER	H/R
4400	0.20	0.25	5.72		4.0E-08	3.5E-03	
4400	0.40	0.23	9.88		7.5E-08	3.5E-03	
4400	0.60	0.23	8.09	36.68	1.1E-07	3.5E-03	1.2E-03
4400	1.00	0.23	11.52		1.8E-07	3.5E-03	
4400	0.20	0.25	5.97		3.9E-08	3.5E-03	
4400	0.40	0.23	9.91	26.20	7.4E-08	3.5E-03	8.3E-04
4400	0.60	0.22	8.91	30.86	1.1E-07	3.5E-03	9.7E-04
4400	1.00	0.22	12.72	48.80	1.8E-07	3.5E-03	1.5E-03
4400	0.20	0.24	5.94	18.71	3.8E-08	3.5E-03	5.9E-04
4400	0.40	0.23	9.74	26.04	7.4E-08	3.5E-03	8.2E-04
4400	0.60	0.23	8.54	32.41	1.1E-07	3.5E-03	1.0E-03
4400	1.00	0.22	12.51	44.43	1.8E-07	3.5E-03	1.4E-03

Table A. 31 0.62% PIB, W = 6400 N/m

0.62 % PIB							
Dimensional					Dimensionless		
W (N/m)	V (m/s)	μ (Pas)	h_{Film} (μm)	H (μm)	μV/ER	W/ER	H/R
6400	0.20	0.24	3.14		3.8E-08	5.1E-03	
6400	0.40	0.22	7.16	15.75	7.0E-08	5.1E-03	5.0E-04
6400	0.60	0.21	6.29	19.89	1.0E-07	5.1E-03	6.3E-04
6400	1.00	0.21	9.41	25.66	1.7E-07	5.1E-03	8.1E-04
6400	0.20	0.23	3.74		3.7E-08	5.1E-03	
6400	0.40	0.22	7.24	14.13	6.9E-08	5.1E-03	4.5E-04
6400	0.60	0.21	6.88	17.51	1.0E-07	5.1E-03	5.5E-04
6400	1.00	0.20	10.44	22.02	1.6E-07	5.1E-03	6.9E-04
6400	0.20	0.23	3.85	7.71	3.7E-08	5.1E-03	2.4E-04
6400	0.40	0.21	7.39	13.55	6.8E-08	5.1E-03	4.3E-04
6400	0.60	0.21	6.84	16.89	1.0E-07	5.1E-03	5.3E-04
6400	1.00	0.20	10.41	20.74	1.6E-07	5.1E-03	6.5E-04

Table A. 32 0.62% PIB, W = 8500 N/m

0.62 % PIB							
Dimensional					Dimensionless		
W (N/m)	V (m/s)	μ (Pas)	h_{Film} (μm)	H (μm)	μV/ER	W/ER	H/R
8500	0.20	0.23	3.07	6.14	3.7E-08	6.8E-03	1.9E-04
8500	0.40	0.21	6.84	12.79	6.8E-08	6.8E-03	4.0E-04
8500	0.60	0.21	5.99	15.90	1.0E-07	6.8E-03	5.0E-04
8500	1.00	0.20	8.91	17.81	1.6E-07	6.8E-03	5.6E-04
8500	0.20	0.23	3.65	7.31	3.6E-08	6.8E-03	2.3E-04
8500	0.40	0.21	7.17	11.57	6.7E-08	6.8E-03	3.6E-04
8500	0.60	0.21	6.56	14.13	9.9E-08	6.8E-03	4.5E-04
8500	1.00	0.20	9.87	19.03	1.6E-07	6.8E-03	6.0E-04
8500	0.20	0.23	3.54	7.08	3.6E-08	6.8E-03	2.2E-04
8500	0.40	0.21	7.09	11.12	6.7E-08	6.8E-03	3.5E-04
8500	0.60	0.21	6.33	13.55	9.8E-08	6.8E-03	4.3E-04
8500	1.00	0.20	9.77	17.97	1.6E-07	6.8E-03	5.7E-04

BIOGRAPHY OF THE AUTHOR

Mitchell A. Johnson was born in St. Paul, Minnesota on September 2, 1972. He attended the University of Minnesota in Minneapolis, Minnesota while working as a Technical Aide at 3M Company in St. Paul, Minnesota to fund his education. Mitchell graduated from the University of Minnesota in 1995 with the Bachelor of Chemical Engineering degree. In 1997 he earned the Master of Science degree in Chemical Engineering from the Institute of Paper Science and Technology at the Georgia Institute of Technology, Atlanta, Georgia. After several professional internships, Mitchell enrolled at the University of Maine in 1998 to pursue his interest in the science and art of coating. A member of the Technical Association of the Pulp and Paper Industry since 1995, Mitchell has presented several papers at technical conferences, and was awarded the Louis Georgevits Memorial Award for the Best Student Paper by the Coating and Graphic Arts Division of TAPPI at the 2000 Coating Conference. He is an active member of the Society of Rheology and the American Institute of Chemical Engineers. Mitchell is currently employed by 3M Company, St. Paul, Minnesota as a Senior Research Engineer and is a candidate for the Doctor of Philosophy degree in Chemical Engineering from The University of Maine in May, 2003.